CATALYTIC CONVERSION OF ETHYLBENZENE OVER ACID ZEOLITES

By

EVANS ITAI MABASO

BSc(Chem. Eng.) (Cape Town)

A thesis submitted to the University of Cape Town

in partial fulfilment of the requirements for the degree of

Master of Science in Engineering

MSc (Eng.)

2000

Acknowledgements

I would like to express my sincere gratitude to my supervisor A/Prof. Jack Fletcher for his help and guidance, and above all, for his professional and enthusiastic supervision without which this work would not have been accomplished.

I would also like to thank Prof. Cyril O'Connor for initially supervising this work. I am indebted to A/Prof. Eric van Steen and Dr. Klaus Möller for their input into this work. I am also grateful to Mr Walter Böhringer for his many helpful and stimulating discussions and for proof-reading the thesis.

I would also like to thank all the members of the Catalysis Research Unit and the Department of Chemical Engineering for all the odd jobs they did for me that were needed so urgently and for creating an environment conducive to study and writing up a thesis.

I thank the Department of Chemical Engineering and the National Research Foundation (NRF) for the funding they gave to this work.

A special thanks goes to one special woman, Evelyn, my wife, for her inspiration, love, support and encouragement. To my parents, Johnson and Eunice who taught me that – determination is the firmness of purpose and no drug is as powerful as hope, I say this thesis is dedicated to you.

Thank you all once again. May God bless you!!!

Synopsis

The disproportionation of ethylbenzene to benzene and diethylbenzene is being considered by the International Zeolite Association (IZA) as a possible standard catalytic test reaction for comparing the acidity of different zeolite catalysts and to distinguish between the effective micropore size of medium and large pore zeolites.

In this study, the performance of this test reaction was employed to compare the acidity of various zeolites, viz. lanthanum/sodium-exchanged zeolite Y (LaNaY-72), hydrogen/sodium-exchanged zeolite Y (LZY-52, LZY-62, LZY-82), hydrogen-exchanged zeolite Beta (H-BEA-15, H-BEA-25) and hydrogen-exchanged ZSM-5 (H-MFI-45). The effects of WHSV, activation temperature and carrier gas were investigated on the LaNaY-72 zeolite only. All experiments were conducted in the vapour phase at 180 °C in an isothermal tubular packed bed reactor operated in down-flow configuration. Product analysis was done off-line via gas chromatography.

All catalyst samples showed the pertinent features of time-on-stream behaviour as expected. Large pore zeolites, LaNaY-72, LZY and H-BEA catalysts, showed a pronounced induction period. It was followed by a quasi-stationary stage during which the conversion decreased slowly. For the medium pore zeolite, H-MFI, there was no observable induction period.

Some of the general trends and correlations described in the literature were found as well. As shown for LaNaY-72, increasing WHSV resulted in a decline of conversion as well as in a reduced induction period. High activation temperature (450 °C instead of 250 °C) reduced the activity of the catalyst, thereby extending the induction period. Conversely, carrier gas (either N_2 or H_2) had no effect on conversion and induction period.

However, results of this study are not consistent with the literature claim that the diethylbenzene deficit during the induction period correlates with the number of accessible Brønsted acid sites. What has been observed is that the

length of the induction period correlates well with the number of acid sites, moreover, that distinctly different relationships are apparent for the sodium containing acid zeolites and for the 'pure' H-form zeolites, respectively.

Significant differences were observed between the diethylbenzene isomer distributions formed over the large pore zeolites during the induction period. Throughout the quasi-steady state period and consistent with literature findings, ortho-diethylbenzene formation occurs far below the thermodynamic equilibrium value whereas the distribution of meta- and para-isomers appears close to an equilibrium level between one another. The diethylbenzene isomer distribution suggests that para-diethylbenzene is the kinetically preferred primary product and that ortho-diethylbenzene forms slowly via secondary isomerisation reactions.

From the overall behaviour of the diethylbenzene selectivity during the induction period, it may be possible to ascribe the changes in diethylbenzene selectivity to selective isomer retention (adsorption and absorption) within the zeolite during this period. However, data from this study is insufficient to prove this hypothesis.

TABLE OF CONTENTS

Acknowledgements i
Synopsis ii
Table of Contents iv
List of Figures viii
List of Tables xiii
Nomenclature xiv

1 INTRODUCTION 1

1.1 BACKGROUND 1

1.2 REACTIONS 1

1.3 CHARACTERISATION OF ZEOLITES FOR PORE SIZE AND ACIDITY. 2

1.4 RESEARCH OBJECTIVES 4
1.4.1 KEY QUESTION 5
1.4.2 TASKS 5

2 LITERATURE REVIEW 6

2.1 ZEOLITES 6
2.1.1 ZEOLITE STRUCTURES 7
2.1.2 FRAMEWORK STRUCTURES OF FAU, BEA AND MFI 9

2.2 CHANNEL STRUCTURE: MICROPOROSITY 10
2.2.1 LARGE PORE ZEOLITES 11
2.2.1.1 Zeolite Y 11
2.2.1.2 Zeolite Beta 12
2.2.2 MEDIUM PORE ZEOLITES 12
2.2.2.1 Zeolite ZSM-5 13
2.2.3 SMALL PORE ZEOLITES 14

2.3 ACIDITY OF ZEOLITES 14
2.3.1 BRØNSTED ACIDITY 14
2.3.2 LEWIS ACIDITY 15
2.3.3 ACTIVATION OF ZEOLITES 17
2.3.3.1 Exchange for polyvalent metal ions 17
2.3.3.2 H-form zeolites 17
2.3.4 LANAY-72 18

2.4 MODIFICATION OF ACIDITY 18
2.4.1 DEALUMINATION 18
2.4.2 ION-EXCHANGE 19
2.4.3 MEASUREMENT OF ACIDITY 19

2.5 SHAPE SELECTIVITY IN ZEOLITES 20

2.6 ACID CATALYZED TRANSALKYLATION OF AROMATICS 23

2.7 EXPERIMENTAL FINDINGS ON ETHYLBENZENE DISPROPORTIONATION 25
2.7.1 MECHANISTIC MODELS FOR THE INDUCTION PERIOD 30
2.7.2 PRODUCT INHIBITION 31

2.8 EQUILIBRIUM CONSIDERATIONS 32

3 EXPERIMENTAL SECTION 33

3.1 ETHYLBENZENE CONVERSION EXPERIMENTS 33
3.1.1 REACTOR AND CATALYST PACKING 35
3.1.1.1 Reactor 35
3.1.1.2 Catalysts and Catalyst Preparation 35
3.1.1.3 Catalyst Loading 36
3.1.1.4 Packed catalyst bed configuration 37
3.1.2 N-DECANE AND ETHYLBENZENE SATURATORS 38
3.1.2.1 Ethylbenzene Feed Purity 39
3.1.3 EXPERIMENTAL PROCEDURE 40
3.1.3.1 Start up 40
3.1.3.2 On-stream period 40
3.1.3.3 Shut down 40

3.1.4 PRODUCT ANALYSIS 41
3.1.4.1 Ampoule Sampling Technique 41
3.1.4.2 Gas Chromatographic Analysis and Data Work-up 41

3.2 AMMONIA TEMPERATURE-PROGRAMMED DESORPTION (NH_3-TPD) 44
3.2.1 APPARATUS 44
3.2.2 PROCEDURE 44
3.2.3 TPD DATA WORK-UP 45

3.3 CATALYSTS SUPPLIED AND EXPERIMENTS CONDUCTED 45

4 RESULTS 46

4.1 ETHYLBENZENE CONVERSION 46
4.1.1 INTRODUCTORY EXPERIMENTS 46
4.1.2 REPRODUCIBILITY 50
4.1.3 LANAY-72 50
4.1.3.1 Effect of Activation Temperature 50
4.1.3.2 Effect of WHSV 53
4.1.3.3 Effect of Carrier Gas 55
4.1.4 LINDE-Y ZEOLITE 55
4.1.5 H-BETA 58
4.1.6 H-MFI-45 60
4.1.7 SELECTION OF COMPARATIVE RESULTS 62

4.2 AMMONIA TEMPERATURE PROGRAMMED DESORPTION (NH_3-TPD) 64
4.2.1 TYPICAL RESULTS 64
4.2.2 EFFECT OF ACTIVATION TEMPERATURE ON THE ACTIVITY OF LANAY-72 65
4.2.3 TPD TRACE FOR LINDE-Y ZEOLITE 66
4.2.4 TPD TRACE FOR ZEOLITE BETA 68
4.2.5 TPD TRACE FOR ZSM-5 68

5 DISCUSSION 70

5.1 GENERAL 70
5.1.1 REPRODUCIBILITY OF EXPERIMENTS 70
5.1.2 CONSISTENCY WITH LITERATURE FINDINGS 70

5.2 CORRELATION OF ETHYLBENZENE DISPROPORTIONATION PERFORMANCE WITH ACIDITY 72

5.2.1 DEFICIT OF DIETHYLBENZENES DURING INDUCTION PERIOD 72

5.2.2 THE NUMBER OF ACID SITES 75

5.3 ISOMER DISTRIBUTION 79

6 CONCLUSION 83

REFERENCES 85

APPENDICES

A-1 CATALYSTS SUPPLIED AND EXPERIMENTS CONDUCTED 90

A-2 EXPERIMENTAL DATA 91

A-3 EVALUATION OF REACTION RATES 95

A-4 CALCULATION OF ACIDITY OF ZEOLITES FROM CHEMICAL COMPOSITION 97

A-5 ESTIMATION OF ETHYLBENZENE DEFICIT 100

LIST OF FIGURES

Figure 1-1 Proposed reaction pathway in large pore zeolites (Beck and Haag, 1997) 1

Figure 1-2 Proposed reaction mechanism in medium pore zeolites (Beck and Haag, 1997). 2

Figure 2-1 TO_4 tetrahedra representation (taken from Breck, 1974) 7

Figure 2-2 Secondary building units identifiable in zeolite frameworks (taken from Gilson, 1992) 8

Figure 2-3 Sodalite unit (taken from van Koningsveld, 1991) 8

Figure 2-4 Stereoscopic representation of the framework structures of zeolites: A) Faujasite (FAU), B) Beta (BEA) and C) ZSM-5 (MFI); T-O-T links in these figures are represented as straight lines (Meier and Olson, 1996)..... 9

Figure 2-5 Schematic representation of the zeolite Y (Faujasite) structure (Kärger and Ruthven, 1992). 11

Figure 2-6 The channel structure of ZSM-5 (Chen et al., 1989) 13

Figure 2-7 Formation of Brønsted acidity on zeolites (Uytterhoeven et al., 1968)..... 15

Figure 2-8 The formation of Lewis acidity from Brønsted acidity. (i) Lewis acid site, (ii) 'true' Lewis acid site (taken from Dwyer, 1992) 15

Figure 2-9 Active sites in aluminosilicate zeolites, (a) hydroxyl group and oxo ligands of aluminium acting as bifunctional Brønsted acid-Lewis base site, (b) bridging hydroxyl group responsible for Brønsted acidity (adapted from Martens et al., 1992). 16

Figure 2-10 Classification of shape-selectivity effects according to Weisz and Csicsery (Taken from Emig and Dittmeyer, 1997)..... 21

Figure 2-11 Reaction scheme occuring via a hydride transfer chain reaction through diphenylethanes as intermediates (Philippou and Anderson, 1997) 23

Figure 2-12 Stepwise mechanism proceeding via a dealkylation-realkylation path (Santilli and Gates, 1997) 24

Figure 2-13 Influence of space velocity at constant feed rate on the conversion of ethylbenzene over LaNaY-72 at 180°C (▲ W = 73 mg; □ W = 145 mg; ▼ W = 290 mg; O W = 580 mg) (Taken from Weiss et al., 1997) 26

Figure 2-14 Influence of space velocity at constant feed rate on the conversion of ethylbenzene over LaNaY-72 at 180°C (▲ $T_{act.}$ = 350°C; O $T_{act.}$ = 300°C; □ Tact. = 250°C) (Taken from Weiss et al., 1997) 27

Figure 2-15 Conversion of ethylbenzene at 180°C over lanthanum exchanged faujasites of different extent of lanthanum exchange (□ LaNaY-63; ▼ LaNaY-72; O LaNaY-92) (Taken from Weiss et al., 1997) 27

Figure 2-16 Influence of reaction temperature on the conversion of ethylbenzene over LaNaY-72 (▲ 160°C; ▼ 180°C; O 200°C; □ 220°C. W/F_{EB} = 580, 290, 290 and 145 g.h/mol, respectively) (Taken from Weiss et al., 1997) 28

Figure 2-17 Isomer distribution of diethylbenzenes from ethylbenzene conversion over LaNaY-72 as a function of time-on-stream at 180 °C (Taken from Karge et al., 1994) 29

Figure 2-18 Conversion of ethylbenzene over H-Beta zeolites (Taken from Karge et al., 1994) 30

Figure 2-19 Catalytic cycle for ethylbenzene disproportionation over large pore zeolites developed from the mechanism of Streitwieser and Reif (1960) (Taken from Weiss et al., 1997) 31

Figure 2-20 Equilibrium conversion and equilibrium distribution of isomers in the diethylbenzene fraction during the disproportionation reaction of ethylbenzene at various temperatures (Thermodynamic data from Stull et al., 1969: Computation method from Smith and van Ness, 1987) 32

Figure 3-1 Process flow diagram for the disproportionation of ethylbenzene. 34

Figure 3-2 Configuration of the glass reactor 35

Figure 3-3 Packed catalyst bed configuration 37

Figure 3-4 Temperature profile in the catalyst bed 38

Figure 3-5 Configuration of ethylbenzene (feed) and n-Decane (internal standard) saturators 39

Figure 3-6 A typical product spectrum obtained from the GC (*Internal standard) 42

Figure 4-1 Conversion of ethylbenzene over LaNaY-72. [Experiment 1, T_{act} = 250°C] .. 47

Figure 4-2 Isomer distribution of diethylbenzene over LaNaY-72. [Experiment 1, T_{act} = 250°C]; (Equilibrium: meta —◆—, para —■—, ortho—▲—) 47

Figure 4-3 The yields of diethylbenzenes and benzene over LaNaY-72, [Experiment 1, T_{act} = 250°C] 49

Figure 4-4 The yield ratios of diethylbenzenes to benzene over LaNaY-72 [Experiment 1, T_{act} = 250°C] 49

Figure 4-5 Reproducibility of conversion versus time-on-stream for the disproportionation of ethylbenzene over LaNaY-72. [Open symbols: Experiment 1; Closed symbols: Experiment 2] 50

Figure 4-6 Reproducibility of isomer distribution versus time-on-stream for the disproportionation of ethylbenzene over LaNaY-72. [Open symbols: Experiment 1; Closed symbols: Experiment 2] 51

Figure 4-7 Reproducibility of product yield versus time-on-stream during the disproportionation of ethylbenzene [Open symbols: Experiment 1; Closed symbols: Experiment 2] 52

Figure 4-8 Reproducibility of product yield ratio versus time-on-stream during the disproportionation of ethylbenzene [Open symbols: Experiment 1; Closed symbols: Experiment 2] 52

Figure 4-9 Effect of activation temperature on the disproportionation of ethylbenzene over LaNaY-72. [Open symbols: Experiment 1; Closed symbols: Experiment 3] 53

Figure 4-10 Effect of activation temperature on the isomer distribution over LaNaY-72. (Closed symbols: T_{act} = 450 °C [Experiment 3]; Open symbols: T_{act} = 250 °C [Experiment 1]) 53

Figure 4-11 Effect of WHSV on the disproportionation of ethylbenzene over LaNaY-72. [Open symbols: Experiment 1; Closed symbols: Experiment 5] 54

Figure 4-12 Effect of WHSV on the isomer distribution over LaNaY-72. (Closed symbols: 0.73 h^{-1} [Experiment 5]; Open symbols: 0.37 h^{-1} [Experiment 1]) .. 54

Figure 4-13 Effect of carrier gas on the disproportionation of ethylbenzene over LaNaY-72. [Open symbols: Experiment 1; Closed symbols: Experiment 4] ... 55

Figure 4-14 Conversion of ethylbenzene over Linde-Y zeolites [Open symbols: Experiment 6; Closed symbols: Experiment 7; Star symbols: Experiment 8].. 56

Figure 4-15 Isomer distribution of diethylbenzenes on zeolites Linde-Y (Open symbols: LZY-82 [Experiment 6]; Closed symbols: LZY-62 [Experiment 7])... 57

Figure 4-16 Conversion of ethylbenzene over zeolite H-Beta, T_{act} = 450°C, W_{cat} = 290 mg, $T_{reaction}$ = 180°C. [Open symbols: Experiment 9; Closed symbols: Experiment 10] 58

Figure 4-17 Isomer distribution of diethylbenzenes on zeolite H-Beta (Open symbols: H-BEA-15 [Experiment 9]; Closed symbols: H-BEA-25 [Experiment 10]) 59

Figure 4-18 Conversion of ethylbenzene over H-MFI-45. [Experiment 11] 60

Figure 4-19 Isomer distribution of diethylbenzenes for the conversion of ethylbenzene over H-MFI-45. [Experiment 11] 61

Figure 4-20 Comparison of maximum conversion, which was attained, to that obtained after 12 hours on-stream on zeolites. [* catalyst activated at 250 °C]. 62

Figure 4-21 The distribution of diethylbenzenes on zeolites after 12 hours on stream. [* Calcination temperature = 250 °C] 63

Figure 4-22 Typical NH_3-TPD trace for LaNaY-72 activated at 450 °C 65

Figure 4-23 TPD traces for LaNaY-72 activated at 250 °C and 450 °C. 66

Figure 4-24 TPD traces for Linde-Y zeolite, all activated at 450 °C. 67

Figure 4-25 TPD traces for zeolite-Beta (Si/Al = 25 and 14.6) both activated at 450 °C 68

Figure 4-26 TPD trace for H-MFI-45 activated at 450 °C. 69

Figure 5-1 Relationship between length of induction period and maximum conversion 71

Figure 5-2 Quantification of the deficit of diethylbenzenes during the induction period (LZY-62, Experiment 7) 72

Figure 5-3 Relationship between diethylbenzene deficit during induction period and the length of the induction period 73

Figure 5-4 Diethylbenzene deficit and number of acid sites as a function of catalyst activity (*LaNaY-72 - catalyst activation at 250 °C) 76

Figure 5-5 Length of induction period as a function of the number of acid sites 77

Figure 5-6 Ethylbenzene conversion as a function of the number of acid sites 77

Figure 5-7 Relationship between the rate of ethylbenzene conversion and the deficit of diethylbenzenes during the induction period, both of which were evaluated when steady state was established. (Weiss et al., 1997). Temperatures refer to activation of samples 78

Figure 5-8 Deficit of diethylbenzene during the induction period as a function of the number of acid sites 79

Figure 5-9 Isomer distribution in the diethylbenzene fraction from ethylbenzene disproportionation over various zeolites expressed in terms of para/(para+meta) ratio 80

Figure 5-10 An expanded view of Figure 5-9 for the less active samples 81

Figure 5-11 Para/(para+meta) ratios as a function of the fractional induction period (*LaNaY-72 - catalyst activation at 250 °C) 82

LIST OF TABLES

Table 2-1 Chemical sources and their function in zeolite synthesis (Jansen, 1991) 6

Table 2-2 Most important characteristics for three well-known zeolites and their major applications (van Hooff and Roelofsen, 1991); (+ relevant, ++ very important) 7

Table 2-3 Pore structures of some zeolites (Meier and Olson, 1996) 10

Table 2-4 Estimated kinetic diameters of compounds 22

Table 3-1 List of all the catalysts supplied 36

Table 3-2 Gas chromatographic conditions 42

Table 3-3 Catalytic experiments conducted 45

Table 4-1 Standard reaction conditions 46

Table 4-2 Pseudo-Stationary phase average diethylbenzene isomer distribution 48

Table 4-3 Pseudo-Stationary phase average diethylbenzene isomer distribution 57

Table 4-4 Pseudo-Stationary phase average diethylbenzene isomer distribution 59

Table 4-5 Pseudo-Stationary phase average diethylbenzene isomer distribution 61

Table 4-6 Results summary of conversion of EB over acid zeolites and the distribution of diethylbenzenes at maximum conversion. 63

Table 4-7 Results summary of conversion of EB over acid zeolites and the distribution of diethylbenzenes after 12 hours 64

Table 5-1 Relationship between zeolite acidity and ethylbenzene conversion. 74

NOMENCLATURE

3WV	Three way valve
DEB	Diethylbenzene
EB	Ethylbenzene
EBS	Ethylbenzene saturator
EFAL	Extra-framework aluminium
GC	Gas chromatograph
H-BEA	Zeolite type catalyst (Beta)
H-MFI	Zeolite type catalyst (H-ZSM-5)
ISS	Internal standard saturator
IZA	International Zeolite Association
LaNaY-72	Code for zeolite Y catalyst (72% La exchanged)
LZY-52	Code for zeolite Y catalyst (Linde zeolite Y, sodium form)
LZY-62	Code for zeolite Y catalyst (Linde zeolite Y, 82% NH_4^+ exchanged)
LZY-82	Code for zeolite Y catalyst (Linde zeolite Y, 99% NH_4^+ exchanged)
m-DEB	meta-diethylbenzene
MFC	Mass flow controller
o-DEB	ortho-diethylbenzene
p-DEB	para-diethylbenzene
SBU	Secondary building unit
Si/Al	Silicon to Aluminium ratio (atomic)
SiO_2/Al_2O_3	Silica/alumina ratio (molar)
TPD	Temperature programmed desorption
UCT	University of Cape Town
WHSV	Weight hourly space velocity

1 INTRODUCTION

1.1 BACKGROUND

For research purposes, the disproportionation of ethylbenzene to benzene and diethylbenzene was first proposed as a model reaction by Karge et al., (1982), to compare the acidity of different zeolite catalysts and distinguish between medium and large pore zeolites. With large pore zeolites more meta isomer is produced whereas with medium pore zeolites, the para isomer is favoured due to the geometric configuration of the diethylbenzene isomers in relation to the zeolite channel geometry.

1.2 REACTIONS

With large pore zeolites such as zeolite Y and at low temperatures (ca. 180°C) the reaction occurs via a hydride transfer chain reaction through diphenylethanes as intermediates (Beck and Haag, 1997). The simplified reaction pathway is shown in Figure 1-1.

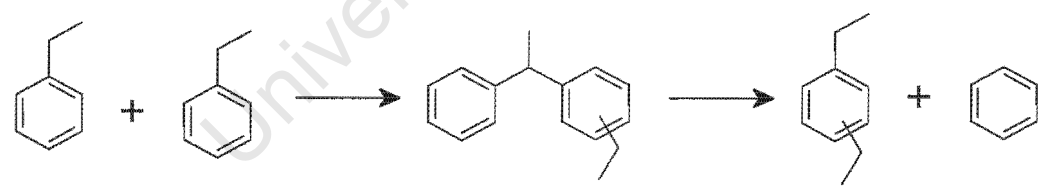

Figure 1-1 Proposed reaction pathway in large pore zeolites (Beck and Haag, 1997)

Medium pore zeolites, such as HZSM-5 and HZSM-11, cannot accommodate the bulky diphenylethane intermediates, and the reaction proceeds via a dealkylation-realkylation path and it requires higher temperatures (Santilli, 1986). The reaction mechanism as described by Beck and Haag. (1997) is shown in Figure 1-2.

Dealkylation:

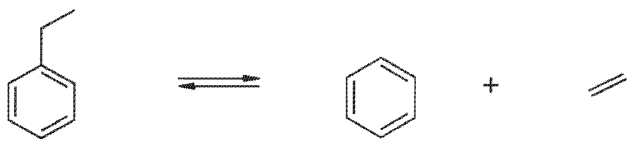

Realkylation:

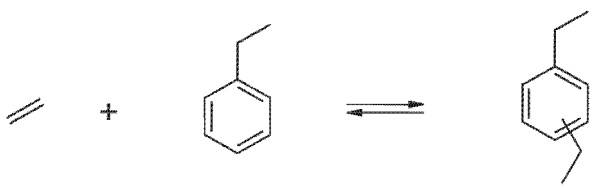

Figure 1-2 Proposed reaction mechanism in medium pore zeolites (Beck and Haag, 1997).

According to the mechanism, the expected ratio of diethylbenzenes to benzene is 1:1, provided no side reactions occur and the rate of dealkylation is equal to the rate of alkylation.

1.3 CHARACTERISATION OF ZEOLITES FOR PORE SIZE AND ACIDITY.

Acid catalysts are widely used in the petroleum industry for the production of fuels and petrochemicals. Since a great variety of reactions are involved, it is important to establish procedures to measure the catalytic properties of acids over a range of acidic characteristics. Catalyst manufacturers and users therefore have a need for simple, reliable methods for characterising this acidity and its catalytic properties (Moscou, 1991, van Hooff and Roelofsen, 1991).

Catalytic properties of zeolite-type materials depend on several factors including, the presence of active sites, the spatial arrangement and size of channels and cavities, and the presence of extraframework compounds within

the channels or on the outer part of the crystallites (Vedrine, 1992). Changing one or several of these factors may affect the catalytic properties and therefore the need to characterise such modifications so as to determine their effects on the catalytic properties of the zeolite (Moscou, 1991, van Hooff and Roelofsen, 1991).

Mostly, characterisation of the acid sites present on molecular sieves involves the chemisorption of basic molecules onto the molecular sieve followed by thermal desorption of the base. The typical method, temperature programmed desorption of ammonia, NH_3-TPD, does not distinguish between protonic (Brønsted) and electrophilic (Lewis) sites (Benesi et al., 1978). The information obtained, i.e. total number of acid sites and their distribution according to their acid strength cannot be linked directly to their catalytic properties. Infrared spectroscopy (IR) distinguishes between adsorption on Lewis or Brønsted acid sites, of bases, in particular pyridine, via the band at 1450 cm^{-1} corresponding to Lewis sites and 1540 cm^{-1} corresponding to Brønsted sites (Bourdillon et al., 1990).

Moreover, the two methods typically need to be employed in tandem. While NH_3-TPD provides reasonable quantitative information (number of sites), it provides no qualitative information (type of sites, Brønsted or Lewis). Pyridine-IR, on the other hand, provides good qualitative data but is notoriously poor for quantification. In addition, both methods are often performed at conditions far from those of the industrial reactions (e.g. under vacuum for IR studies) and with probe molecules (NH_3, pyridine, etc.) often quite dissimilar to the reactants of interest in terms of molecular size and basicity (Bourdillon et al., 1990).

The most commonly used methods to determine the pore size and geometry are the adsorption of specific molecules and detailed crystal X-ray diffraction. While both are perhaps insensitive to small modifications (e.g. resulting from dealumination), the latter is typically impractical since in all cases large crystals would be required (Rohrbaugh and Wu, 1989).

Often, a preferred method of characterising catalysts is subjecting them to a test reaction, which is considered to yield more reliable data because the catalyst may be studied under typical reaction conditions (van Hooff and Roelofsen 1991). Even so, such probe reactions must be chosen such that the probe molecule has easy access to the active sites and the production of reaction intermediates must not be inhibited. Reactions that produce water and alcohol might modify the catalyst (e.g. transformation of Lewis to Brønsted acid sites by water) and, hence, probe reactions to determine acidity should preferably involve exclusively hydrocarbon reactions (Bourdillon et al., 1990).

The disproportionation of ethylbenzene has been proposed to be a suitable probe reaction for characterising the Brønsted acidity and effective pore geometry of zeolites, (Karge et al., 1983, Rhodes et al., 1993 and Weiss et al., 1997).

1.4 RESEARCH OBJECTIVES

The conversion of ethylbenzene has been proposed by the International Zeolite Association (IZA) as an officially recognised standard test reaction for zeolite catalysts. It is intended that the probe reaction be used to characterise zeolites in terms of effective channel size and acidity (Weitkamp, 1994).

The main objective of this study is to evaluate the ethylbenzene disproportionation reaction as a reliable standard test reaction for acidic zeolites, and to consider the catalytic performance of certain typical acidic zeolite catalysts via comparison with the standard reference catalyst recommended.

1.4.1 KEY QUESTION

- Can ethylbenzene disproportionation be used as a standard test reaction to indicate effective zeolite channel size and to compare the acidity of a range of acid zeolite materials?

1.4.2 TASKS

- To benchmark the performance of the standard catalyst LaNaY-72 for the disproportionation of ethylbenzene. Also to investigate the effect of WHSV and that of the carrier gas.

- To compare the performance of various typical acid zeolites, viz. H-BEA, H-MFI, HNa-FAU and the reference catalyst, LaNa-Y for consistent interpretation in terms of acid strength and effective zeolite pore diameter.

- To provide the Catalysis Research Unit at UCT with a reliable test reaction for modified acid zeolites.

2 LITERATURE REVIEW

2.1 ZEOLITES

Zeolites are crystalline aluminosilicates with three-dimensional structures arising from a framework of $[SiO_4]^{4-}$ and $[AlO_4]^{5-}$ tetrahedra. These units are linked via the oxygen atoms to generate an open framework containing channels and cavities (Jansen, 1991). The chemical sources, which are needed in principle for zeolite synthesis, are given in Table 2-1.

Table 2-1 Chemical sources and their functions in zeolite synthesis (Jansen, 1991)

Source	Functions
SiO_2	Primary building unit of framework
AlO_2^-	Origin of framework charge
OH^-	Mineraliser, guest molecule
Alkali cation, template	Counterion of framework charge, guest molecule
H_2O	Solvent, guest molecule

The most important characteristics and major applications of zeolites are shown in Table 2-2. The table illustrates that not all the properties of zeolites are of the same importance for every application. For example, particle size and morphology are important in the application of zeolite A in detergents, while acidity and stability play a major role for the application of zeolite Y in cracking catalysts.

Table 2-2 Most important characteristics for three well-known zeolites and their major applications (van Hooff and Roelofsen, 1991); (+ relevant, ++ very important)

IMPORTANT CHARACTERISTIC	TYPE OF ZEOLITE		
	ZEOLITE A	ZEOLITE Y	ZSM-5
Structure, structural defects		+	++
Pore size	++	+	++
Chemical composition	++	++	++
Framework Si/Al ratio		++	+
Acidity		++	++
Stability		++	+
Morphology, particle size	++	+	++
IMPORTANT APPLICATION	ADSORBENT, ION EXCHANGE IN DETERGENTS	CRACKING CATALYST	SHAPE SELECTIVE CATALYST

2.1.1 ZEOLITE STRUCTURES

The "Atlas of Zeolite Structure Types" (Meier and Olson, 1996) categorises 98 topologically distinct tetrahedral TO_4 frameworks. In Figure 2-1, the T atoms lie at the centers of tetrahedra, with oxygen atoms at the corners. Aluminium, Al, and silicon, Si, atoms dominate T atoms.

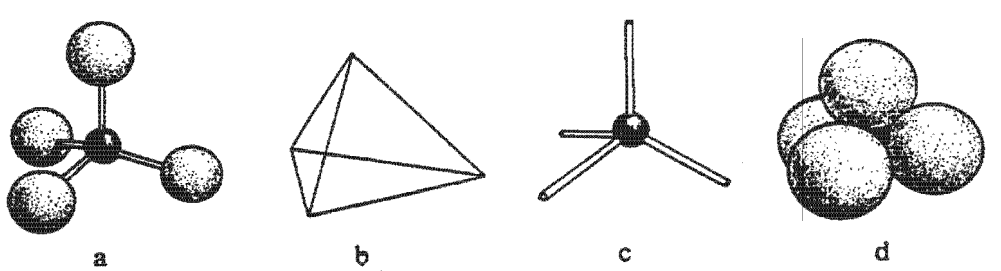

Figure 2-1 TO_4 tetrahedra representation (taken from Breck, 1974)

These tetrahedral or primary units can be linked in various ways to form secondary building units (SBUs) as per Figure 2-2. All zeolites can be reduced to combinations of such secondary building units.

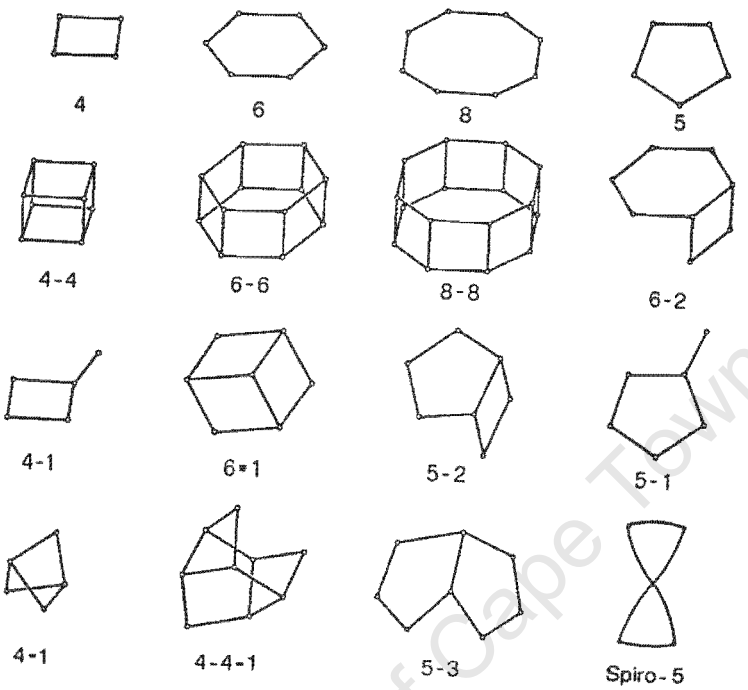

Figure 2-2 Secondary building units identifiable in zeolite frameworks (taken from Gilson, 1992)

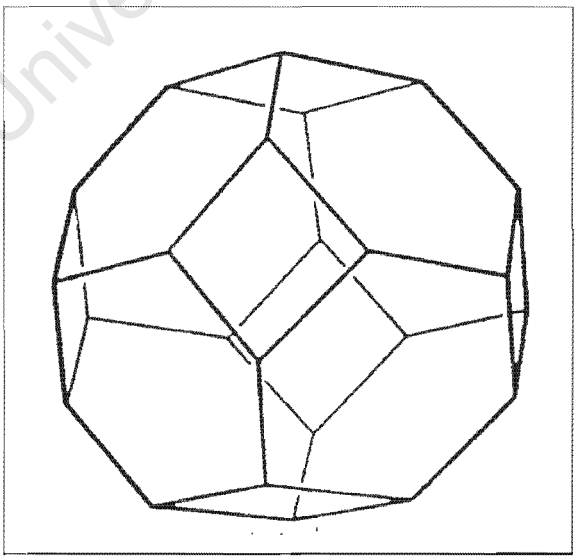

Figure 2-3 Sodalite unit (taken from van Koningsveld, 1991)

These SBUs may be interconnected in various topologies to give rise to a wide range of polyhedra (tertiary units). An example of such a tertiary unit is shown in Figure 2-3, the sodalite unit, which is found in Zeolite A and in faujasites (types X and Y) (van Koningsveld, 1991).

2.1.2 FRAMEWORK STRUCTURES OF FAU, BEA AND MFI

The framework structures of FAU, BEA and MFI are shown in Figure 2-4 (Meier and Olson, 1996).

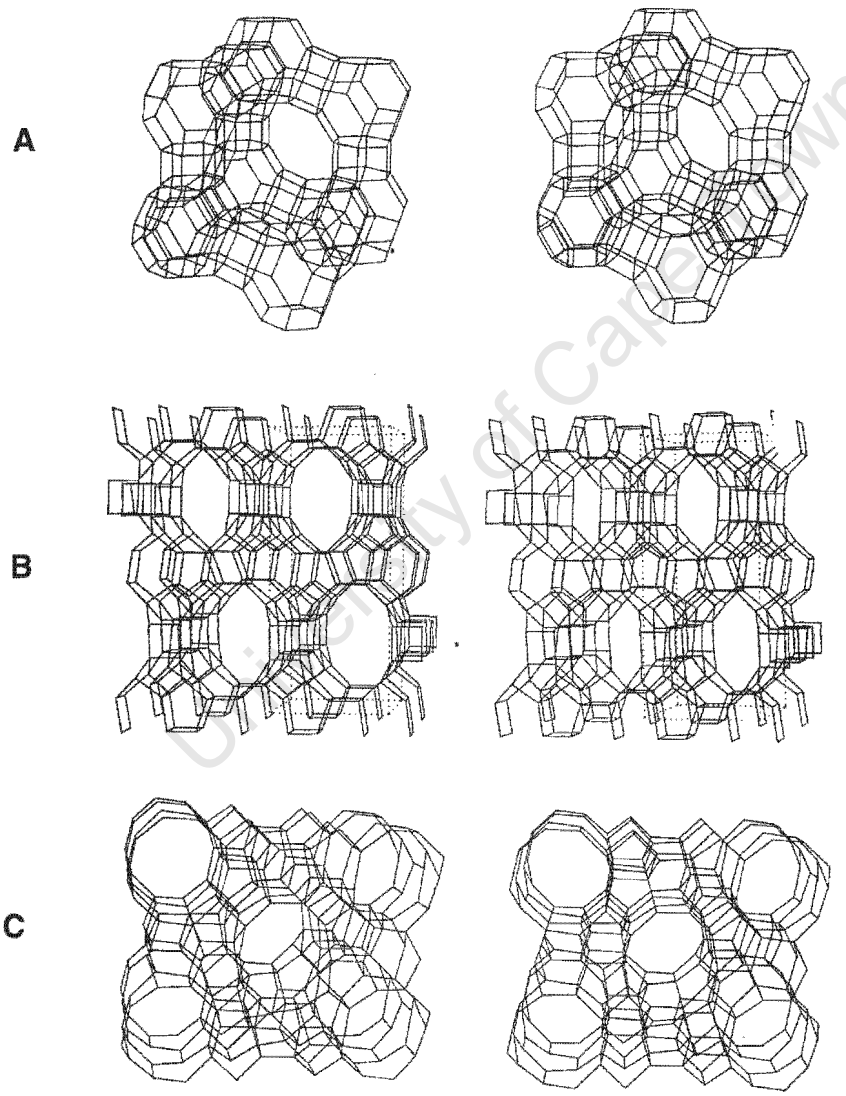

Figure 2-4 Stereoscopic representation of the framework structures of zeolites: A) Faujasite (FAU), B) Beta (BEA) and C) ZSM-5 (MFI); T-O-T links in these figures are represented as straight lines (Meier and Olson, 1996)

2.2 CHANNEL STRUCTURE: MICROPOROSITY

There are 98 different zeolite structures (Meier and Olson, 1996), which may be categorized into three broad classes on the basis of their channel (micropore) dimensions, namely, small, medium and large pore zeolites (Chen et al., 1996). A key factor of zeolites, important in many catalytic processes, is their microporous character with uniform pore dimensions (Moscou, 1991). This uniform pore dimension, of the order of a few Å in size (Table 2-3) is advantageous in catalysis in that it may impose shape selectivity in chemical transformations. Effective pore diameters depend on both the cation present in the zeolite as well as on the particular framework structure of the zeolite (Kärger and Ruthven, 1992).

Table 2-3 Pore structures of some zeolites (Meier and Olson, 1996)

Zeolite	Pore size (Å)	Si/Al	Channel system
8-membered rings			
A	4.1	1	3-D
Rho	3.6	6	3-D
10-membered rings			
ZSM-5	5.3 x 5.6	>5	3-D
	5.1 x 5.5		
ZSM-11	5.3 x 5.4	20 – 90	3-D
12-membered rings			
Beta	5.5 x 5.5	5 – 100	1-D
	6.4 x 7.6		2-D
Faujasites (Y)	7.4	3 – 6	3-D

2.2.1 LARGE PORE ZEOLITES

Channel openings bounded by 12-membered oxygen rings yield zeolites with micropore sizes typically in range 6 – 8 Å. A well known example of such a zeolite is faujasite (FAU) (Figure 2-4 A), such as zeolites X and Y and used as cracking catalyst (Kärger and Ruthven, 1992) .

2.2.1.1 Zeolite Y

The primary structural unit in zeolite Y (FAU) is the so-called sodalite cage, which is a truncated octahedron containing 24 silicon (or aluminium) tetrahedra. It is composed of six four-membered rings and eight six-membered rings, Figure 2-3. The three dimensional, open, porous structure of zeolite Y is derived by joining the sodalite cages in a tetrahedral arrangement through hexagonal prisms, with such prism being joined via a six-ring face of a sodalite cage, Figure 2-5.

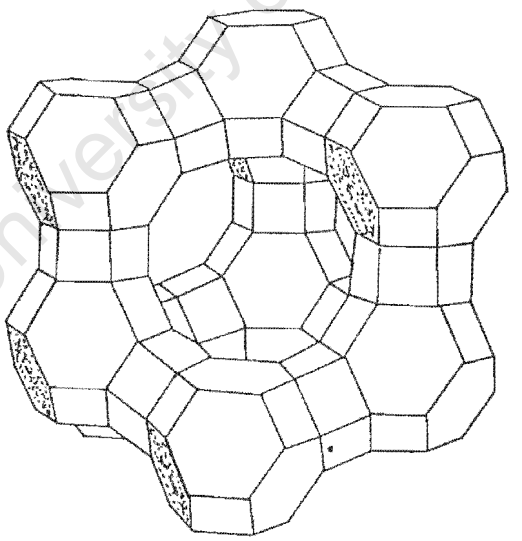

Figure 2-5 Schematic representation of the zeolite Y (Faujasite) structure (Kärger and Ruthven, 1992).

The joining of the sodalite cages in this manner produces the characteristic supercage, which is the major cavity in the zeolite Y structure. The free diameter of the supercage is approximately 13 Å (Leach, 1971), and the diameter of the pore opening is 7.4 Å. The composition of the Y type material has the general formula shown below (Meier and Olson, 1996).

$$Na_{58}[Al_{58}Si_{134}O_{384}] \cdot 240H_2O$$

2.2.1.2 Zeolite Beta

Zeolite Beta (BEA) is a high silica, crystalline aluminosilicate. The unit cell formula of the sodium form of zeolite Beta is shown below (Meier and Olson, 1996).

$$Na_n[Al_nSi_{64-n}O_{128}] \text{ where } n < 7$$

The pore structure of zeolite Beta consists of channels of 12-membered rings as well as channels of 10-membered rings interconnected by cages constituted by the intersections of the channels. The secondary building units that form the tertiary structure include both 4-rings and 5-rings, Figure 2-2. The channels formed by the 12-membered rings have a diameter of 6.4 x 7.6 Å whereas the channels formed by the 10-membered rings have a diameter of 5.5 x 5.5 Å, Figure 2-4 B.

2.2.2 MEDIUM PORE ZEOLITES

Zeolites containing channels bounded by 10-membered oxygen rings exhibit pore sizes typically in the range 4 – 6 Å. Included in this category are several catalytically important zeolites, in particular the widely used ZSM-5 (Chen et al., 1996).

2.2.2.1 Zeolite ZSM-5

Zeolite ZSM-5 (MFI) consists of 10-membered rings (5-1 secondary building units, Figure 2-2). These units link up to form the three dimensional pore structure with 10-membered ring openings. The framework contains two intersecting elliptical channel systems, one sinusoidal (diameter 5.1 x 5.5 Å) and the other straight and parallel (diameter 5.3 x 5.6 Å). The parallel pore system is easily seen in Figure 2-4 C. The overall channel system, shown schematically in Figure 2-6, is said to give rise to the shape selective properties of ZSM-5.

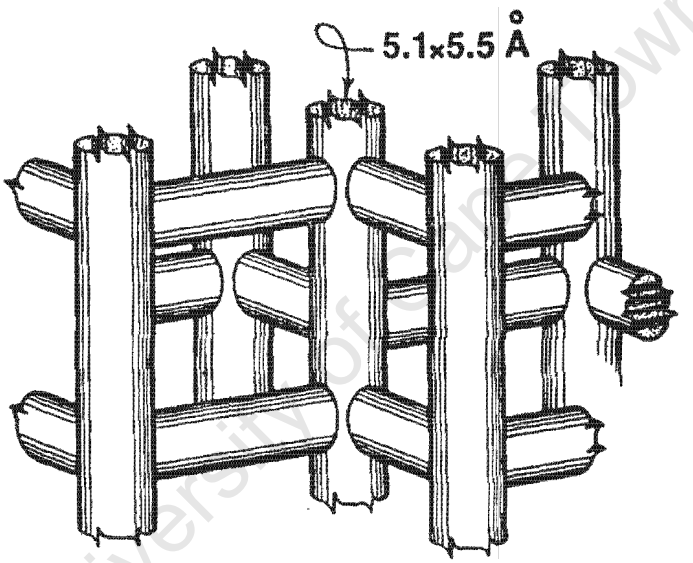

Figure 2-6 The channel structure of ZSM-5 (Chen et al., 1989)

The unit cell formula of the sodium form of zeolite ZSM-5 is shown below (Meier and Olson, 1996).

$$Na_n [Al_nSi_{96-n}O_{192}] \sim 16H_2O \text{ where } n \leq 27$$

2.2.3 SMALL PORE ZEOLITES

Small pore zeolites are those for which the channel openings are formed by six- to eight-membered oxygen rings, resulting in free pore diameters in the range of 3 – 5 Å. Examples of eight-membered ring zeolites are given in Table 2-3. Under normal conditions only very small molecules, e.g. water and carbon monoxide, can penetrate these zeolites. These materials are not normally used as catalysts but they can be used for drying of feed streams, as they would selectively adsorb water from hydrocarbon streams (Chen et al., 1996).

2.3 ACIDITY OF ZEOLITES

The isomorphic substitution of silicon T-atoms in the zeolite framework by aluminium results in a net negative framework charge for each aluminium in tetrahedral co-ordination. Charge balancing cations, typically alkaline or other positively charged ions are accommodated in the zeolite structure to balance this framework charge deficit. If the charge balancing species are either proton donating or electron accepting species, acidic properties are thus introduced into the zeolite (Dwyer, 1992).

2.3.1 BRØNSTED ACIDITY

Zeolites are usually prepared in the sodium form (i.e. Na^+ as charge balancing cation). If the sodium ions are exchanged with ammonium cations and the solid then heated to drive off ammonia one is left with a protonated solid (Figure 2-7), which behaves as a solid Brønsted-type acid (Uytterhoeven et al., 1968). Zeolites, which instead of metal or alkali metal ions have H^+ ions as charge balancing species, are the most active for acid catalyzed reactions.

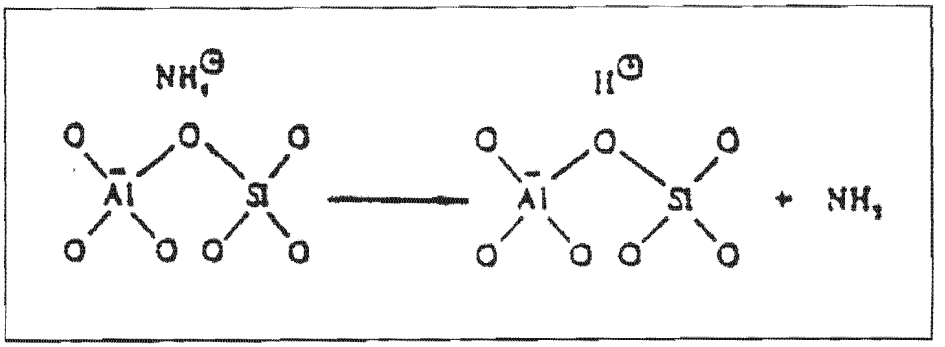

Figure 2-7 Formation of Brønsted acidity on zeolites (Uytterhoeven et al., 1968)

2.3.2 LEWIS ACIDITY

Calcination at higher temperatures (well above 500°C) results in conversion of the Brønsted acids to Lewis acids via pairwise dehydration of adjacent Brønsted acid hydroxyl groups (Dwyer, 1992). The source of Lewis acidity in decationated zeolites (H-forms) may be assigned, on the basis of infrared spectra, to the generation of trico-ordinated (≡Al and ≡Si^+) sites within the zeolite framework as shown in Figure 2-8 (Dwyer, 1992). The trico-ordinated Al* in Figure 2-8(i) acts as a weak acid.

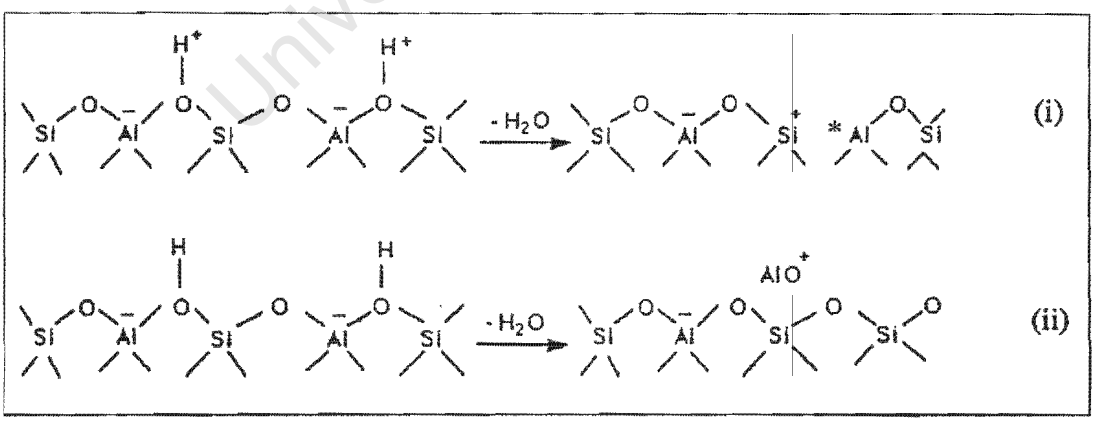

Figure 2-8 The formation of Lewis acidity from Brønsted acidity. (i) Lewis acid site, (ii) 'true' Lewis acid site (taken from Dwyer, 1992)

Lewis acid sites may be unstable, particularly in the continued presence of water, because this leads to the formation of non-framework sites resulting from the ejection of Al species from the framework as depicted in Figure 2-8(ii) and resulting in so-called extra-framework aluminium (EFAL) species. The EFAL Lewis sites are postulated to be $(AlO)^+$ species which are strong acid sites whereas the Al* species are thought to act as weak acid sites (Dwyer, 1992).

There is general agreement that bridging hydroxyl groups, linking a silicon with an aluminium atom in the framework of zeolites, are responsible for the Brønsted acidity and the catalytic activity. However, some favour a bifunctional active site (Martens et al., 1992), comprising a Brønsted acid (hydroxyl on the silicon) and one or more Lewis bases (oxo ligands of the aluminium) (Figure 2-9a), which interact and form a bridging hydroxyl, as shown schematically in Figure 2.9b.

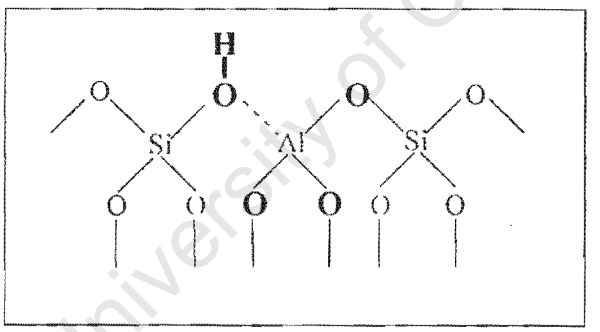

(a)

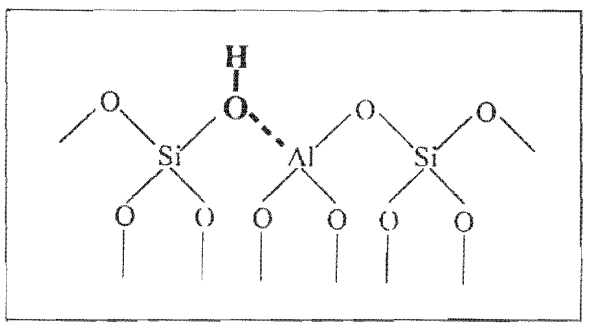

(b)

Figure 2-9 Active sites in aluminosilicate zeolites, (a) hydroxyl group and oxo ligands of aluminium acting as bifunctional Brønsted acid-Lewis base site, (b) bridging hydroxyl group responsible for Brønsted acidity (adapted from Martens et al., 1992).

The interaction of the oxygen atom of the hydroxyl group with the aluminium leads to the weakening of the hydrogen-oxygen bond. This results in an increase in acidity and enhances the basicity of the oxo ligands of aluminium (Martens et al., 1992).

2.3.3 ACTIVATION OF ZEOLITES

2.3.3.1 Exchange for polyvalent metal ions

At least two steps are required for activation of the acidic catalytic properties (Hickson and Csicsery, 1968). Firstly, the monovalent metal cations present (e.g. sodium ions from synthesis) must be exchanged for polyvalent metal ions (such as La^{3+}), which can be done by solid-state ion exchange or in solution. Secondly, the ionically exchanged zeolite must be heated in order to develop the acidic catalytic properties. This process is called activation. It is required to remove physically adsorbed water from the zeolite and thus open up the structure to hydrocarbon reactants.

Total acidity and acid strength of acidic protons generated by activation is dependent on: the extent of ion-exchange, the nature of the cation (its size and charge), the temperature of activation and the Si/Al ratio (Hickson and Csicsery, 1968).

2.3.3.2 H-form zeolites

An active H-zeolite catalyst may be prepared from the sodium form in one step through repeated ion exchange with diluted mineral acid. An active zeolite may also be prepared in two steps through repeated ion exchange in ammonium solution and subsequent heating up in order to drive off ammonia and thus transform the zeolite to the protonated, acid form (Uytterhoeven et al., 1968).

2.3.4 LaNaY-72

An active LaNaY-72 catalyst may be prepared through solid-state ion exchange between $LaCl_3$ and the sodium form of a faujasite-type zeolite followed by brief washing with water at room temperature. The contact with water is essential to generate, after solid-state ion exchange, acidic Brønsted centres. According to the Hirschler-Plank mechanism water molecules are split into H^+ and OH^- groups upon interaction with the bare La^{3+} cations introduced by solid-state exchange. The protons form bridging hydroxyls by interaction with the framework and the OH-groups are attached to the La^{3+} cations giving rise to acidic $La(OH)^{2+}$ or $La(OH)_2^+$ species (Karge, 1992).

2.4 MODIFICATION OF ACIDITY

2.4.1 DEALUMINATION

It is a well-established fact that aluminium can be removed from the zeolite by various methods in a process referred to as dealumination (Barrer, 1988). Since the intrinsic source of acidity in zeolites results from the isomorphous framework substitution of silicon by aluminium, the extent of Al substitution and subsequent removal of Al from the zeolite framework will strongly influence both the extent of zeolite acidity and the nature thereof. The most common processes for dealumination are leaching with mineral acids and hydrothermal treatment. In the former procedure mineral acid removes framework aluminium and typically solubilizes the extracted Al-species such that little, if any, EFAL species are left in the zeolite channel system after subsequent washing.

Hydrothermal treatment of zeolites also results in the removal of aluminium from the framework. However, unlike in the case of acid washing, extra-framework aluminium species often remain within the pores. Severe steaming usually results in decreased activity whereas mild steaming often increases activity (Lago et al., 1986).

Similarly, despite the overall loss of framework Brønsted acid sites, Anderson (1991) reported increased hexene oligomerisation activity after mild hydrothermal treatments of ZSM-5. The reason for increased activity, despite fewer framework Brønsted sites, is thought to be due to the formation of strong/superacid sites (as outlined e.g. in Figure 2-8(ii)).

2.4.2 ION-EXCHANGE

Zeolites are often synthesized in the sodium form and, hence, non-acidic form. These may be ion exchanged in ammonium solution and then deammoniated by heating in order to transform the NH_4^+ form to the acidic, proton form. The degree of cation exchange depends on the exchange cations' equilibrium concentrations in solution and on the solid. Solution concentration and temperature permits control of the degree of exchange. Consequently, zeolites exchanged with metal cations (e.g. LaNaY-72) or with metal cations and protons (e.g. NaH-Y), each with acidity varying with degree of exchange, can readily be produced.

2.4.3 MEASUREMENT OF ACIDITY

Temperature programmed desorption of ammonia is commonly used to determine the number and strength of the acid sites. In this technique, a sample of zeolite is saturated with NH_3, which chemisorbs to the acid sites. Excess NH_3 (physisorbed species) are removed by extensive flushing with inert gas or by evacuation, after which the sample temperature is linearly increased in a flowing stream of inert gas. Analysis of the effluent stream permits the determination of the moles of desorbed NH_3 as a function of temperature (Szostak, 1989).

The quantity and strength of acid sites on the sample is obtained from the TPD traces. Integrating the area under the trace, with calibration, will yield the quantity of acid sites, assuming a one-to-one relationship between NH_3 and acid sites. Information on the strength of the acid sites is obtained by observing the peak temperature at which the ammonia desorbs. High

desorption temperatures correspond to strong acid sites while low temperatures correspond to weaker acid sites. Therefore, the peak-maximum-temperature (T_m) provides information about the acid strength (Szostak, 1989).

Although NH_3-TPD is a simple and rapid method to characterise zeolite acidity, it has its limitations:

- It is not possible to distinguish between ammonia desorbing from Brønsted or Lewis acidic sites and even desorption from non-acidic sites is recorded (Bourdillon et al., 1990).
- Particularly in the case of zeolites, however, the possibility of diffusional constraints during the desorption of ammonia as well as readsorption in the pores and cavities of the zeolite, may yield peak-maximum-temperatures significantly higher than those corresponding to the true, unconstrained desorption temperatures (van Hooff et al., 1991). Consequently, experimentally determined T_m values should be compared with due caution, especially when comparing values for different zeolites and Si/Al ratios.

2.5 SHAPE SELECTIVITY IN ZEOLITES

The micropores or channels in zeolites are uniform in size and are of the same dimensions as many industrially relevant organic molecules (Tables 2-3 and 2-4). Consequently, the size and shape of the channels may influence the shape or structure of molecular interactions that occur within these spaces. This influence of the channel structure on the geometry of the permissible reactants, products and reaction intermediates is referred to as shape selectivity (Weisz et al, 1962).

Shape-selective effects may occur whenever the pore size of a microporous catalyst is in the same range as the diameter of the molecules or transition states involved in the reacting system. Shape-selective effects are routinely

classified into three categories namely "reactant-", "product-" and "transition state-" selectivity (Weisz et al, 1962), as illustrated in Figure 2-10.

Reactant selectivity occurs when only those reactants physically capable of entering the pore structure are converted while reactants too large to enter are not converted. Product selectivity refers to situations where only certain of several possible products are capable of diffusing out of the zeolite, while those with a rather bulky structure do not emerge from the zeolite prior to interconversion to other species capable of egress. Transition state selectivity arises when certain reactions for which the intermediate formation of a bulky transition state is required are suppressed due to size limitations imposed by the size of the channels.

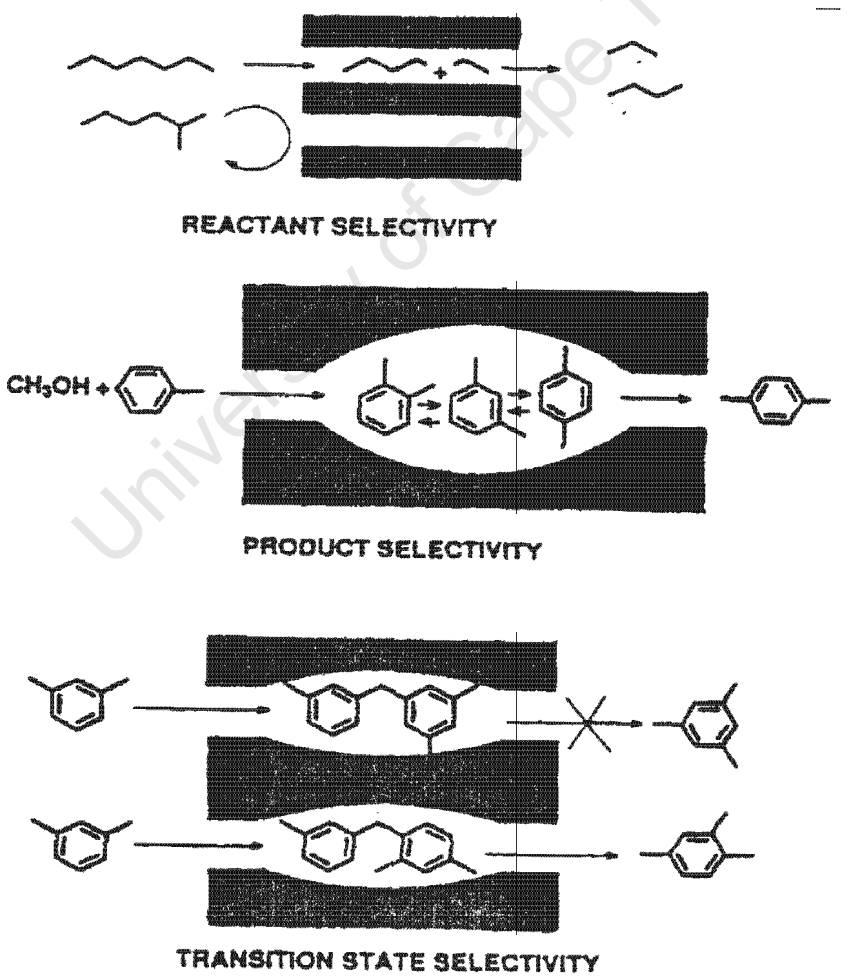

Figure 2-10 Classification of shape-selectivity effects according to Weisz and Csicsery (Taken from Emig and Dittmeyer, 1997)

In general, reactant and product selectivities are mass transfer effects, arising from the relative rates of diffusion of the various molecular species involved in a reaction, and not merely a result of whether reactants or products fit into the channel system of the zeolite (Emig and Dittmeyer, 1997). Given the molecular dimensions of the species involved in the disproportionation reaction (Table 2-4) and the channel dimensions of zeolite catalysts (Table 2-3) shape selective effects may be of significance.

Shape selective effects are of great importance for the product distribution in many zeolite-catalyzed reactions. As an example, consider HZSM-5, a medium pore MFI zeolite which, when used for disproportionation of ethylbenzene, results in the formation of the linear para-ethylbenzene isomer in yields far exceeding those expected from thermodynamic predictions (Klemm et al., 1997). Other well-known industrial reactions for which the shape selective effects of zeolite catalysts are essential include toluene-disproportionation, xylene-isomerisation and the production of several other para-dialkylated aromatics.

As the channel dimensions of crystalline aluminosilicates are comparable to those of reactant ethylbenzene, and product diethylbenzenes and benzene (Tables 2-3 and 2-4), micropore diffusional resistance cannot be avoided. Therefore, the kinetic parameters computed will include the diffusional effects.

Table 2-4 Estimated kinetic diameters of compounds

Compound	Kinetic Diameter (Å)
Ethylbenzene	5.85
Benzene	5.85
para-Diethylbenzene	5.85
meta-Diethylbenzene	6.46
ortho-Diethylbenzene	6.46

2.6 ACID CATALYZED TRANSALKYLATION OF AROMATICS

Zeolite catalysts, which are effective for alkylation and transalkylation reactions, contain strong protonic acid centres. Work done by Philippou and Anderson (1997) provides spectroscopic evidence as to the reaction mechanisms operating during the catalytic ethylbenzene disproportionation.

Over acid zeolites, the reaction is found to commence with the formation of diethylbenzenes retaining the radioactive label at the α-position of the side chain. This observation strongly suggests that disproportionation proceeds via the intermediacy of diphenylethane structures (Figure 2-11).

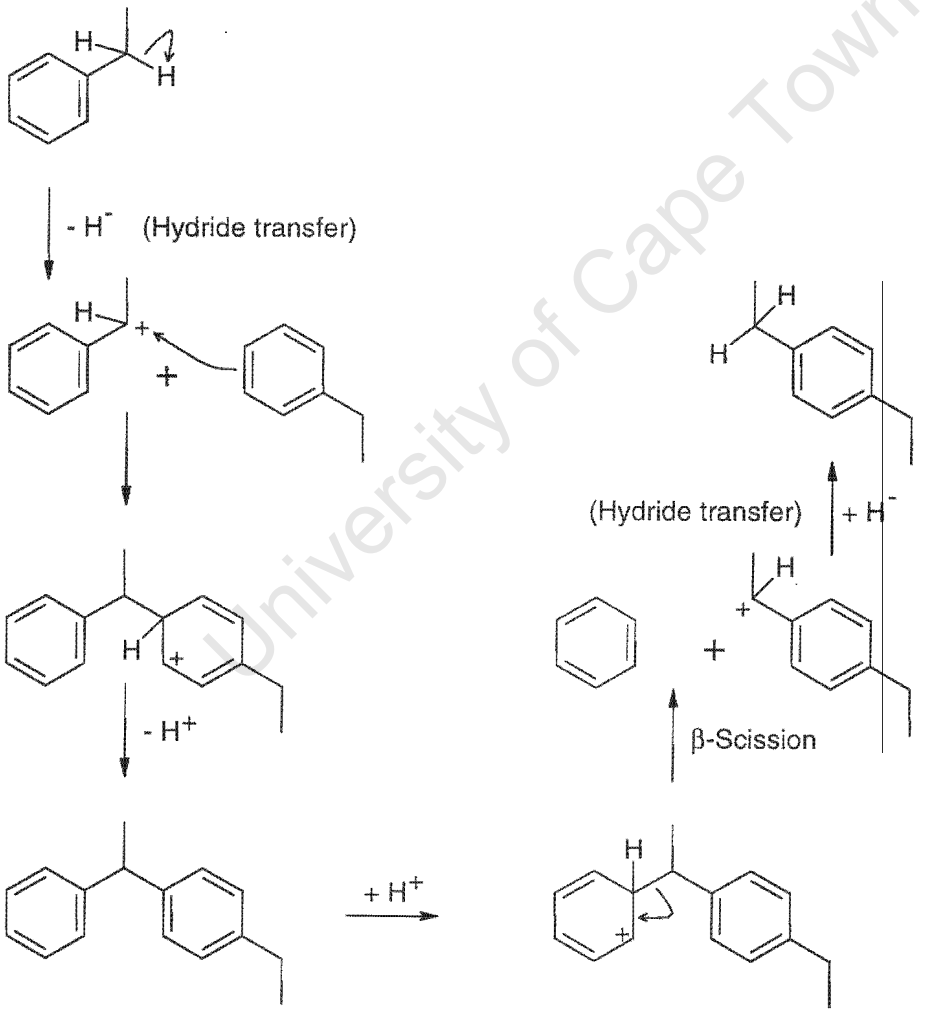

Figure 2-11 Reaction scheme occuring via a hydride transfer chain reaction through diphenylethanes as intermediates (Philippou and Anderson, 1997)

In Figure 2-11, hydride abstraction activates the aromatic on the α-carbon of the side chain. The activated aromatic then adds to another aromatic to form the diphenylethane reaction intermediate. A proton is removed from the ring and the aromatic system is restored. In a second step, a proton is added to the other ring (which might be a simultaneous step, involving the very same proton), followed by a β-scission to produce the reaction products. The reaction sequence is terminated by hydride addition.

However, externally imposed steric constraints can force this reaction to proceed by an otherwise higher-energy route. This involves formation of carbenium ion by protonation of the aromatic system (Figure 2-12) followed by β-scission to release the aromatic and the carbenium ion $CH_3CH_2^+$ that is thereby alkylated to another feed molecule. Proton abstraction terminates the reaction sequence.

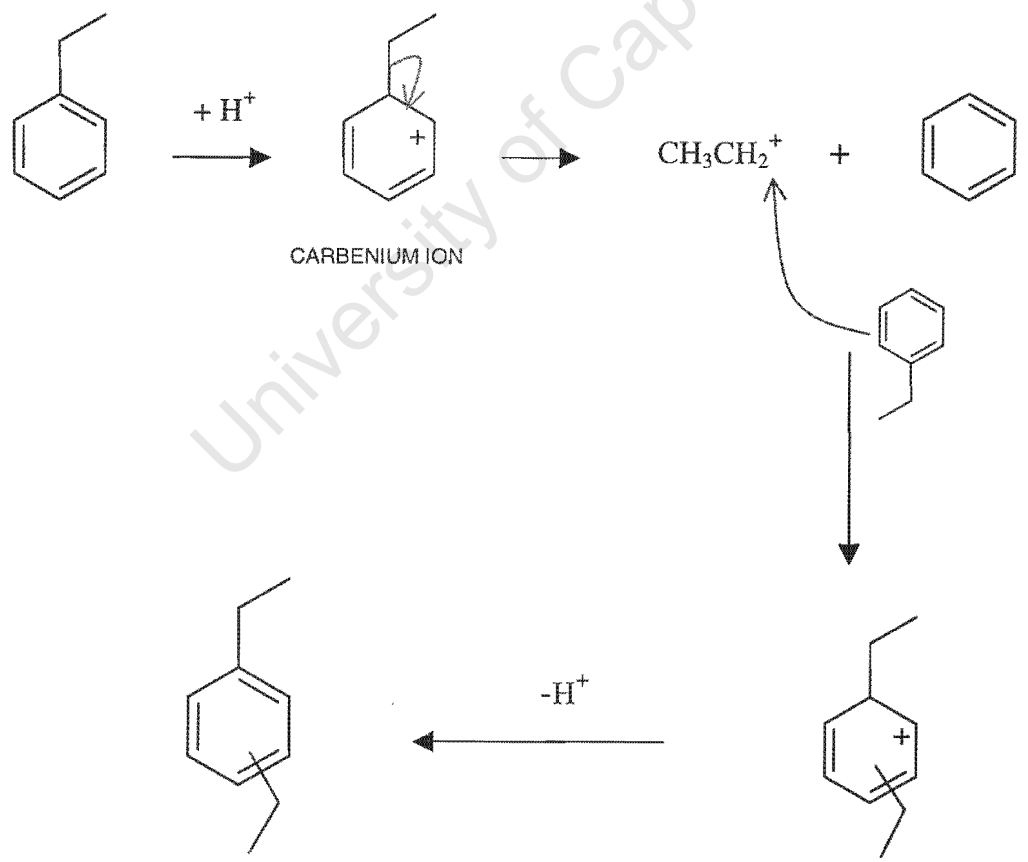

Figure 2-12 Stepwise mechanism proceeding via a dealkylation-realkylation path (Santilli and Gates, 1997)

As depicted in Figure 2-11, with large pore zeolite catalysts such as zeolite Y, the reaction occurs via a hydride transfer chain reaction through diphenylethanes as intermediates (Philippou and Anderson, 1997). In medium pore zeolites such as HZSM-5, the bimolecular aromatic step shown in Figure 2-11 does not occur because the formation of the diphenylethane intermediate is sterically hindered in the narrow channels (a form of transition state-selectivity). Rather, the stepwise mechanism shown in Figure 2-12, which proceeds via a dealkylation-realkylation path prevails, even though this would be a higher-energy reaction (Santilli and Gates, 1997). Consequently, the product distribution observed with medium pore zeolites such as HZSM-5 differs considerably from that observed with large pore zeolites. In general, the disproportionation reaction is influenced by transition state shape selectivity in zeolites.

2.7 EXPERIMENTAL FINDINGS ON ETHYLBENZENE DISPROPORTIONATION

Karge et al. (1982) undertook pioneering work in the late 70s on ethylbenzene disproportionation as a test reaction. Thereafter, extensive studies were conducted in different research laboratories (Kaeding et al., 1981; Weitkamp et al., 1986; Neuber et al., 1988; Rhodes and Rudham, 1993; Karge et al., 1994; Weiss et al., 1997 etc.).

Studies on large pore zeolite Y showed that early in the experiment there is an induction period during which the conversion increases. After several hours, a maximum conversion is passed and a (quasi-) stationary stage is reached as per Figure 2-13, which illustrates the time-on-stream behaviour at different space velocities (Weiss et al., 1997). Space velocity, of course, influences conversion but has little effect on the length of the induction period under the conditions pertaining to Figure 2-13. In the case of the latter, a slight increase in induction period with decreasing space velocity might result from the concomitantly lower average reactant concentration. Moreover, the subtle changes in induction period with changing space velocity as illustrated in

Figure 2-13 is not generally observed and, indeed, large effects have been reported, e.g. in the case of zeolite Beta as per Figure 2-18, and for several other acidic zeolites (Weitkamp et al., 1986; Karge et al., 1994).

The activation temperature has influence on both conversion and the induction period (Figure 2-14). Increased activation temperature decreases the activity of the LaNaY-zeolite and, concurrently, shifts the maximum conversion towards longer time-on-stream.

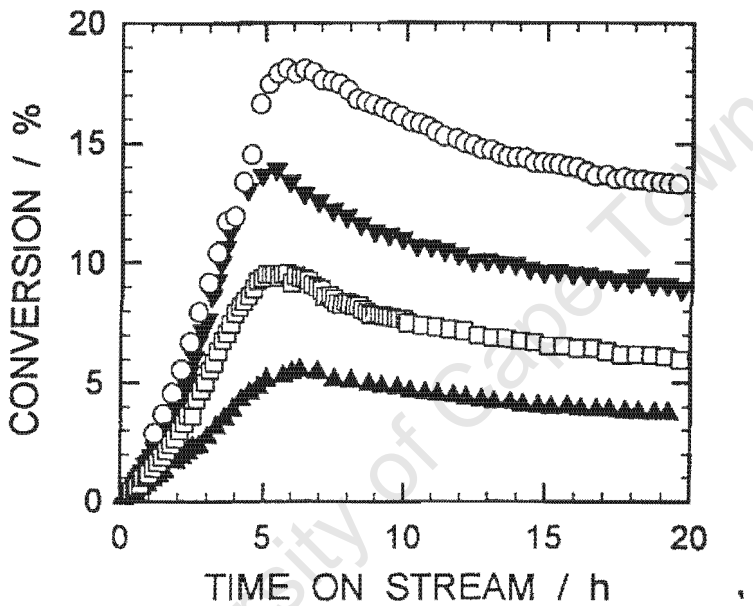

Figure 2-13 Influence of space velocity at constant feed rate on the conversion of ethylbenzene over LaNaY-72 at 180°C (▲ W = 73 mg; □ W = 145 mg; ▼ W = 290 mg; O W = 580 mg) (Taken from Weiss et al., 1997)

Weiss et al. (1997), showed that the duration of the induction period strongly depends on the density of acid sites as effected by both of the activation temperature (Figure 2-14) and the degree of lanthanum exchange (Figure 2-15). They further showed that the length of the induction period also depends strongly on the reaction temperature (Figure 2-16). In the case of the latter, note from Figure 2-13 that space velocity (F_{EB}/W) has negligible effect on the induction period at 180 °C and, hence, that the variation in induction period shown in Figure 2-16 results overwhelmingly from the influence of reaction temperature.

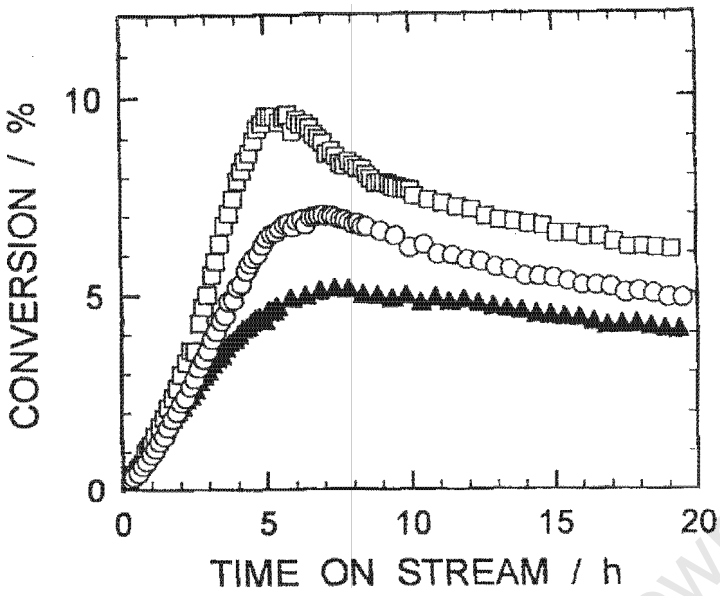

Figure 2-14 Influence of space velocity at constant feed rate on the conversion of ethylbenzene over LaNaY-72 at 180°C (▲ $T_{act.}$ = 350°C; ○ $T_{act.}$ = 300°C; □ $T_{act.}$ = 250°C) (Taken from Weiss et al., 1997)

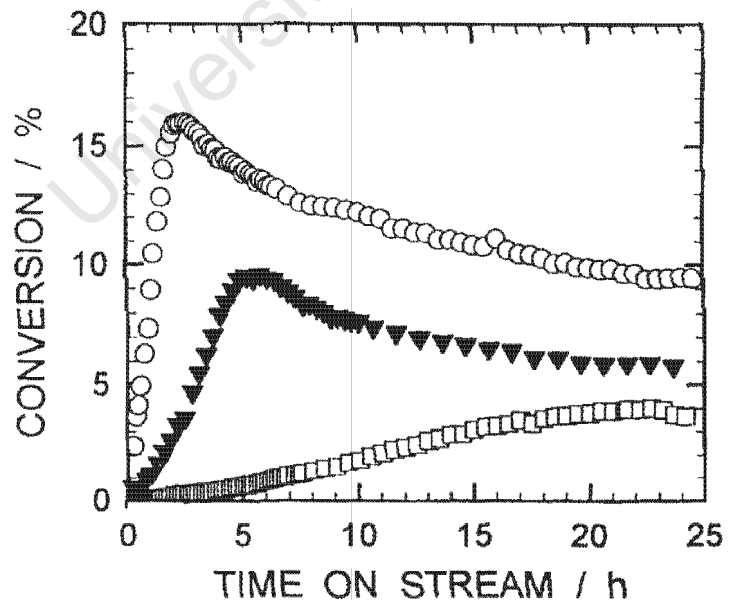

Figure 2-15 Conversion of ethylbenzene at 180°C over lanthanum exchanged faujasites of different extent of lanthanum exchange (□ LaNaY-63; ▼ LaNaY-72; ○ LaNaY-92) (Taken from Weiss et al., 1997)

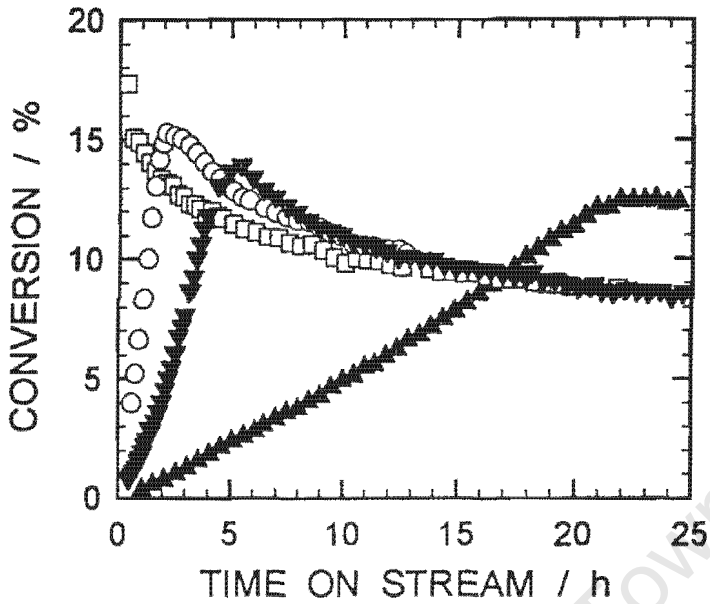

Figure 2-16 Influence of reaction temperature on the conversion of ethylbenzene over LaNaY-72 (▲ 160°C; ▼ 180°C; O 200°C; □ 220°C. W/F_{EB} = 580, 290, 290 and 145 g.h/mol, respectively) (Taken from Weiss et al., 1997)

It can be seen as per Figure 2-16 that at 160°C, the induction period extends over more than 20 hours whereas it is completed within less than one hour at 220°C.

Interesting as well, are the changes in isomer distribution during the induction period, Figure 2-17. On the basis of the Streitwieser-Reif mechanism (Streitwieser and Reif, 1960) and the rule of electrophilic substitution in aromatics, one would expect 1,4-DEB as the primary product and the selectivity thereof to be higher than that of the other isomers. Consecutive isomerization steps could account for the occurrence of 1,3-DEB and 1,2-DEB. Indeed, the isomer distribution very roughly approaches an equilibrium distribution (Figure 2-20), but for a significantly depressed 1,2-DEB component. A 1,2-DEB level significantly lower than the equilibrium level is a common observation across a wide variety of acid zeolites. However, the relative levels of 1,3- and 1,4-DEB varies significantly as a function of zeolite type (Weitkamp et al., 1986; Karge et al., 1994).

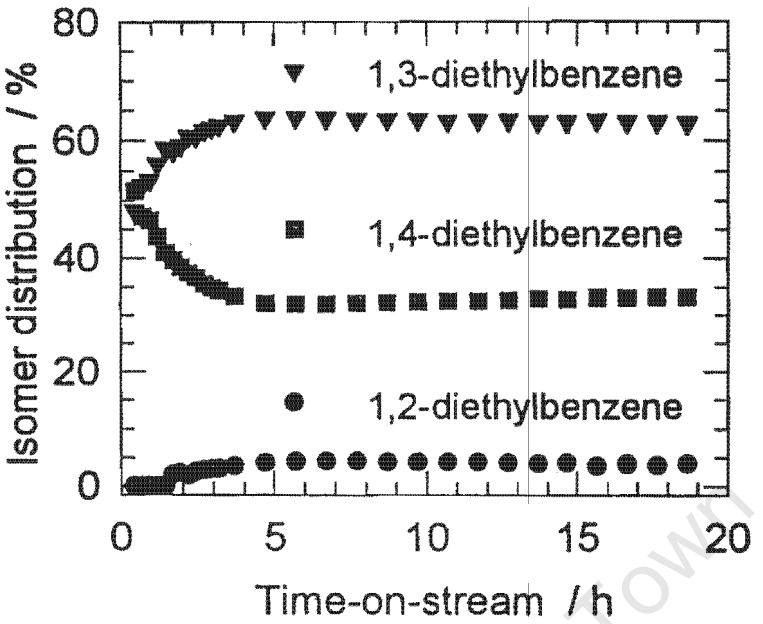

Figure 2-17 Isomer distribution of diethylbenzenes from ethylbenzene conversion over LaNaY-72 as a function of time-on-stream at 180 °C (Taken from Karge et al., 1994)

Karge et al. (1994) and Weiss et al. (1997) concluded, therefore, that the induction period itself is directly connected with the number and/or strength of the Brønsted acid sites. It was also proposed that polyalkylated diphenylethanes might be species that build up during the induction period (section 2.7.1).

Two samples of H-Beta zeolite which differed in their aluminium content and, hence, the density of acid sites, were used as catalysts by Karge et al. (1994), (Figure 2-18). From the figure it can be seen that the general time-on-stream behaviour of the large pore H-Beta is similar to that for LaNaY-72. The catalyst with higher density of acid sites was found to be more active as expected.

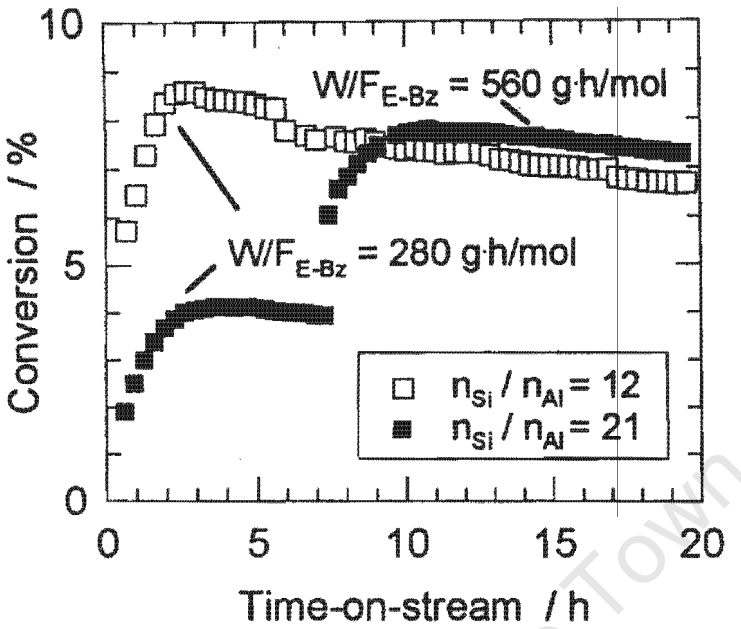

Figure 2-18 Conversion of ethylbenzene over H-Beta zeolites (Taken from Karge et al., 1994)

In summary, ethylbenzene disproportionation over large pore zeolites is characterised by an induction period indicative of a reaction mechanism involving diphenylethane-type-intermediates. By contrast, over medium pore zeolites, the reaction occurs without an induction period presumably because the reaction proceeds via a dealkylation-realkylation mechanism.

2.7.1 MECHANISTIC MODELS FOR THE INDUCTION PERIOD

Correlation of the length of the induction period with the catalyst activity during ethylbenzene disproportionation suggests that the catalytically active species, presumably higher alkylated aromatics (Figure 2-19), are progressively built up in transalkylation reactions according to a mechanism which was developed from that of Streitwieser and Reif (1960). Such species are most easily formed on catalysts with a large number of strong Brønsted acid sites and at elevated reaction temperature, resulting in a shorter induction period.

The number of Brønsted sites with a sufficiently high acid strength for the formation of such species seems to be reflected by both the ethylbenzene disproportionation reaction rate during the stationary stage and the deficit of diethylbenzenes during the induction period (Weiss et al., 1997). Consequently, Weiss et al. (1997) postulated that the polyalkylated diphenylethanes are species, which build up, during the induction period.

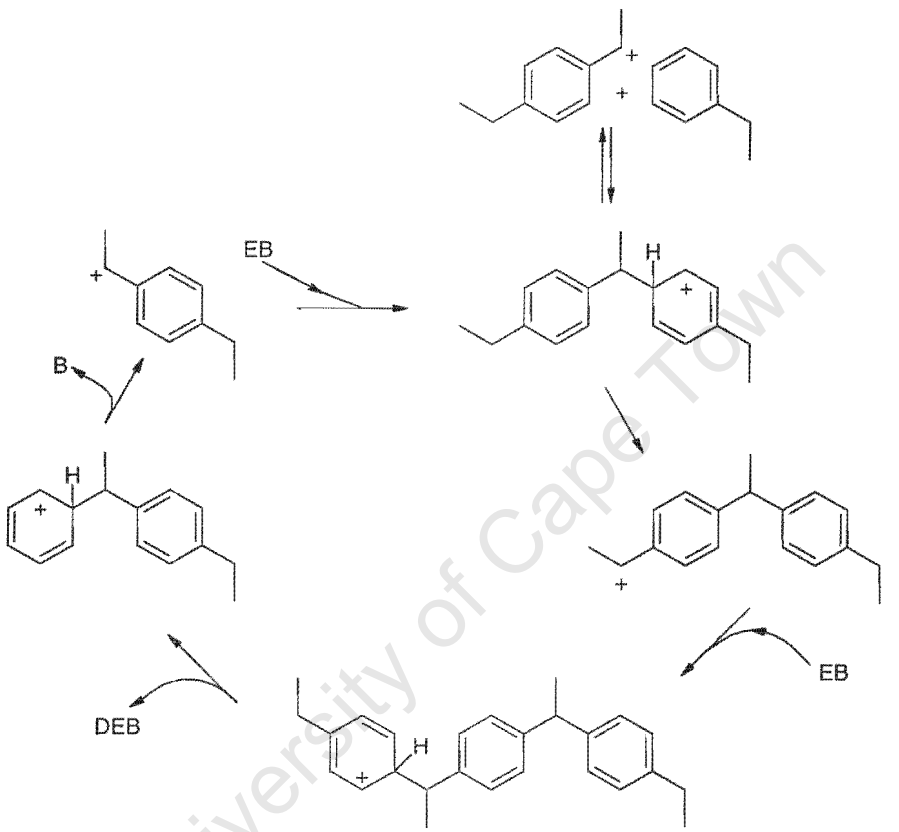

Figure 2-19 Catalytic cycle for ethylbenzene disproportionation over large pore zeolites developed from the mechanism of Streitwieser and Reif (1960) (Taken from Weiss et al., 1997)

2.7.2 PRODUCT INHIBITION

Arsenova et al. (1995) have studied the kinetics of ethylbenzene disproportionation over HY zeolite. Kinetic studies showed that the reaction is complex but can be described by a Langmuir-type rate law if one takes into consideration an inhibiting effect of diethylbenzenes produced. The inhibitory effect of diethylbenzene was confirmed by admixing this product to the feed stream.

2.8 EQUILIBRIUM CONSIDERATIONS

The thermodynamic equilibrium composition of the gaseous products of ethylbenzene disproportionation at various temperatures and one atmosphere have been calculated from the ΔG_f^o data values taken from Stull et al. (1969). The reaction is slightly endothermic and higher temperatures therefore favour conversion. The equilibrium conversion between 150 and 300°C is about 50%, almost invariant with temperature. Figure 2-20 shows the isomer distribution for the disproportionation reaction at various temperatures.

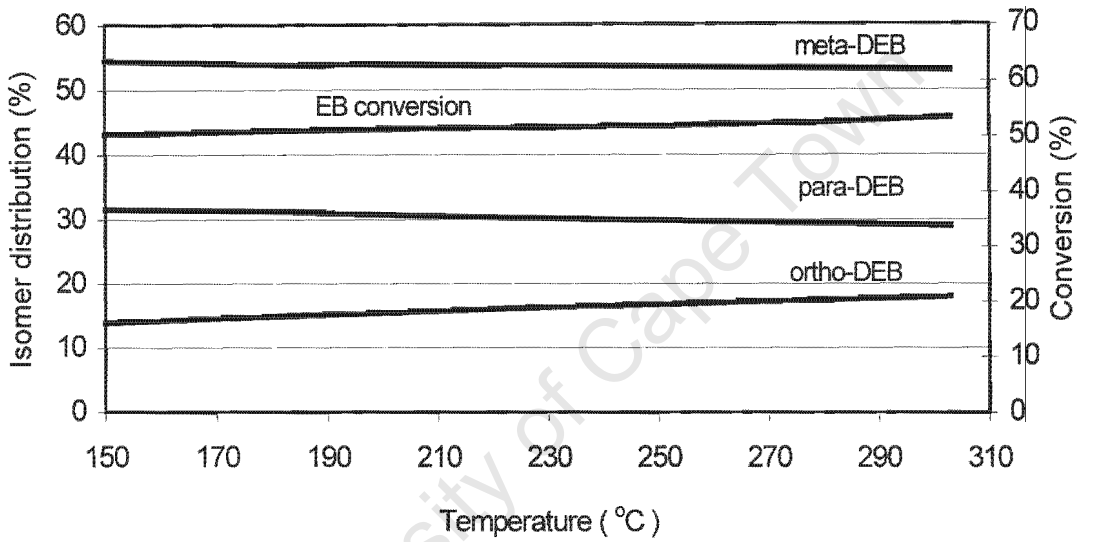

Figure 2-20 Equilibrium conversion and equilibrium distribution of isomers in the diethylbenzene fraction during the disproportionation reaction of ethylbenzene at various temperatures (Thermodynamic data from Stull et al., 1969: Computation method from Smith and van Ness, 1987)

Calculated thermodynamic equilibria for the reaction at 180°C indicate a para/meta/ortho ratio of roughly 30/55/15, showing that the meta isomer is the most favoured and the ortho isomer is the least favoured. Kaeding (1985), and Forni et al. (1993), also reported similar thermodynamic equilibrium values. From Figure 2-20, it can be seen that the equilibrium conversion and isomer distribution is essentially insensitive to temperature in the range of interest (i.e. +/- 180°C).

3 EXPERIMENTAL SECTION

3.1 ETHYLBENZENE CONVERSION EXPERIMENTS

The physical arrangement of equipment for ethylbenzene conversion experiments is shown schematically in Figure 3-1. It consists essentially of a tubular packed bed reactor operated in down-flow configuration with thermostated vapour saturators (21 °C) for ethylbenzene feed and internal standard (n-decane) for chromatographic analysis.

Carrier gas, either H_2 or N_2, is supplied from cylinders via mass flow controllers. During operation, carrier gas is fed to the system via valves V_1 or V_2 in Figure 3-1 and mass-flow-controllers MFC_1 and MFC_2. Valves V_3, V_4, and V_5, are open and the carrier gas-flow flows through the reactant and internal standard saturators, EBS and ISS respectively, which are kept constant at 21 °C.

The carrier gas flow for ethylbenzene feed and n-decane internal standard are set to 40 sccm with MFC_1 and MFC_2, respectively. The combined reactor effluent and internal standard are maintained in the vapour phase by keeping the lines at 100 °C. The total composition of the combined stream is sampled in the vapour phase in a heated glass ampoule according to the method of Schulz et al., 1986 (see section 3.1.3). Analysis is off-line via gas chromatography (section 3.1.3).

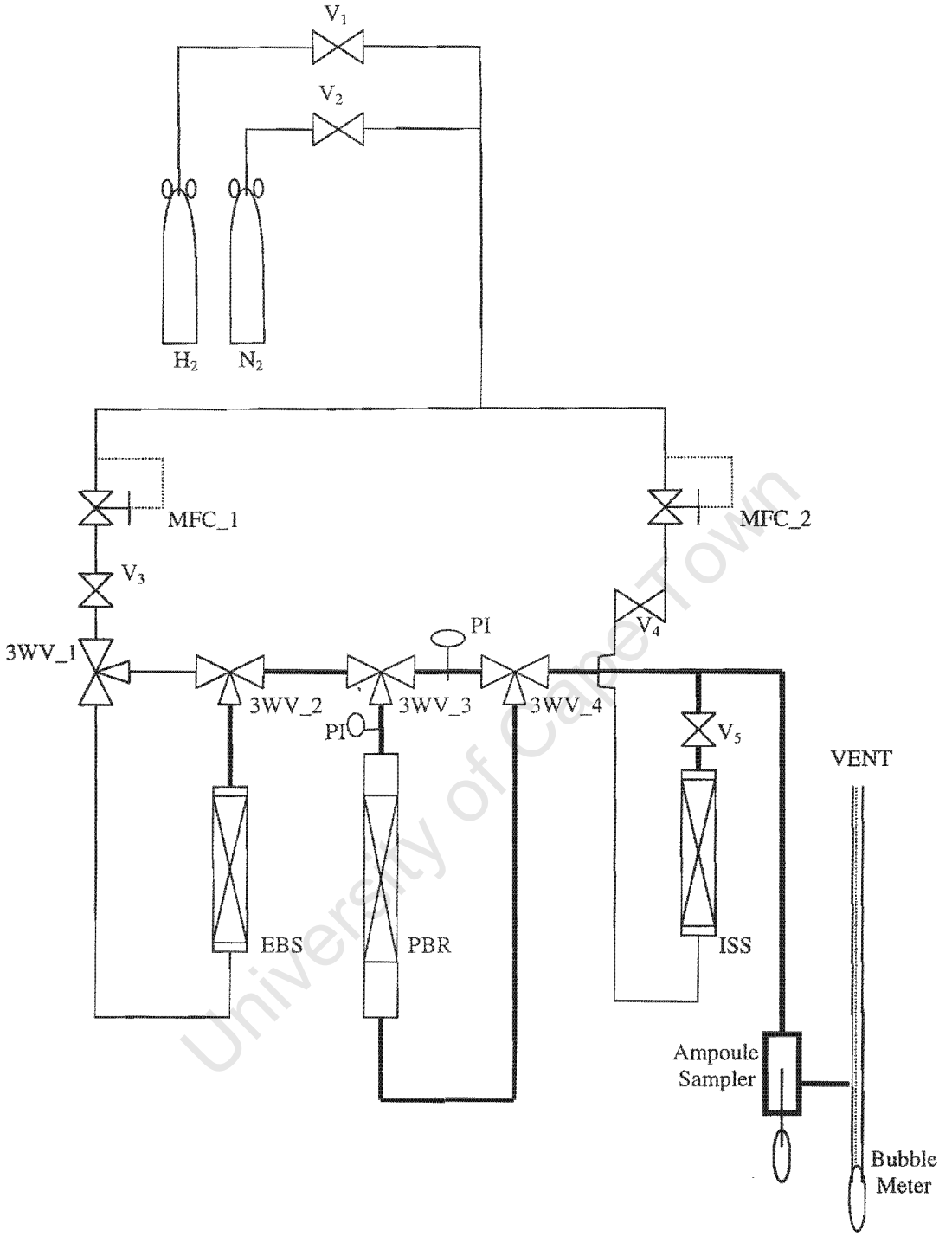

Key:
V = on/off Valve **3WV** = Three-Way Valve **MFC** = Mass Flow Controller
PI = Pressure Indicator **EBS** = EthylBenzene Saturator **ISS** = Internal Standard Saturator
PBR = Tubular Packed Bed Reactor ——— = Heated Lines

Figure 3-1 Process flow diagram for the disproportionation of ethylbenzene.

3.1.1 REACTOR AND CATALYST PACKING

3.1.1.1 Reactor

Catalytic experiments were conducted in a down-flow preheated fixed bed plug-flow reactor under atmospheric pressure (Figure 3-2). The catalyst bed section of the reactor has an internal diameter of 10 mm and is made from glass. The catalyst bed (section 3.1.1.3) was packed inside the reactor on a plug of glass wool and the feed mixture (ethylbenzene and carrier gas) was passed through the catalyst bed from top to bottom. A thermocouple placed in an axial thermowell approximately 10 mm above the section of the packed bed containing catalyst is used to monitor and control temperature.

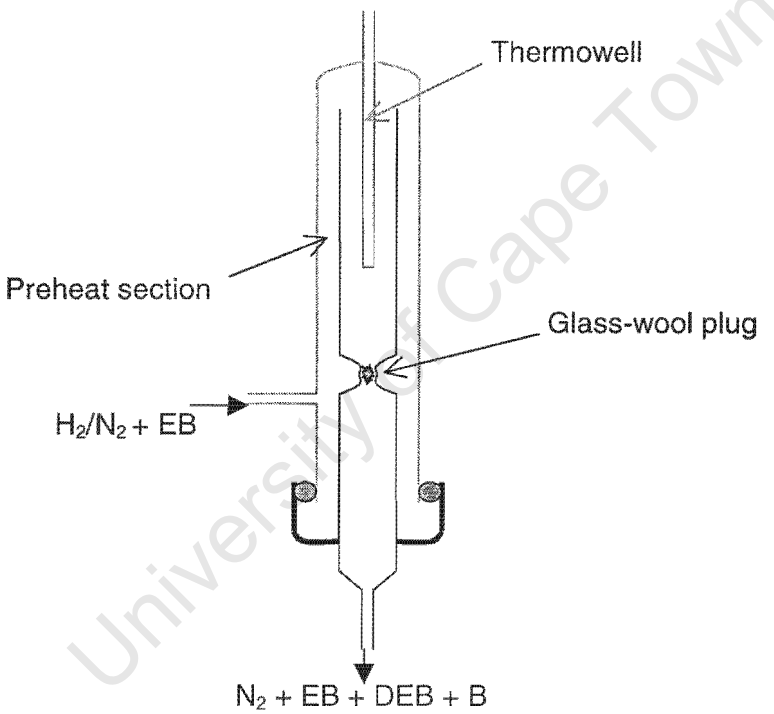

Figure 3-2 Configuration of the glass reactor

3.1.1.2 Catalysts and Catalyst Preparation

Catalyst was used in the form of granulate of size fraction 0.2 – 0.3 mm. For catalysts supplied in the form of powder, LaNaY, H-BEA and H-MFI, granulate was prepared by pelletizing without binder, at 9 tons pressure, followed by crushing and sieving. In the case of the H-FAU (LZY) catalysts, 1/16 inch extrudates (80 % H-FAU, 20 % alumina binder) were crushed and sieved to

the same size fraction. The mass of catalyst used was determined after allowing for the binder content (LZY series of catalysts) and moisture content.

Table 3-1 List of all the catalysts supplied

Catalyst Sample	Si / Al Ratio	Form	Source
LaNaY-72	2.6	Powder	International Zeolite Association (IZA) †
LZY-82	2.7	Extrudate	Union Carbide Corporation
LZY-62	2.5	Extrudate	Union Carbide Corporation
LZY-52	2.4	Powder	Union Carbide Corporation
H-BEA-25	25	Powder	SÜD-Chemie AG
H-BEA-15	14.6	Powder	SÜD-Chemie AG
H-MFI-45	45	Powder	SÜD-Chemie AG

† Prof. S. Ernst, Germany

3.1.1.3 Catalyst Loading

Before operation, the reactor is filled with the catalyst in the following way: Approximately 1 cm^3 of washed, inert sand is placed into the reactor on a supporting plug of glass wool. The required catalyst mass is diluted with 3 cm^3 inert sand, (0.2-0.3 mm granulate containing 290 or 145 mg catalyst after adjustment for moisture content and binder) and placed on top of the 1 cm^3 of pure sand, such that the active catalyst bed is positioned in the isothermal zone of the reactor (section 3.1.1.4). A further 2.5 cm^3 of sand is placed on top of the catalyst bed to act as an additional packed zone to facilitate plug flow behaviour.

The total packed bed length is approximately 12 cm deep with the catalyst containing section between 4 cm and 4.2 cm in length depending on the amount of catalyst required for the particular experiment. The overall configuration is shown schematically in Figure 3-3. For ethylbenzene conversion experiments the axial thermowell extends into the uppermost layer

of sand in the packed bed to a point 10 mm above the catalyst-containing layer as per Figure 3-3.

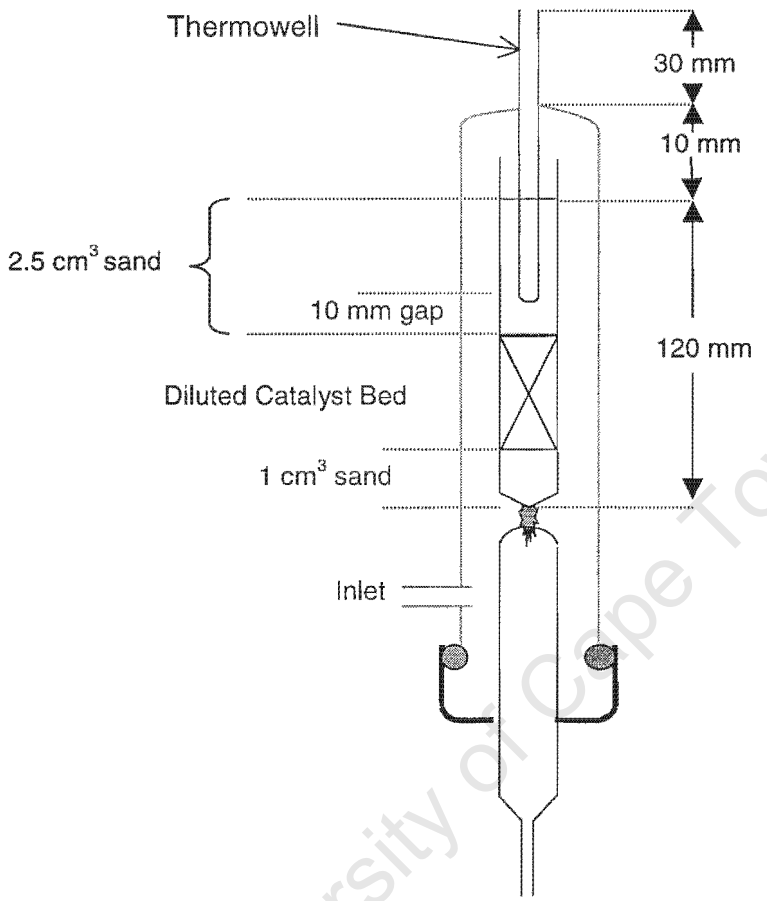

Figure 3-3 Packed catalyst bed configuration

3.1.1.4 Packed catalyst bed configuration

Prior to the conduction of ethylbenzene reactions, experiments were performed to measure the packed bed temperature profile under typical reaction conditions of temperature and flow rate (nitrogen). For these experiments the axial thermowell extended the full depth of the packed bed so as to determine a complete bed temperature profile.

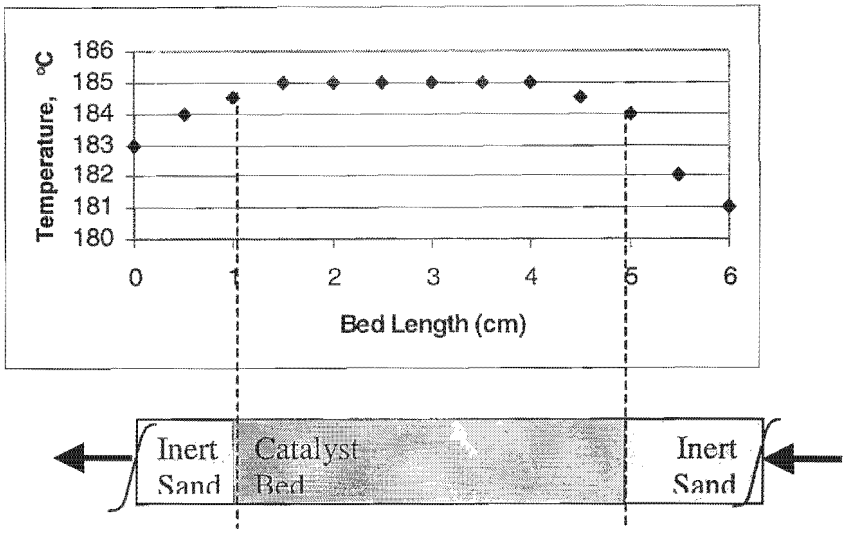

Figure 3-4 Temperature profile in the catalyst bed

As can be seen in Figure 3-4, the isothermal region within the reactor is approximately 5 cm long and extends slightly above and below the catalyst containing section of the bed.

3.1.2 N-DECANE AND ETHYLBENZENE SATURATORS

Ethylbenzene feed and n-decane internal standard are supplied to the experimental system via saturation of carrier gas streams at controlled conditions of flow rate, temperature and pressure.

The saturators are stainless steel vessels consisting of an upper packed section for carrier gas saturation and a lower liquid reservoir. The upper section is packed with Chromosorb P between plugs of glass wool. The Chromosorb packing is saturated with liquid ethylbenzene/n-decane via capilliary action as the bottom of the packed column extends below the level of liquid in the reservoir. Carrier gas is passed upward through the liquid filled packing at 1 atm. The packed upper section is jacketed to maintain a constant temperature of 21 °C. The design of the saturators is shown schematically in Figure 3-5.

Constant saturator head pressure and temperature ensure a constant partial pressure of ethylbenzene or n-decane, respectively. N-decane is employed as an internal standard for the purpose of a carbon balance by chromatographic analysis.

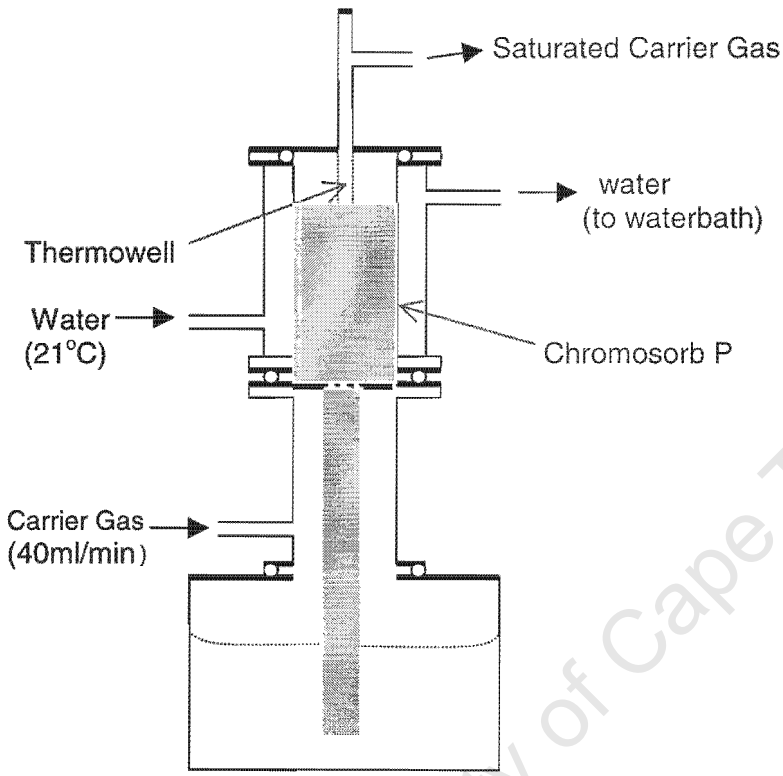

Figure 3-5 Configuration of ethylbenzene (feed) and n-Decane (internal standard) saturators

3.1.2.1 Ethylbenzene Feed Purity

High-purity Analar^{R}, analitical grade ethylbenzene (from ALDRICH) was used. Ethylbenzene readily oxidises in the presence of oxygen, forming a number of oxygenated compounds, which can retard the catalytic reaction. Consequently, all fresh ethylbenzene was tested for such poisons by colorimetric evaluation of ethylbenzene reacted with 20 % by volume of concentrated sulphuric acid. In all cases no coloration was evident and consequently the ethylbenzene was used without further purification.

3.1.3 EXPERIMENTAL PROCEDURE

3.1.3.1 Start up

All catalyst samples were activated in-situ prior to reaction in a 50 sccm stream of nitrogen for 12 hours at an activation temperature of 250 °C or 450 °C, depending on catalyst type. During catalyst activation, nitrogen fed via MFC_1 bypasses the ethylbenzene saturator. After activation the reactor is switched to bypass and the catalyst bed temperature is reduced to the reaction temperature, 180 °C. While the catalyst bed is cooling, carrier gas is set to flow at 40 sccm via both saturators and the temperature of the saturators and the heated feed and product lines allowed to stabilise at 21 °C and 100 °C, respectively. Stable carrier flow and saturator temperature is determined by consistent chromatographic analysis of the bypass mixed ethylbenzene/n-decane stream over several consecutive samples. After steady state is established, with the reactor stable at reaction temperature, the system is switched from bypass to flow through the reactor. This point defines the start of the experiment. Progress of the reaction is followed by regular sampling of the combined product/internal-standard stream.

3.1.3.2 On-stream period

The first sample is collected 15 minutes after ethylbenzene is switched to flow through the reactor. Subsequent samples are collected after every additional 15 minutes for 3 hours, then every 30 minutes for the following two hours and thereafter on an hourly basis. The ampoule sampling technique was used on all the experiments conducted.

3.1.3.3 Shut down

When the last sample is collected, valve 3WV_2 is switched to bypass, valve V_4 is closed and the heating tape is switched off. Carrier gas is allowed to pass through the reactor until the reactor temperature has dropped to room temperature. Thereafter the mass flow controllers are switched off.

3.1.4 PRODUCT ANALYSIS

3.1.4.1 Ampoule Sampling Technique

Complete product stream samples were obtained via the ampoule sampling technique of Schulz et al., (1986). A simplified procedure is as follows:

Vacuum ampoules are made from pasteur pipettes by sealing the capillary end with an acetylene flame. A vacuum (1 kPa absolute pressure) is then applied to the open end of the pipette for +/- 30 seconds after which this end is heated, drawn and sealed in the flame yielding an evacuated sealed ampoule of approximately 30 – 40 mm length and 5 mm diameter with a narrow protruding capillary of approximately 50 – 60 mm in length.

To obtain samples of the reactor effluent stream, the capillary end of the ampoule is inserted, through the septum of a sampling device, into the effluent stream. The capillary is broken in the sampling device, so drawing a total vapour phase sample into the ampoule after which the capillary is partially withdrawn and sealed with a butane flame.

The sealed ampoule containing the sample is introduced into the carrier gas of a gas chromatograph via a heated sample injection device. Once the ampoule is stabilized at the injection temperature, the ampoule is crushed within the device so releasing the sample contents into the chromatograph in the form of a pulse.

3.1.4.2 Gas Chromatographic Analysis and Data Work-up

A HP 5890A Gas Chromatograph fitted with a 12 m long x 0.32-mm diameter OV-1 capillary column is used for the analysis of the ampoule samples. Details of the method are provided in Table 3-2.

Table 3-2 Gas chromatographic conditions

Gas chromatograph	HP 5890A
Column	12 m x 0.32 mm
Stationary phase	OV-1 (methylpolysiloxane)
Carrier gas	Argon
Head pressure	140 kPa
Split flow	100 ml/min
Column flow	1.8 ml/min (at 50 °C oven/column temperature)
Temperature programme	
Initial oven temperature	50 °C (1 min)
Temperature ramp	10 °C/min to 150 °C
Final temperature	150 °C (1 min)

A typical product chromatogram and analysis is shown in Figure 3-6.

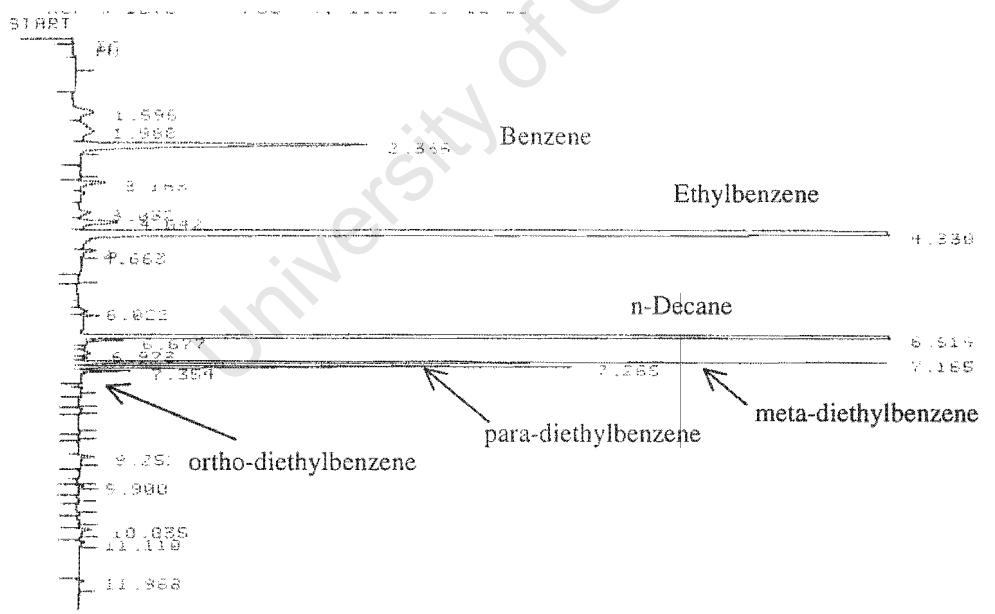

Product I.D	RT (min)	Area
Benzene	2.336	123309
Ethylbenzene	4.330	5906400
n-Decane*	6.614	1301882
Meta-DEB	7.165	114638
Para-DEB	7.265	62207
Ortho-DEB	7.354	6973

Figure 3-6 A typical product spectrum obtained from the GC (*Internal standard)

The molar yields of benzene (Y_B) and diethylbenzenes (Y_{DEB}) were calculated from the areas (A_i) of the peaks in the gas chromatogram according to:

$$Y_B = \frac{A_B / CN_B}{A_B / CN_B + A_{DEB} / CN_{DEB} + A_{EB} / CN_{EB}} \qquad (3.1)$$

$$Y_{DEB} = \frac{A_{DEB} / CN_{DEB}}{A_B / CN_B + A_{DEB} / CN_{DEB} + A_{EB} / CN_{EB}} \qquad (3.2)$$

where subscripts are

B = Benzene; EB = EthylBenzene; DEB = DiEthylBenzene

A_i = Peak area of compound i in the gas chromatogram;

CN_i = Number of carbon atoms in compound i

Ethylbenzene conversion (X_{EB}) is calculated from the sum of the yields of benzene and diethylbenzenes (Weitkamp, 1994):

$$X_{EB} = Y_B + Y_{DEB} \qquad (3.3)$$

The distribution of the DEB isomers with respect to the total DEB product are calculated from the areas of the peaks in the gas chromatogram according to:

$$DEB\_distribution = \frac{A_i}{A_{m-DEB} + A_{p-DEB} + A_{o-DEB}} \qquad (3.4)$$

The molar yield ratio of diethylbenzenes to benzene is calculated as follows:

$$\frac{Y_{DEB}}{Y_B} = \frac{A_{DEB} / CN_{DEB}}{A_B / CN_B} \qquad (3.5)$$

A carbon balance was performed for each sample using equation 3.6 based on the internal standard n-decane:

$$C_{Total} = \frac{\left(\frac{\sum_i A_i - A_{n-Decane}}{A_{n-Decane}}\right)_{Reactor}}{\left(\frac{\sum_i A_i - A_{n-Decane}}{A_{n-Decane}}\right)_{Bypass}} \qquad (3.6)$$

$\sum_i A_i$ includes all impurities of the feed in case of the bypass sample and all impurities of the feed plus all products in case of the reactor sample. The closer C_{Total} is to 1, the better the total carbon mass balance.

3.2 AMMONIA TEMPERATURE-PROGRAMMED DESORPTION (NH_3-TPD)

3.2.1 APPARATUS

The analyses were performed by an external laboratory on an AUTOCHEM 2910 supplied by Micromeritics.

3.2.2 PROCEDURE

Approximately 0.15 grams of sample are loaded into the sample cell followed by degassing in flowing helium while the temperature is raised to 120 °C at 5 °C/min. After holding at 120 °C for 10 minutes, the sample temperature is raised at 10 °C/min under flowing helium up to a final activation temperature of either 250 °C or 450 °C. After holding the sample at the final activation temperature for 30 minutes, the sample was cooled to 100 °C. At this temperature the sample is saturated with ammonia by exposure to a stream of 4.98 % NH_3/He for 60 minutes, followed by purging in pure helium for 30 minutes at the same temperature to remove physisorbed ammonia.

Temperature programmed desorption of the remaining adsorbed ammonia is achieved by ramping the sample temperature from 100 °C to 750 °C at 10 °C/min in flowing helium. The effluent stream containing desorbed ammonia is monitored by thermal conductivity detector (TCD).

3.2.3 TPD DATA WORK-UP

Proprietary software supplied by the instrument manufacturer, including appropriate calibration procedures, presents the data as desorbed NH_3 concentration as a function of temperature.

3.3 CATALYSTS SUPPLIED AND EXPERIMENTS CONDUCTED

Table 3-3. Catalytic experiments conducted

Exp. No.	Catalyst Type	Si/Al Ratio	W_{cat} (mg)	Carrier Gas	T_{rxn} °C	T_{act} °C	(%) NH_4 Exch.	(%) La Exch.
1	LaNaY-72	2.4	290	Nitrogen	180	250	-	72
2*	LaNaY-72	2.4	290	Nitrogen	180	250	-	72
3	LaNaY-72	2.4	290	Nitrogen	180	450	-	72
4	LaNaY-72	2.4	290	Hydrogen	180	250	-	72
5	LaNaY-72	2.4	145	Nitrogen	180	250	-	72
6	LZY-82	5.38	290	Ntrogen	180	450	99	-
7	LZY-62	4.94	290	Nitrogen	180	450	82	-
8	LZY-52	4.74	290	Nitrogen	180	450	0	-
9	H-BEA-15	14.6	290	Nitrogen	180	450	-	-
10	H-BEA-25	25	290	Nitrogen	180	450	-	-
11	H-MFI-45	45	290	Nitrogen	180	450	-	-

*Repeat of experiment 1

4 RESULTS

For easy and concurrent readability of this section, you are referred to Appendix 1, a "fold-out" tabulated summary of all catalytic experiments conducted. Standard reaction conditions are shown on Table 4-1. Deviations from these standard conditions are indicated in the figure captions. Complete tabulated experimental data may be found in Appendix 2.

Table 4-1 Standard reaction conditions

Reaction temperature, T_{rxn}	180 °C
Catalyst weight, $W_{cat.}$	290 mg
Activation temperature, $T_{act.}$	450 °C
Carrier gas	Nitrogen

4.1 ETHYLBENZENE CONVERSION

4.1.1 INTRODUCTORY EXPERIMENTS

Figure 4-1 depicts the catalytic results obtained with LaNaY-72. The characteristic time-on-stream behaviour of large pore zeolites can be seen as was observed by others (Karge et al., 1994 and Weiss et al., 1997). Early in the experiment, there is an induction period during which the conversion increases. After several hours the so-called (quasi-) stationary stage or deactivation period is reached.

The distribution of diethylbenzene isomers formed over LaNaY-72 is plotted versus time-on-stream in Figure 4-2. Substantial changes in the distribution occur with time-on-stream during the induction period. Soon after the point of maximum conversion is reached, the distribution of diethylbenzene isomers becomes stable and remains essentially unchanged for the remainder of the experiment (i.e. throughout the deactivation period).

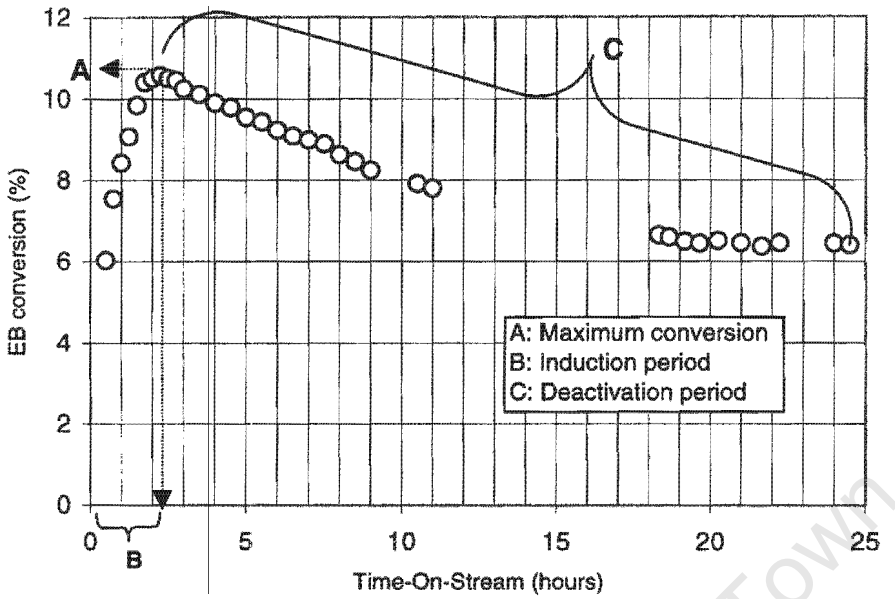

Figure 4-1 Conversion of ethylbenzene over LaNaY-72. [Experiment 1, T_{act} = 250°C]

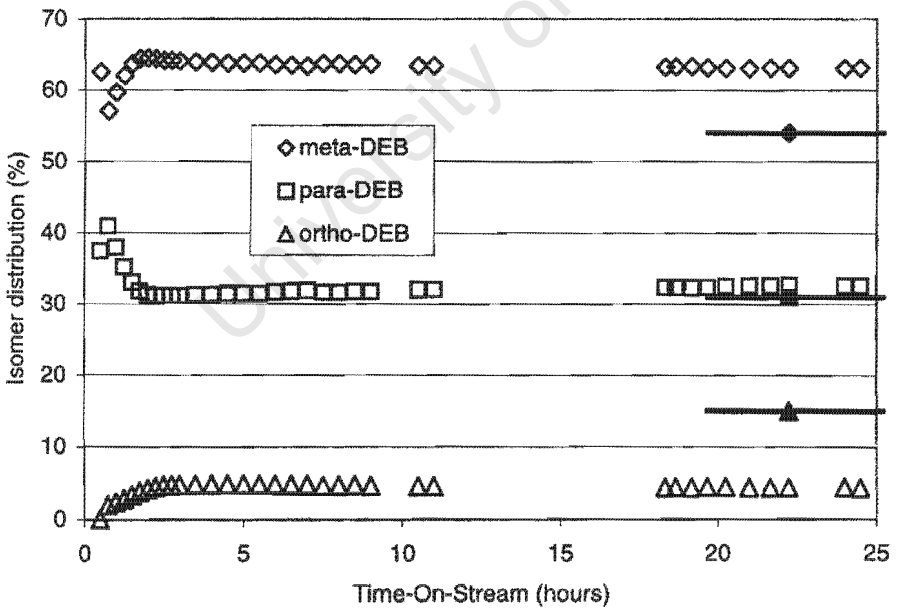

Figure 4-2 Isomer distribution of diethylbenzene over LaNaY-72. [Experiment 1, T_{act} = 250°C]; (Equilibrium: meta —◆—, para —■—, ortho —▲—)

The isomer distribution is clearly not in equilibrium, with the ortho-isomer far below the equilibrium value. However, from Table 4-2 it can be considered that the meta- and para-isomer distribution approaches equilibrium between one another.

Table 4-2 Pseudo-Stationary phase average diethylbenzene isomer distribution

	Meta-	Para-	Ortho-
LaNaY-72 (Experiment 1)	64	31	5
Equilibrium (at 180 °C)	54	31	15
	Normalised distribution between meta- and para-isomer only		
LaNaY-72 (Experiment 1)	67	33	-
Equilibrium (at 180 °C)	64	36	-

The molar yields of diethylbenzene (DEB) and benzene (B) as well as the molar yield ratio of DEB:B, are shown in Figures 4-3 and 4-4, respectively, as a function of time-on-stream. A considerable deficit of diethylbenzenes is observed during the initial part of the induction period. The ratio increases rapidly during the induction period, stabilizing at a maximum ratio of approximately 0.9 at the point of maximum ethylbenzene conversion.

Throughout the deactivation period the molar DEB:B ratio remains essentially constant between 0.95 – 0.85 (declining slightly with time-on-stream) and close to the ratio of 1:1 expected from stoichiometry in the absence of side reactions. All the above results are consistent with the previously published literature on ethylbenzene conversion over LaNaY-72 catalyst (Karge et al., 1994, Weiss et al., 1997).

Similar features were observed for all catalysts employed in this study except ZSM-5, for which no induction period could be seen, and LZY-52 for which no noticeable activity was recorded.

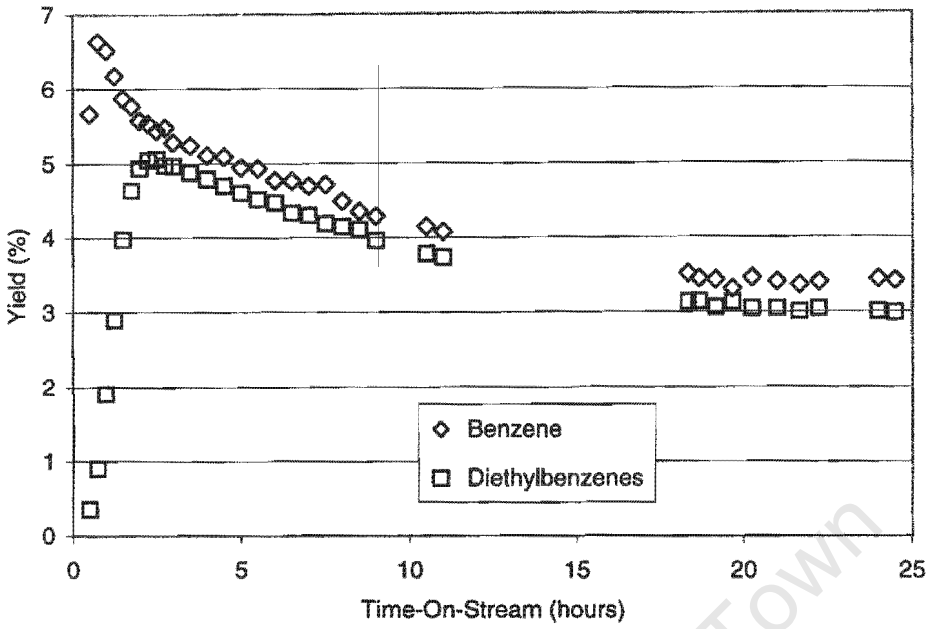

Figure 4-3 The yields of diethylbenzenes and benzene over LaNaY-72, [Experiment 1, T_{act} = 250°C]

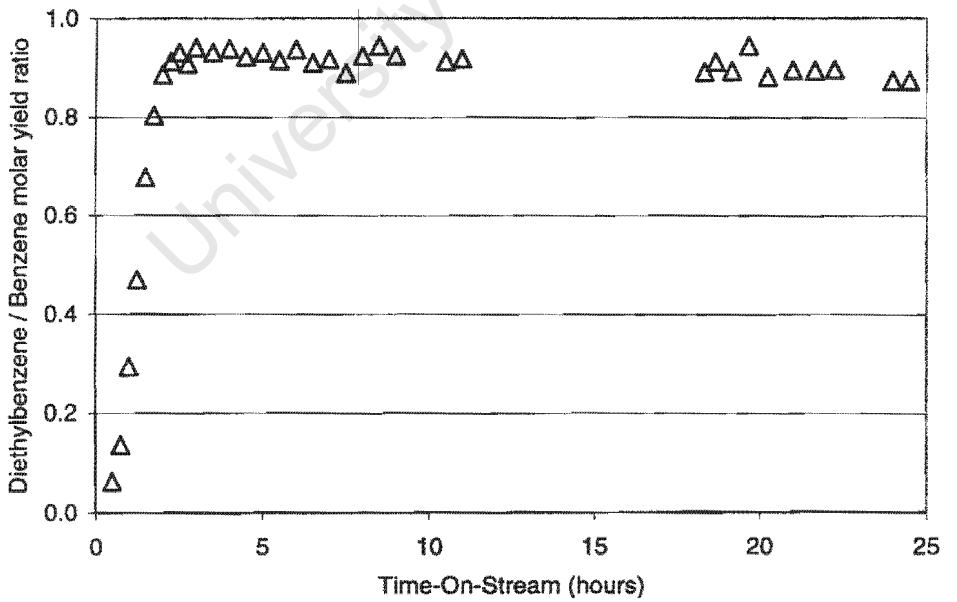

Figure 4-4 The yield ratios of diethylbenzenes to benzene over LaNaY-72 [Experiment 1, T_{act} = 250°C]

4.1.2 REPRODUCIBILITY

A repeat experiment of that described in section 4.1.1 was conducted to demonstrate the experimental reproducibility that is obtainable at set conditions. Figures 4-5 – 4-8 show the reproducibility of conversion, DEB isomer distribution and DEB: B ratio, respectively, for the ethylbenzene disproportionation reaction over LaNaY-72. From the figures it is apparent that the experimental reproducibility is of an acceptable level. Importantly, all the pertinent features of the time-on-stream behaviour are reproduced in significant detail.

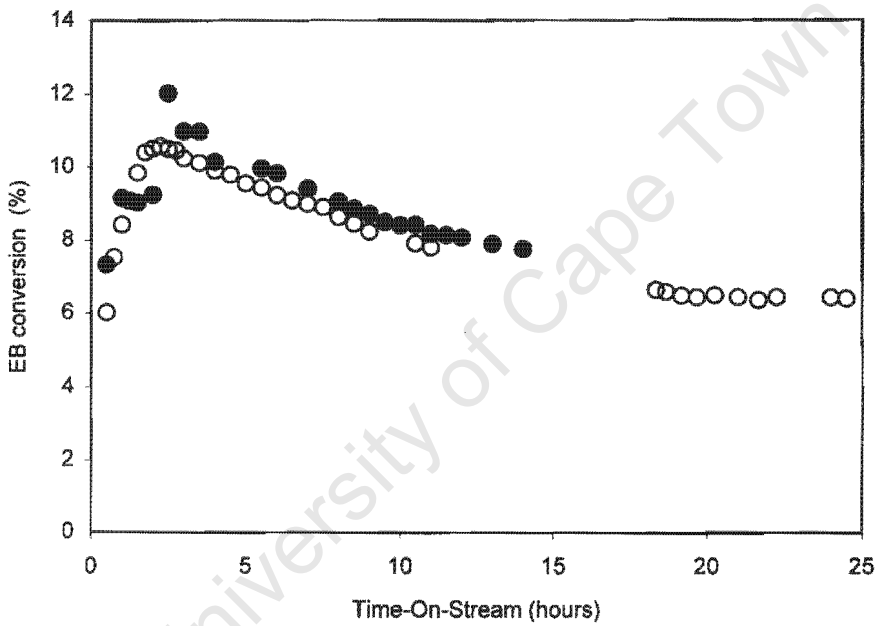

Figure 4-5 Reproducibility of conversion versus time-on-stream for the disproportionation of ethylbenzene over LaNaY-72. [Open symbols: Experiment 1; Closed symbols: Experiment 2]

4.1.3 LaNaY-72

4.1.3.1 Effect of Activation Temperature

As can be seen from Figure 4-9, conversion of EB strongly depends on the activation temperature. An increase in activation temperature from 250 °C to 450 °C results in a decrease in the activity of the catalyst. Also of interest is the length of the induction period, which increased from 2.3 hours to 3.1 hours

with an increase in activation temperature. Deactivation during the quasi-stationary stage remains essentially unaffected by activation temperature.

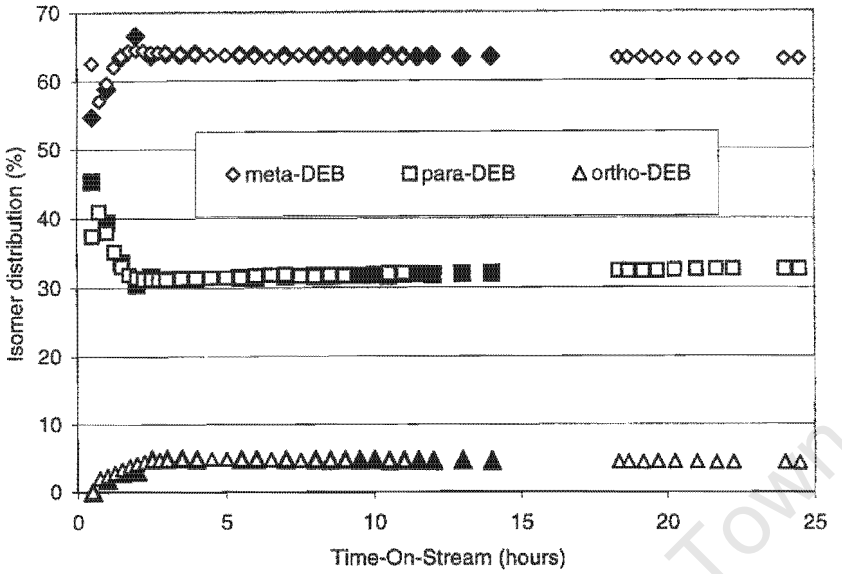

Figure 4-6 Reproducibility of isomer distribution versus time-on-stream for the disproportionation of ethylbenzene over LaNaY-72. [Open symbols: Experiment 1; Closed symbols: Experiment 2]

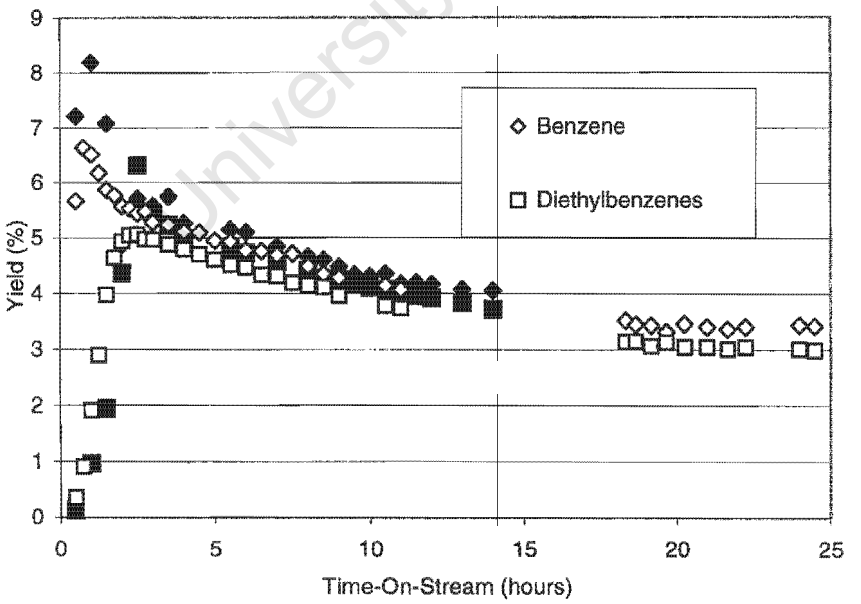

Figure 4-7 Reproducibility of product yield versus time-on-stream during the disproportionation of ethylbenzene [Open symbols: Experiment 1; Closed symbols: Experiment 2]

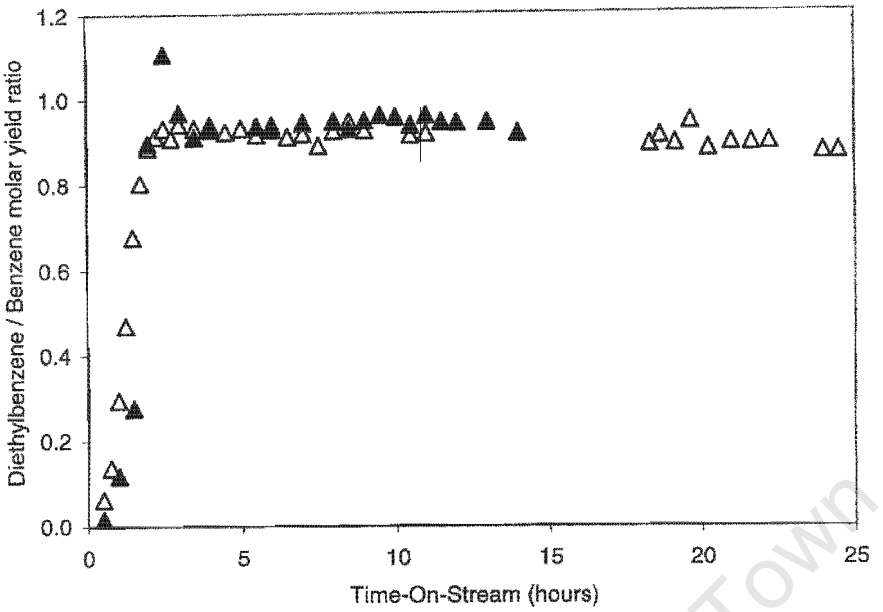

Figure 4-8 Reproducibility of product yield ratio versus time-on-stream during the disproportionation of ethylbenzene [△ Experiment 1; ▲ Experiment 2]

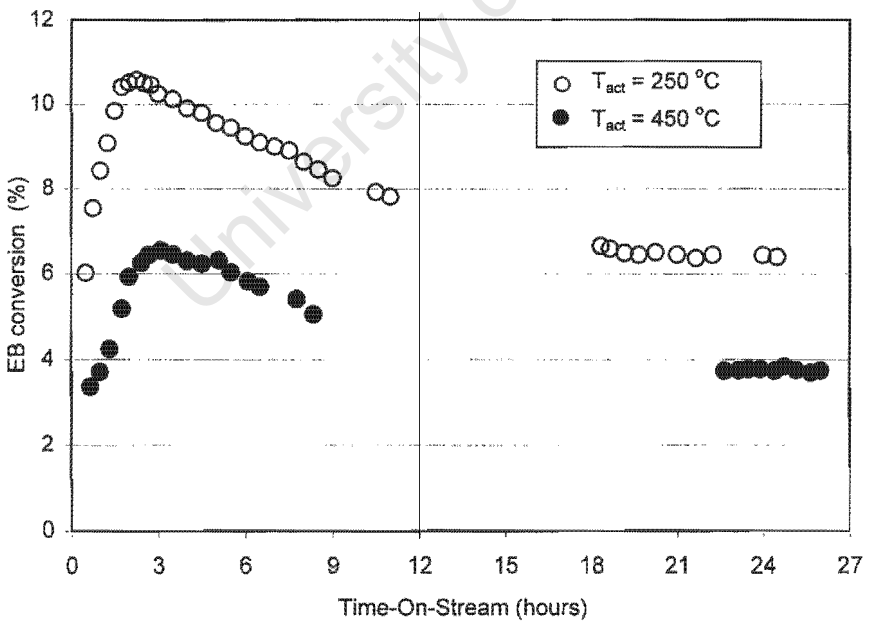

Figure 4-9 Effect of activation temperature on the disproportionation of ethylbenzene over LaNaY-72. [Open symbols: Experiment 1; Closed symbols: Experiment 3]

Figure 4-10 shows the diethylbenzene isomer distribution for the different activation temperatures.

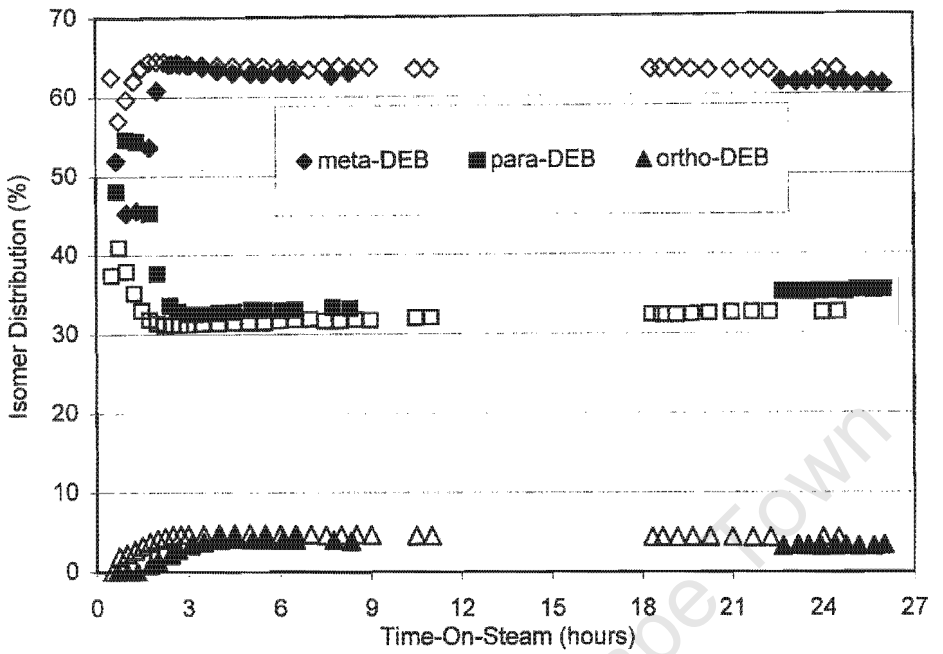

Figure 4-10 Effect of activation temperature on the isomer distribution over LaNaY-72. (Closed symbols: T_{act} = 450 °C [Experiment 3]; Open symbols: T_{act} = 250 °C [Experiment 1])

4.1.3.2 Effect of WHSV

WHSV was varied by changing the dry mass of catalyst with constant feed rate. The effect of this variable on conversion and product spectrum is shown in Figures 4-11 and 4-12. Doubling the WHSV results in an apparent decrease in the induction period, from 2.3 hours to about 1.8 hours consistent with the trends observed for LaNaY-72 (Weiss et al., 1997) and for other zeolites (Karge et al., 1994). As expected, the conversion decreases with increasing WHSV. The diethylbenzene isomer distribution for different space velocities is shown in Figure 4-12.

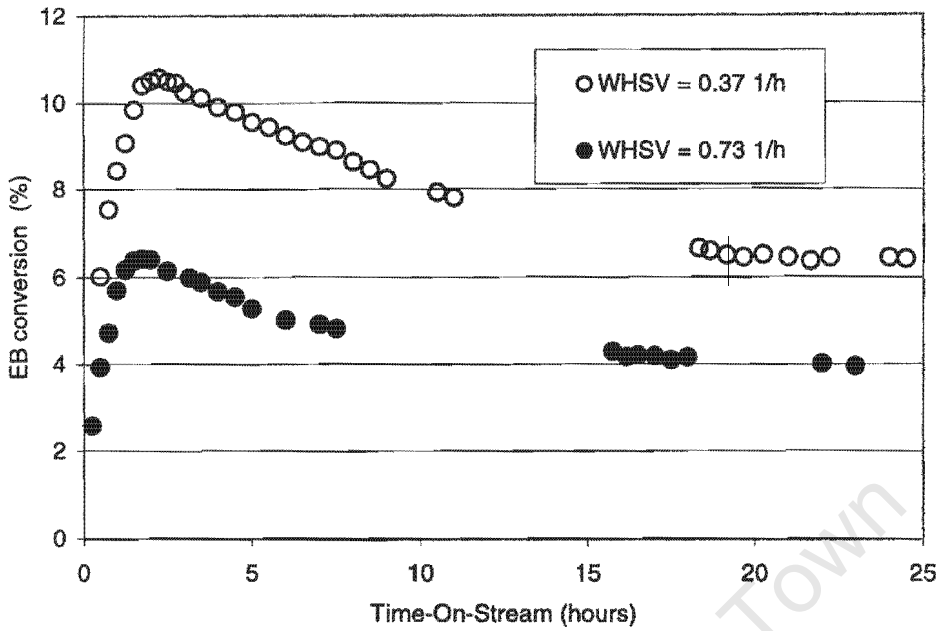

Figure 4-11 Effect of WHSV on the disproportionation of ethylbenzene over LaNaY-72. [Open symbols: Experiment 1; Closed symbols: Experiment 5]

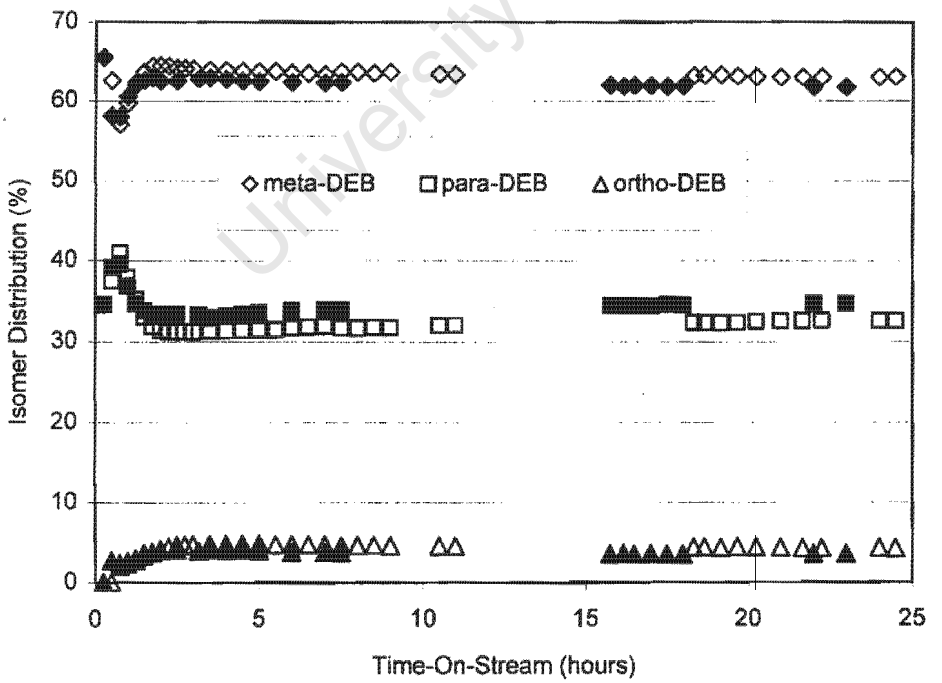

Figure 4-12 Effect of WHSV on the isomer distribution over LaNaY-72. (Closed symbols: 0.73 h^{-1} [Experiment 5]; Open symbols: 0.37 h^{-1} [Experiment 1])

4.1.3.3 Effect of Carrier Gas

Carrier gas was found to have no effect on both catalyst activity and induction period (Figure 4-13).

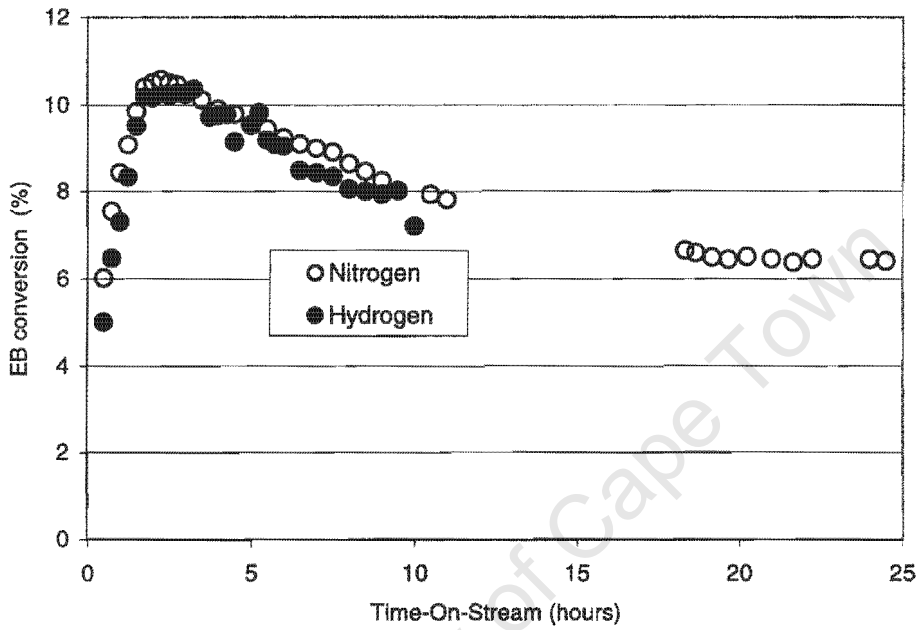

Figure 4-13 Effect of carrier gas on the disproportionation of ethylbenzene over LaNaY-72. [Open symbols: Experiment 1; Closed symbols: Experiment 4]

4.1.4 LINDE-Y ZEOLITE

Figure 4-14 depicts ethylbenzene conversion over activated Linde-Y zeolites (T_{act} = 450°C) of different levels of NH_3-Na exchange. The highest activity can be seen for LZY-82 (99% NH_4-form). Virtually no activity was observed for LZY-52 (Na-form). The induction period recorded for LZY-62 (82% NH_4-form) is 2.3 hours whereas that for LZY-82 is less than 1 hour. Both active catalysts show conversion versus time on stream behaviours typical of large pore zeolites.

The maximum conversion for LZY-82 catalyst is about 47% and that for the LZY-62 catalyst is about 8%, consistent with the greater ammonium/sodium exchange and, hence, proton acidity of the former catalyst. As per the findings of Weiss et al. (1997) on LaNaY of different La-Na exchange levels, a relatively strong decrease in activity is observed for LZY-62 versus LZY-82. LZY-52, which is fully sodium exchanged, exhibits no observable activity. As can be seen in Figure 4-14 for LZY-82 and LZY-62, relative deactivation during the stationary stage is more or less similar.

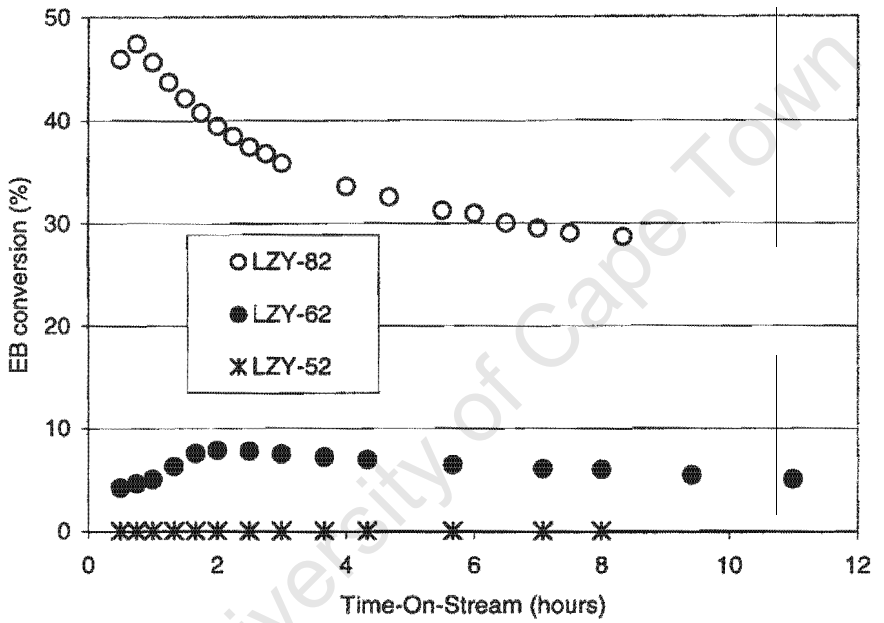

Figure 4-14 Conversion of ethylbenzene over Linde-Y zeolites [Open symbols: Experiment 6; Closed symbols: Experiment 7; Star symbols: Experiment 8]

Of particular interest is the distribution of the diethylbenzene isomers formed on zeolite Linde-Y (Figure 4-15). As was observed in Figure 4-2 and Table 4-2 for LaNaY-72, the isomer distribution is not in equilibrium. However, the meta- and para-isomer distribution approaches equilibrium between one another (Table 4-3).

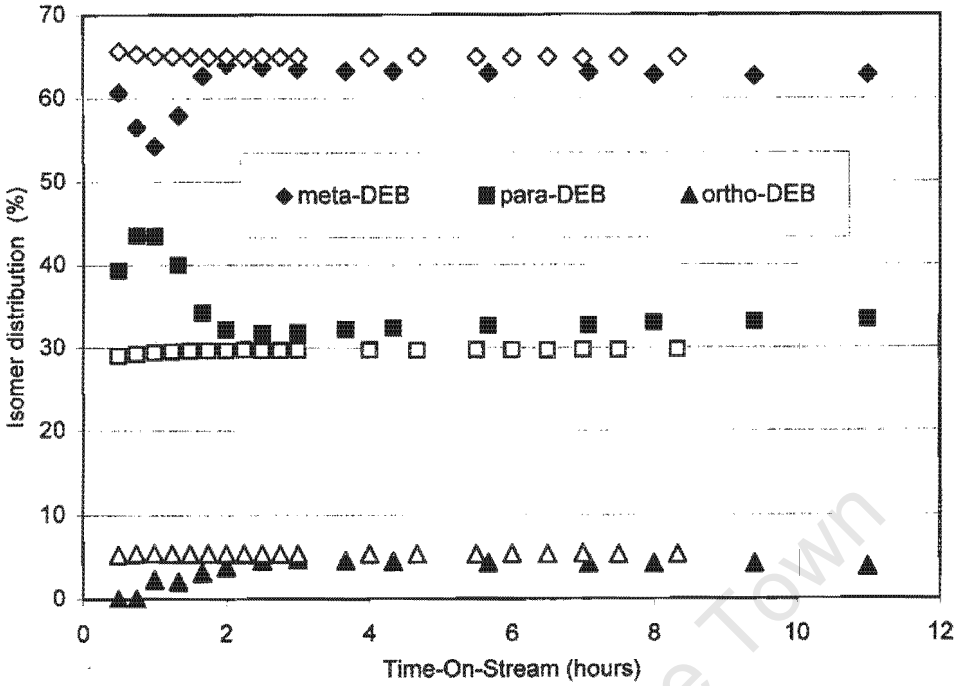

Figure 4-15 Isomer distribution of diethylbenzenes on zeolites Linde-Y (Open symbols: LZY-82 [Experiment 6]; Closed symbols: LZY-62. [Experiment 7])

Table 4-3 Pseudo-Stationary phase average diethylbenzene isomer distribution

	Meta-	Para-	Ortho-
LZY-82 (Experiment 6)	65	30	5
Equilibrium (at 180 °C)	54	31	15
	Normalised distribution between meta- and para-isomer only		
LZY-82 (Experiment 6)	69	31	-
Equilibrium (at 180 °C)	64	36	-

4.1.5 H-BETA

Two samples of zeolite H-Beta with different aluminium content (Si/Al = 15 and 25) and, hence, density of acid sites, were used as catalysts for ethylbenzene disproportionation (Figure 4-16). The catalyst with the higher density of acid sites (H-BEA-15) is more active, as expected. Also as expected for large pore zeolites, an induction period is indicated in Figure 4-16 and the more active sample (H-BEA-15) exhibits a shorter induction period.

As previously observed for LaNaY of different acidity (Figure 4-9), deactivation during the stationary stage is similar for the two H-BEA catalysts of different total acidity. Moreover, both catalysts exhibit similar qualitative and quantitative features as previously observed with Y-type zeolites, both LaNaY-72 (Figure 4-2) and Linde-Y types (Figure 4-15).

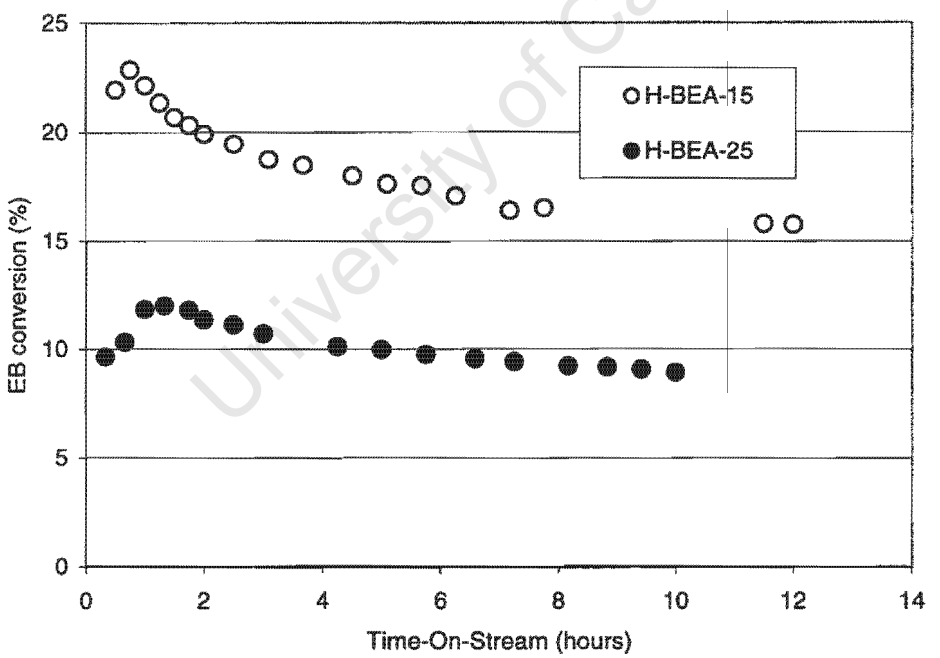

Figure 4-16 Conversion of ethylbenzene over zeolite H-Beta, T_{act} = 450°C, W_{cat} = 290 mg, $T_{reaction}$ = 180°C. [Open symbols: Experiment 9; Closed symbols: Experiment 10]

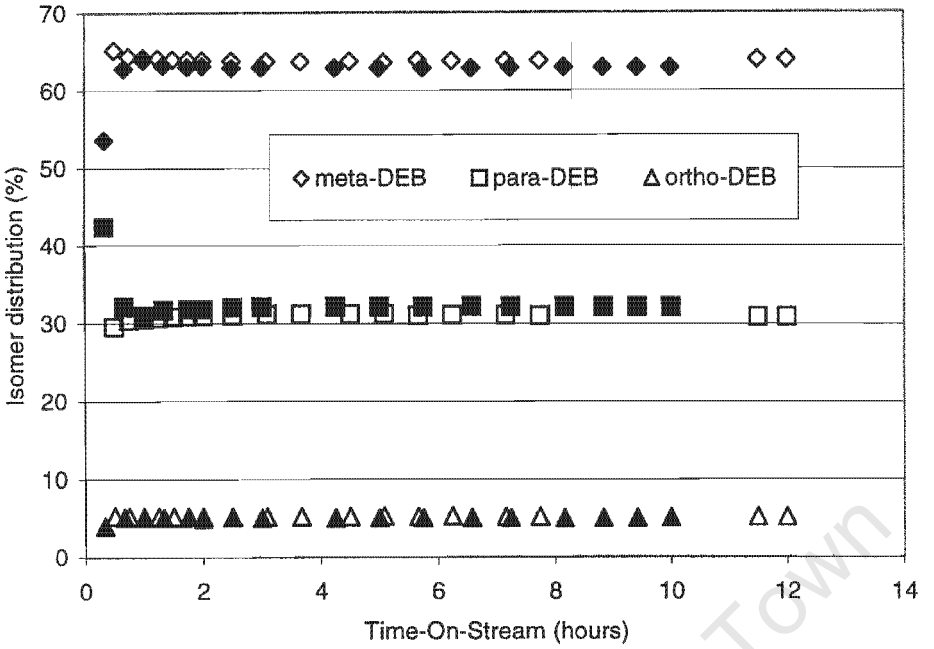

Figure 4-17 Isomer distribution of diethylbenzenes on zeolite H-Beta (Open symbols: H-BEA-15 [Experiment 9]; Closed symbols: H-BEA-25 [Experiment 10])

Also, as was observed for the Y-type zeolites, the diethylbenzene isomer distributions over the H-Beta samples are not in equilibrium (Table 4-4), but the meta- and para-isomer distribution approaches equilibrium between one another.

Table 4-4 Pseudo-Stationary phase average diethylbenzene isomer distribution

	Meta-	Para-	Ortho-
H-BEA-15 (Experiment 9)	64	31	5
Equilibrium (at 180 °C)	54	31	15
	Normalised distribution between meta- and para-isomer only		
H-BEA-15 (Experiment 9)	67	33	-
Equilibrium (at 180 °C)	64	36	-

4.1.6 H-MFI-45

The results of ethylbenzene conversion over H-MFI-45 are shown in Figures 4-18 and 4-19. Ethylbenzene conversion drops rapidly from an initially higher value to a constant lower level within two hours. In contrast to the Y and Beta zeolites tested, H-MFI-45 shows no induction period and a true, constant steady-state conversion is rapidly established. Under the test conditions of 180 °C, the steady state conversion is relatively low at 0.5 mol%. Moreover, ortho-diethylbenzene was undetectable, consistent with the reported findings of Weitkamp et al. (1986).

Therefore, it can be stated that the diethylbenzene isomers are not in thermodynamic equilibrium and, as in the case of the large pore zeolites studied here, equilibrium is almost approached between the meta- and para-isomers (Table 4-5).

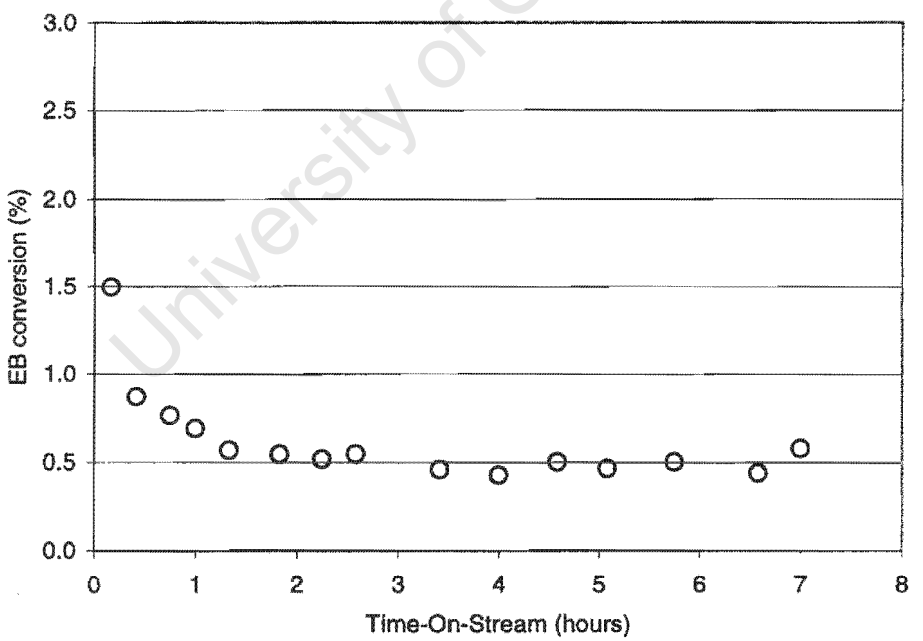

Figure 4-18 Conversion of ethylbenzene over H-MFI-45. [Experiment 11]

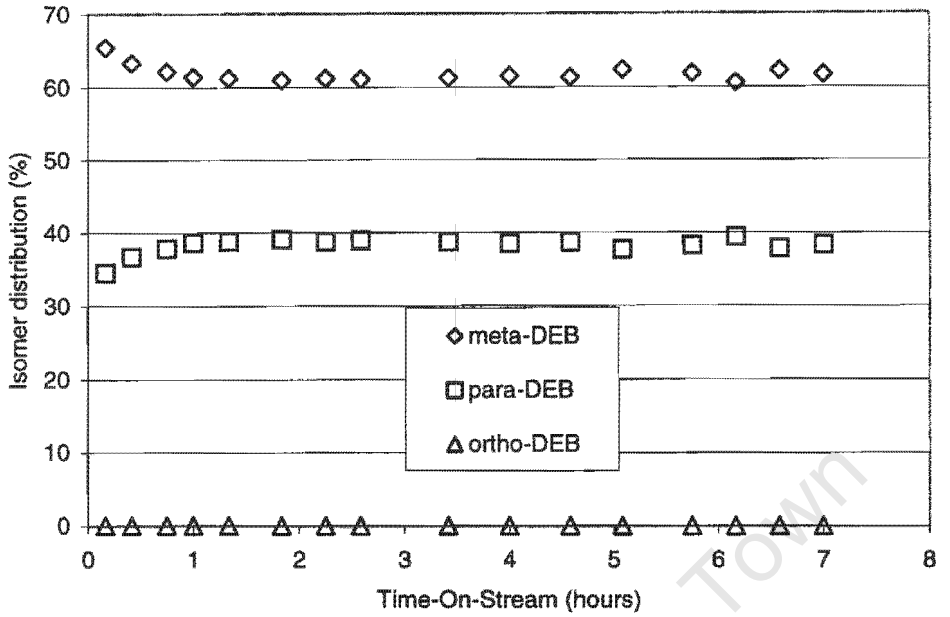

Figure 4-19 Isomer distribution of diethylbenzenes for the conversion of ethylbenzene over H-MFI-45. [Experiment 11]

Table 4-5 Pseudo-Stationary phase average diethylbenzene isomer distribution

	Meta-	Para-	Ortho-
H-MFI-45 (Experiment 11)	61	39	0
Equilibrium (at 180 °C)	54	31	15
	Normalised distribution between meta- and para-isomer only		
H-MFI-45 (Experiment 11)	61	39	-
Equilibrium (at 180 °C)	64	36	-

4.1.7 SELECTION OF COMPARATIVE RESULTS

Maximum conversion and conversion after 12 hours for each and every catalyst employed in this study is shown in Figure 4-20 and is tabulated in Tables 4-6 and 4-7. LZY-82 is the most active catalyst initially but also exhibits the largest absolute activity decline compared to the other catalysts. On a relative basis, all catalysts, except H-MFI-45, show similar deactivation behaviour when comparing conversion after 12 hours on stream relative to the maximum conversion level.

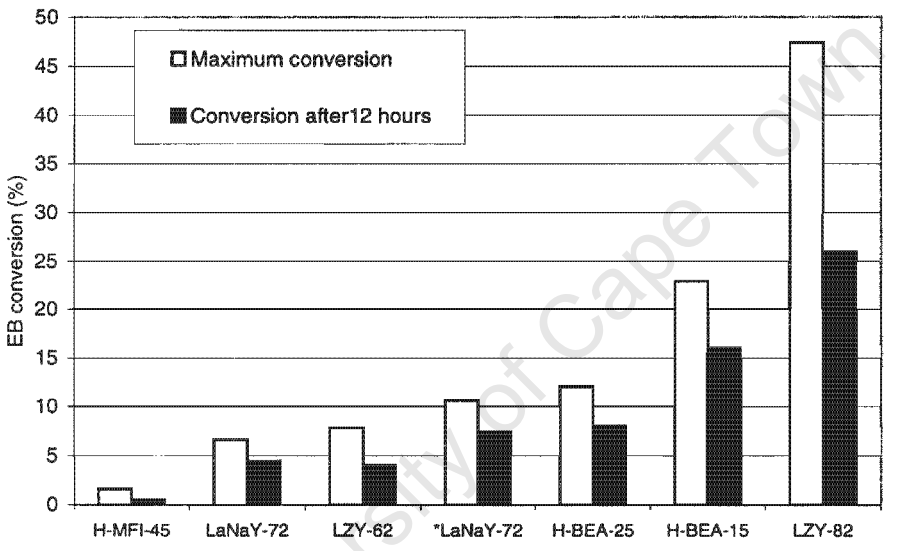

Figure 4-20 Comparison of maximum conversion, which was attained, to that obtained after 12 hours on-stream on zeolites. [* catalyst activated at 250 °C].

The distribution of diethylbenzenes over zeolites after 12 hours on stream is presented in Figure 4-21 and Tables 4-6 and 4-7. The catalysts are arranged in order of increasing maximum activity. Close inspection of Figure 4-21, suggests that the selectivity of para-DEB decrease very slightly with increasing activity, whereas the meta- and ortho-DEB become slightly more favoured.

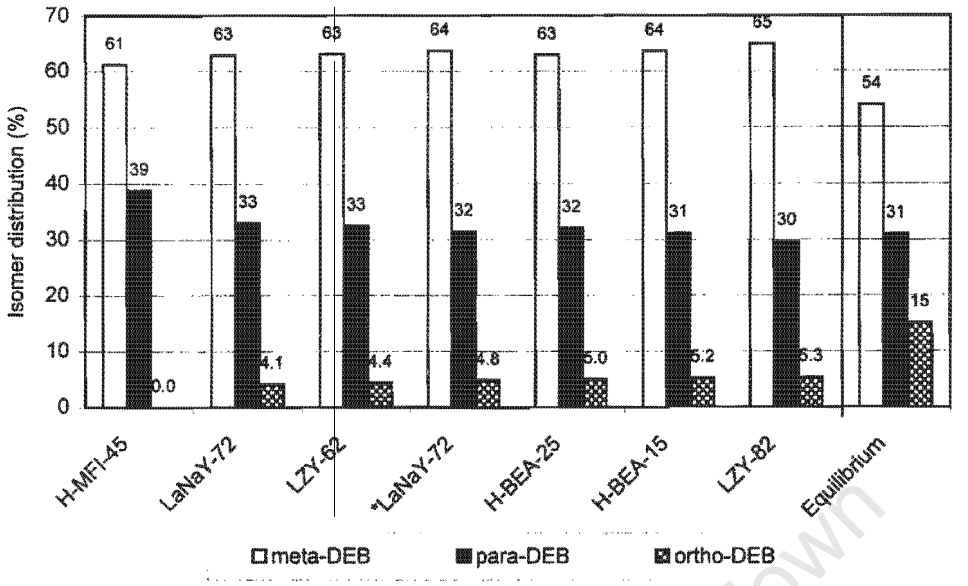

Figure 4-21 The distribution of diethylbenzenes on zeolites after 12 hours on stream. [* Calcination temperature = 250 °C]

Table 4-6 Results summary of conversion of EB over acid zeolites and the distribution of diethylbenzenes at maximum conversion.

Catalyst	Induction period (h)	Maximum Conversion $X_{EB,Max.}$ (%)	Conversion after 12 h (%)	DEB distribution at $X_{EB,Max.}$				
				All isomers			m- / p- only**	
				meta	para	ortho	meta	para
H-MFI-45	-	1.7	0.5	66	34	0.0	66	34
LaNaY-72	3.1	6.6	4.4	64	33	3.0	66	34
LZY-62	2.3	7.8	4.0	64	32	4.0	67	33
LaNaY-72*	2.3	11	7.4	65	31	4.0	68	32
H-Beta-25	1.3	12	8.0	63	32	5.0	66	34
H-Beta-15	0.8	23	16	65	30	5.0	68	32
LZY-82	0.8	47	26	66	29	5.0	69	31
Thermodynamic equilibrium (at 180 °C)				54	31	15	64	36

* Catalyst activation at 250 °C

** Normalized distribution between meta- and para-isomer only

Table 4-7 Results summary of conversion of EB over acid zeolites and the distribution of diethylbenzenes after 12 hours

Catalyst	Induction period (h)	Maximum Conversion (%)	Conversion after 12 h (%)	DEB distribution after 12 h				
				All isomers			m- / p- only**	
				meta	para	ortho	meta	para
H-MFI-45	-	1.7	0.5	61	39	0.0	61	39
LaNaY-72	3.1	6.6	4.4	63	33	4.0	66	34
LZY-62	2.3	7.8	4.0	63	33	4.0	66	34
LaNaY-72*	2.3	11	7.4	64	31	5.0	67	33
H-Beta-25	1.3	12	8.0	63	32	5.0	66	34
H-Beta-15	0.8	23	16	64	31	5.0	67	33
LZY-82	0.8	47	26	65	30	5.0	69	31
Thermodynamic equilibrium (at 180 °C)				54	31	15	64	36

* Catalyst activation at 250 °C

** Normalized distribution between meta- and para-isomer only

4.2 AMMONIA TEMPERATURE PROGRAMMED DESORPTION (NH_3-TPD)

Analyses were conducted at an external laboratory and were provided without absolute quantification of the desorbed ammonia signal. Consequently, the results are presented here for qualitative interpretation only.

4.2.1 TYPICAL RESULTS

Figure 4-22 depicts the typical trace for the TPD of ammonia for LaNaY-72. Desorption peaks are observed in the temperature ranges 100 °C – 300 °C (Peak A); 300 °C – 500 °C (Peak B) and > 500 °C (Peak C). Peak A in the TPD profiles is assigned to weakly adsorbed ammonia at surface hydroxyls (Rane et al., 1993, Karge et al., 1990) and other sites not typically associated with catalytic activity. Peak B is generally assigned to desorption of ammonia

from the strong, catalytically active, acid sites (Kapustin et al., 1988, Rane et al., 1993). Peak C is due to pairwise dehydroxylation of Brønsted acid sites (Karge et al., 1991) yielding water which is detected by the thermal conductivity detector of the TPD apparatus.

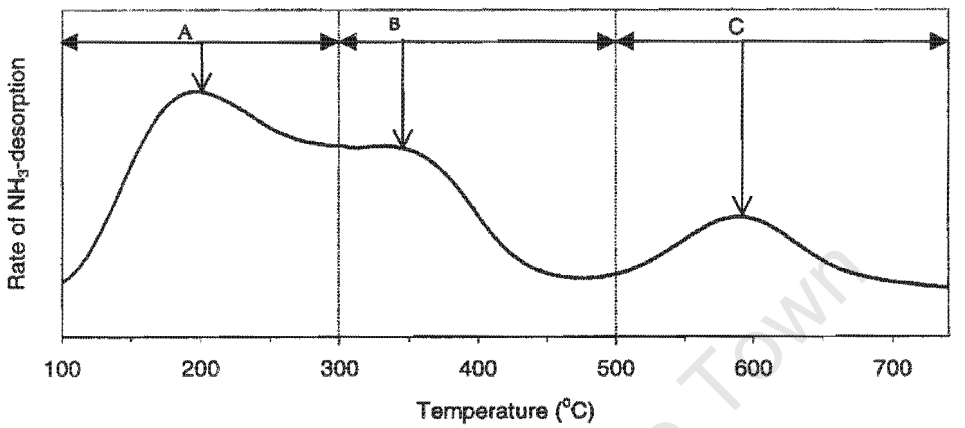

Figure 4-22 Typical NH_3-TPD trace for LaNaY-72 activated at 450 °C.

The TPD profiles obtained for the different zeolite samples used for the conversion of ethylbenzene are shown in Figures 4-23 to 4-26. A summary of the peak maximum temperatures for Peak B is presented in Table 5-1.

4.2.2 EFFECT OF ACTIVATION TEMPERATURE ON THE ACTIVITY OF LANAY-72

The NH_3-TPD results for the LaNaY-72 catalyst, Figure 4-23, show that the uptake of weakly adsorbed NH_3 increases dramatically when the activation temperature is increased from 250 °C to 450 °C similar to the findings of Weiss et al. (1997) for pyridine-TPD. As expected, the dehydroxylation peak at about 600 °C is not influenced by pretreatment at much lower temperature. The slightly higher B-peak maximum temperature for the sample activated at 250 °C is perhaps indicative of the expected stronger acidity of this sample versus that activated at 450 °C.

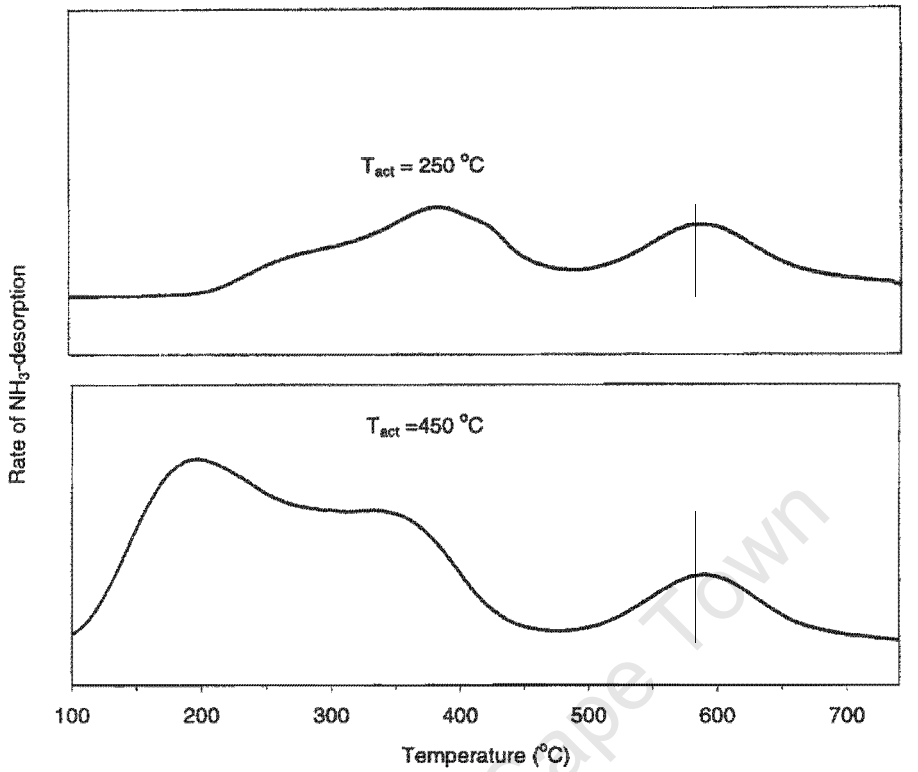

Figure 4-23 TPD traces for LaNaY-72 activated at 250 °C and 450 °C.

4.2.3 TPD TRACES FOR LINDE-Y ZEOLITE

For LZY samples (Figure 4-24), Peak A appears in a narrow temperature range (190+/-10 °C) and is of approximately the same magnitude, suggesting that for all samples the source of this adsorbed NH_3 is not related to structural protonic centers. Further support for this assignment comes from the fact that it is most prominent for the fully Na-exchanged LZY-52.

However, Peak B appearing for LZY-62 and LZY-82 at approximately 310 °C and 360 °C, respectively, is assigned to framework acidity (Rane et al., 1993). The significant shift to higher desorption temperature in the completely exchanged sample, LZY-82, indicates an increase in the strength of the Brønsted acid sites, as expected. Peak C is insignificant with LZY samples.

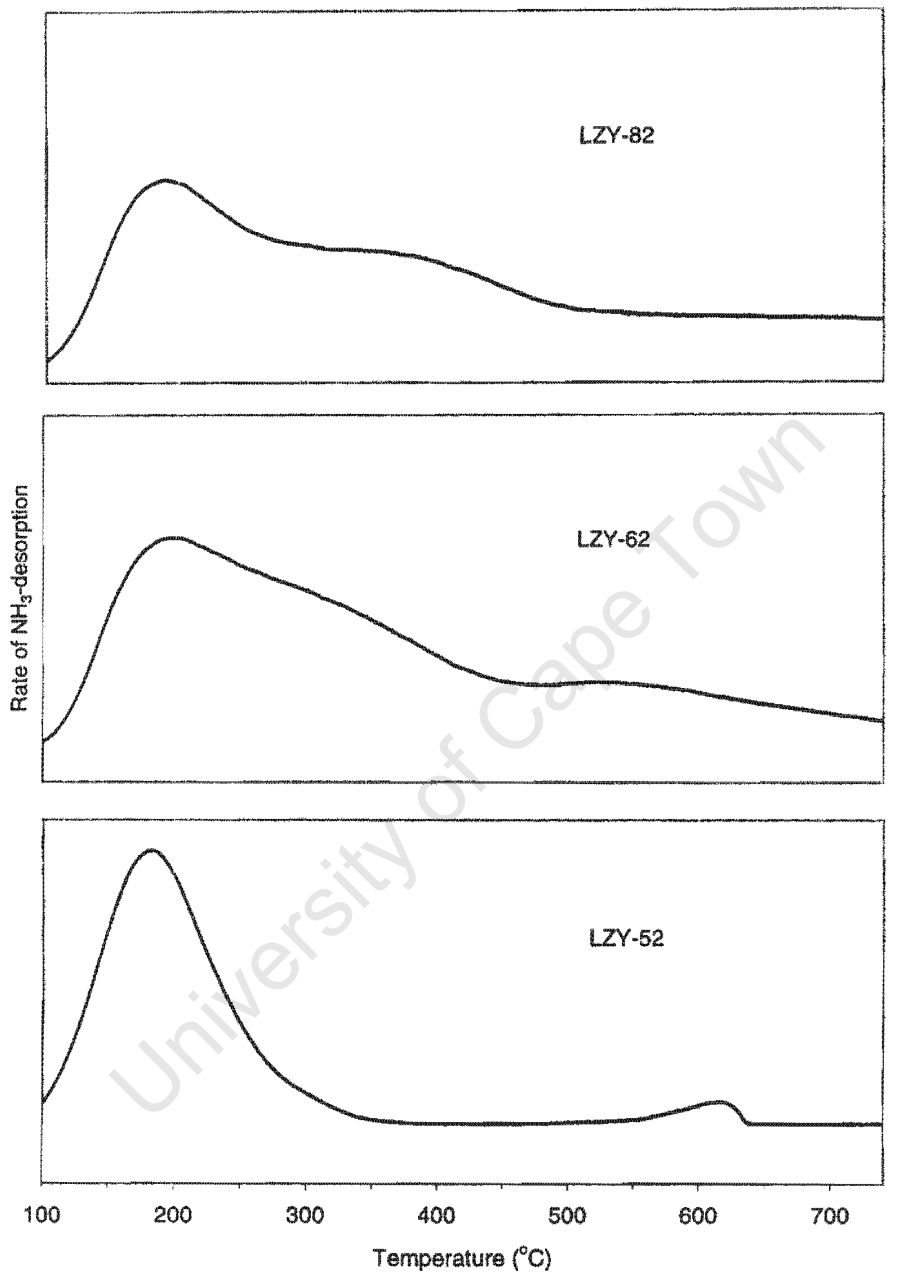

Figure 4-24 TPD traces for Linde-Y zeolite, all activated at 450 °C.

4.2.4 TPD TRACES FOR ZEOLITE BETA

Peak A in the TPD traces of the Beta zeolites (Figure 4-25) is associated with weak surface sites as per the situation for the LZY-types. Peak B is assigned to framework acidic sites. Consistent with expectations, more such acid sites are present for the lower Si/Al ratio catalyst, H-BEA-15, than for the H-BEA-25 sample. The apparent higher B-peak maximum temperature for H-BEA-25 may be ascribed to the effect of greater NH_3 readsorption during TPD due to the higher density of acid sites on this sample.

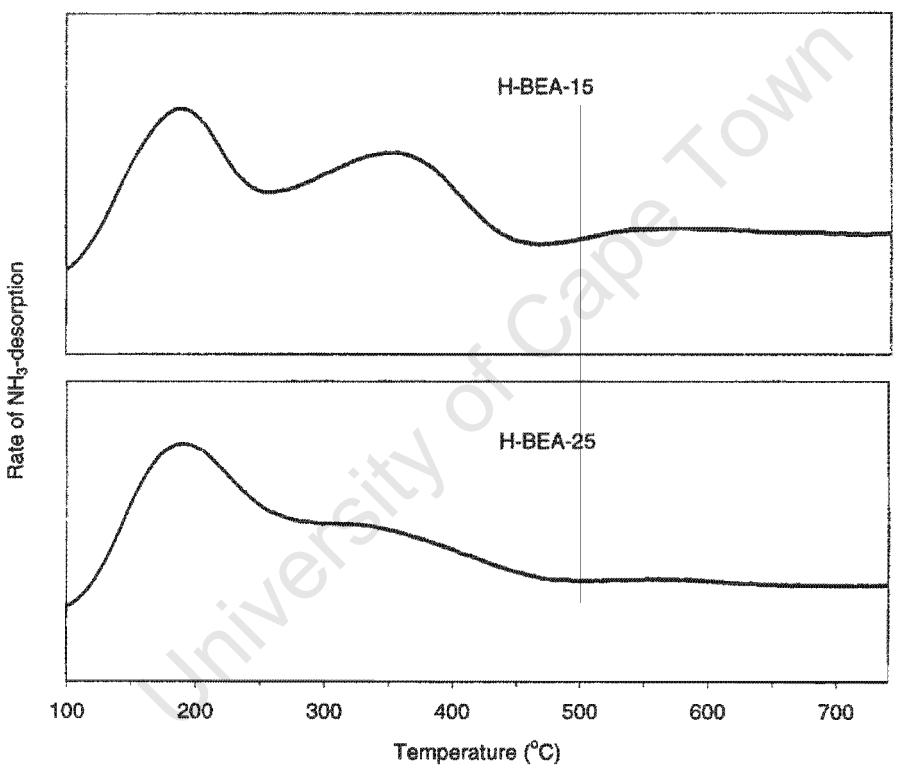

Figure 4-25 TPD traces for zeolite-Beta (Si/Al = 25 and 14.6) both activated at 450 °C

4.2.5 TPD TRACE FOR ZSM-5

Peak B in Figure 4-26 is ascribed to framework acidity, whereas peak A is associated with weakly adsorbing centres of insignificant catalytic activity.

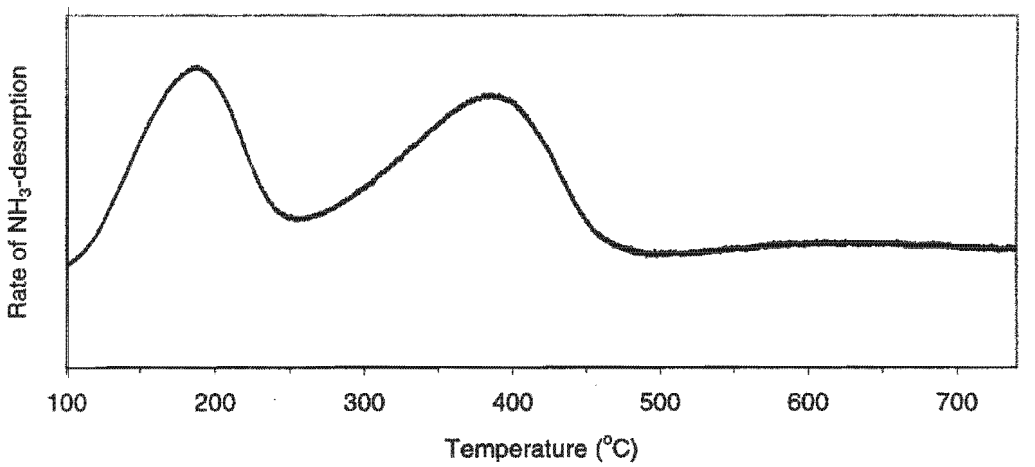

Figure 4-26 TPD trace for H-MFI-45 activated at 450 °C.

5 DISCUSSION

5.1 GENERAL

5.1.1 REPRODUCIBILITY OF EXPERIMENTS

A repeat experiment over LaNaY-72 showed acceptable reproducibility of conversion and isomer distribution. Time-on-stream behaviour is reproduced in significant detail as well (Figures 4-5 to 4-8).

5.1.2 CONSISTENCY WITH LITERATURE FINDINGS

All catalyst samples show the pertinent features of time-on-stream behaviour as expected (Weitkamp et al., 1986, Karge et al., 1994 and Weiss et al., 1997). Also, all catalysts show a long-term decline in activity during the quasi-steady state period. Large pore zeolites – LaNaY-72, LZY and H-BEA catalysts show a pronounced induction period; for the medium pore zeolite, H-MFI, there is no observable induction period (Figures 4-1, 4-14, 4-16 and 4-18 respectively).

The induction period shows the characteristic deficit of diethylbenzenes as compared to co-product benzene (Figure 4-3) and correspondingly, the diethylbenzene/benzene molar yield ratio increases from the beginning of the experiment to about 0.9 at the end of the induction period (Figure 4-4).

Consistent with literature findings, there is far less ortho-diethylbenzene than in thermodynamic equilibrium. The distribution between meta- and para-isomer is close to equilibrium during the quasi-steady state (Tables 4-2 to 4-5). The induction period shows enhanced para-selectivity.

The effect of reaction conditions, catalyst pretreatment and catalyst properties is as expected. As shown for LaNaY-72, increasing WHSV results in a decline in conversion as well as in a shorter induction period (Figure 4-11). High activation temperature (450 °C versus 250 °C) reduces the activity of the

catalyst thereby also extending the induction period (Figure 4-9). The carrier gas, either N_2 or H_2 has no effect on conversion or induction period. The effect of reaction conditions on isomer distributions is small (Figures 4-10 and 4-12).

The more active the catalyst, the shorter the induction period. This is particularly pronounced within series of the same zeolite type (Figures 4-9, 4-14, 4-16 and Table 4-6) and generally holds within the entire range of samples studied (Figure 5-1). These findings correspond to a general trend, which can be derived from the literature as well.

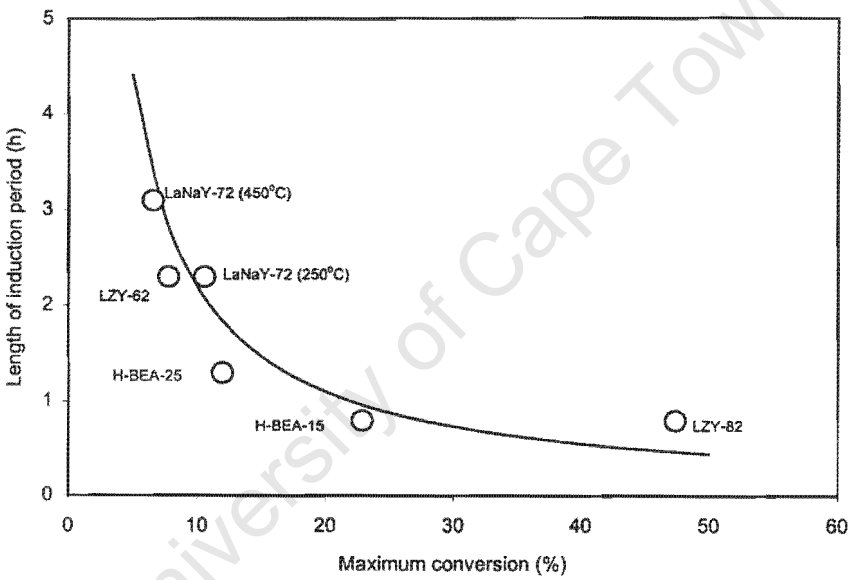

Figure 5-1 Relationship between length of induction period and maximum conversion

5.2 CORRELATION OF ETHYLBENZENE DISPROPORTIONATION PERFORMANCE WITH ACIDITY

5.2.1 DEFICIT OF DIETHYLBENZENES DURING THE INDUCTION PERIOD

For all the large pore zeolites employed in this study, a significant deficit of diethylbenzenes was observed during the induction period. This is consistent with literature and was explained by Weiss et al. (1997) to be due to the accumulation of dimers and trimers of ethylbenzene and diethylbenzenes in the pore system of large pore zeolites during the induction period, forming the catalytically active species in the zeolite (Figure 2-19). The amount of this deficit can be quantified as shown in Figure 5-2.

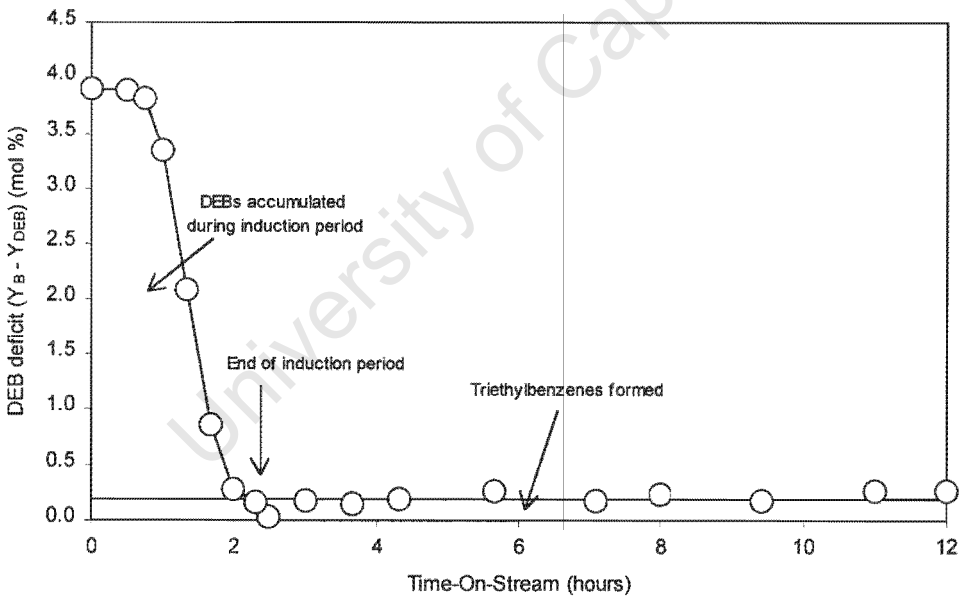

Figure 5-2 Quantification of the deficit of diethylbenzenes during the induction period (LZY-62, Experiment 7)

The integrated yield differences derived from plots like Figure 5-2, are given in Table 5-1 for the various catalyst samples. These yield differences have been suggested to represent the accumulation of diethylbenzenes on the catalyst and the quantities are thought to correlate with the number of accessible Brønsted acid sites (Weiss et al., 1997). Consequently, the magnitude of the diethylbenzene deficit during the induction period should show a strong dependence on Si / Al ratio and extent of sodium exchange and also, particularly in case of LaNaY zeolites, on activation temperature. However, Table 5-1 indicates that there is probably no correlation between the acidity of the catalysts and the diethylbenzene deficit for the experiments of this study. Figure 5-3 shows the diethylbenzene deficit as a function of the length of the induction period, which was found to be a strong indicator of activity (see Figure 5-1). As can be seen from the figure, there is no correlation between the length of induction period and the diethylbenzene deficit.

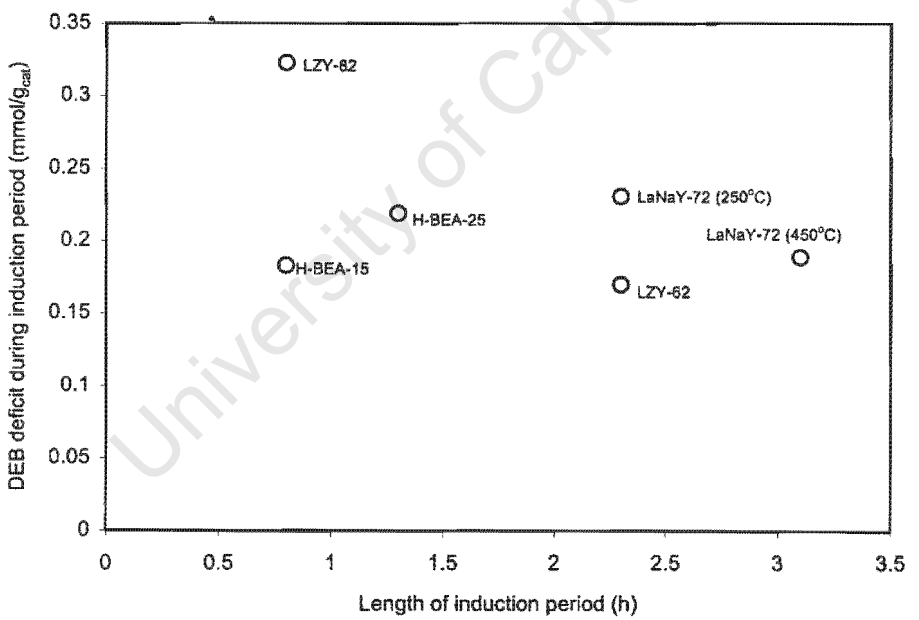

Figure 5-3 Relationship between diethylbenzene deficit during induction period and the length of the induction period.

Table 5-1 Relationship between zeolite acidity and ethylbenzene conversion.

Zeolite (activated at 450 °C)	Chemical Composition	T_{max} [4] °C	No. of acid sites [5] mmol/g_{cat}	DEB deficit [6] mmol/g_{cat}	TEB formed [7] mmol/g_{cat}	$t_{induction}$ [8] h
LaNaY-72 (450 °C)	$(La(OH))_{13.6}H_{13.6}Na_{15.8}[Al_{56.5}Si_{135.5}O_{384}]$ [2]	340	0.97	0.189	0.021	3.1
LaNaY-72 (250 °C) [1]	$(La(OH)_2)_{13.6}H_{27.1}Na_{15.8}[Al_{56.5}Si_{135.5}O_{384}]$ [3]	380	1.91	0.231	0.037	2.3
LZY-52	$Na_{33.4}[Al_{33.4}Si_{158.6}O_{384}]$	-	0.0	-	-	-
LZY-62	$Na_{5.8}H_{26.5}[Al_{32.3}Si_{159.7}O_{384}]$	330	1.86	0.170	0.012	2.3
LZY-82	$Na_{0.3}H_{29.8}[Al_{30.1}Si_{161.9}O_{384}]$	380	2.06	0.323	0.688	0.8
H-BEA-25 [9]	$H_{2.5}[Al_{2.5}Si_{61.5}O_{128}]$	350	0.64	0.219	0.006	1.3
H-BEA-15 [9]	$H_{4.1}[Al_{4.1}Si_{59.9}O_{128}]$	360	1.07	0.183	0.040	0.8
H-MFI-45 [9]	$H_{2.1}[Al_{2.1}Si_{93.9}O_{192}]$	390	0.36	-	-	-

[1] Catalyst activation at 250 °C;

[2] hydration of 1 of the 2 sites on La only assumed;

[3] complete hydration of sites assumed;

[4] Peak maximum temperature of the TPD B-peak;

[5] Estimated from chemical composition;

[6] Integrated yield(benzene-diethylbenzenes) from onset of experiment to $t_{induction}$;

[7] Integrated yield of triethylbenzenes from the onset of experiment to $t_{induction}$;

[8] At maximum conversion;

[9] Numbers 15, 25 and 45 indicate Si/Al atomic ratio here

However, the deficit of diethylbenzenes remains, albeit at a low level, even during the pseudo-steady state period (see Figure 4-3), during which the diethylbenzene to benzene molar ratio reaches an ultimate level of only 0.9 (Figure 4-4). This holds generally for all large pore zeolite samples and was found to be attributable to small amounts of polyethylbenzenes (mainly triethylbenzenes) which were observed in the product spectrum by GC (see chromatogram in Appendix 2). No lower carbon number fragments were observed, therefore no evidence was observed for a dealkylation-realkylation reaction mechanism (Figure 2-12) being operative for the experiments of this study.

Weiss et al. (1997) reported that for LaNaY-type zeolites an activation temperature above 250 °C results in a decrease of the catalytic activity and an increased length of the induction period. The results of this study, where the activity of the catalyst was almost halved when activated at 450 °C, support this finding (Table 5-1). Hence, it might be inferred that the (Lewis) acid sites resulting from the higher temperature activation process do not catalyse the disproportionation reaction to the same degree as do the Brønsted acid sites.

5.2.2 THE NUMBER OF ACID SITES

The number of acid sites refers to Brønsted acid sites and was derived from the chemical composition of the zeolites as given in Table 5-1. The number of Brønsted sites in the LaNaY-72 samples was estimated according to the Hirschler-Planck mechanism. Two sites per lanthanum ion were considered for samples activated at 250 °C, whereas for samples activated at 450 °C it was estimated that only one Brønsted site exists per lanthanum ion.

Figure 5-4 shows no clear correlation between the number of acid sites and the amount of diethylbenzene accumulated during the induction period.

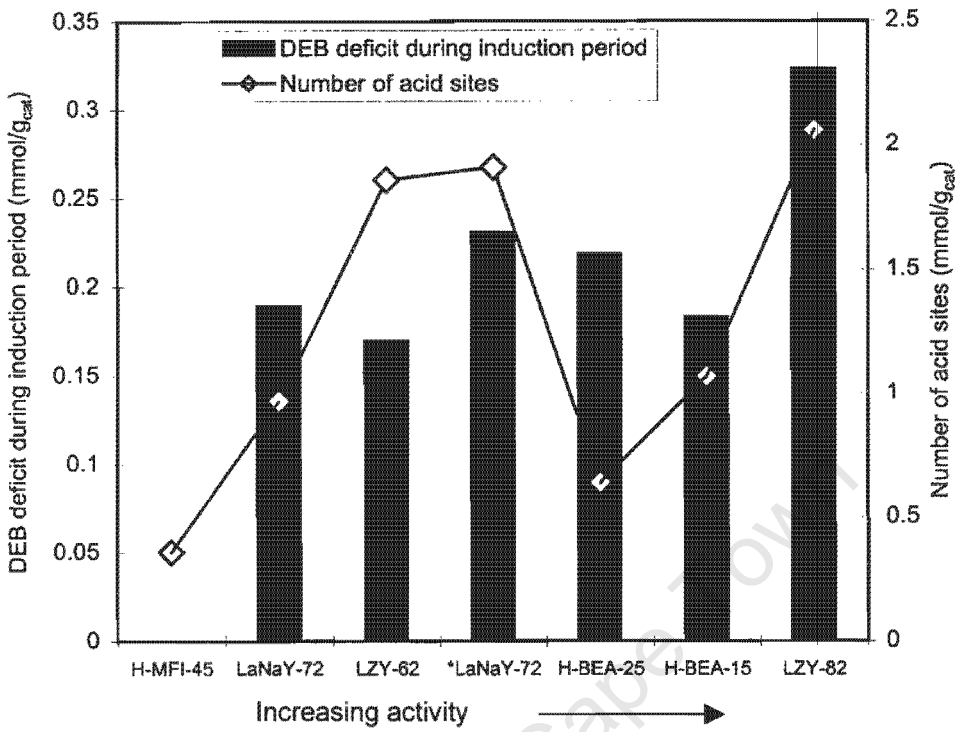

Figure 5-4 Diethylbenzene deficit and number of acid sites as a function of catalyst activity (*LaNaY-72 - catalyst activation at 250 °C)

From Figures 5-5 to 5-7, however, several distinct interrelations can be derived. In Figure 5-5, the length of the induction period is plotted as a function of acidity. Discriminating between sodium free samples (short induction period) and sodium containing samples (long induction period), two sets of data are apparent. The trend is the same for both data sets, viz. the higher the number of acid sites the shorter the induction period (the sodium containing samples, in rough approximation, have similar Na / Al ratios - see Table 5-1). This is pronounced in the case of the LZY samples, where the number of acid sites is almost unchanged by the presence of sodium (LZY-62 versus LZY-82; see the chemical composition of the unit cell, Table 5-1) but where the effect on the induction period is substantial.

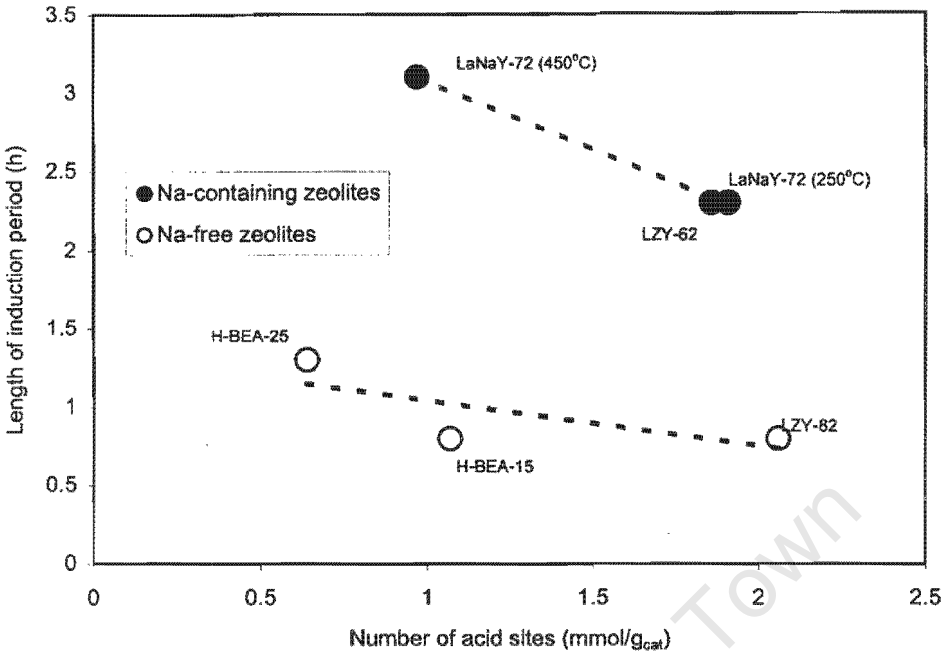

Figure 5-5 **Length of induction period as a function of the number of acid sites**

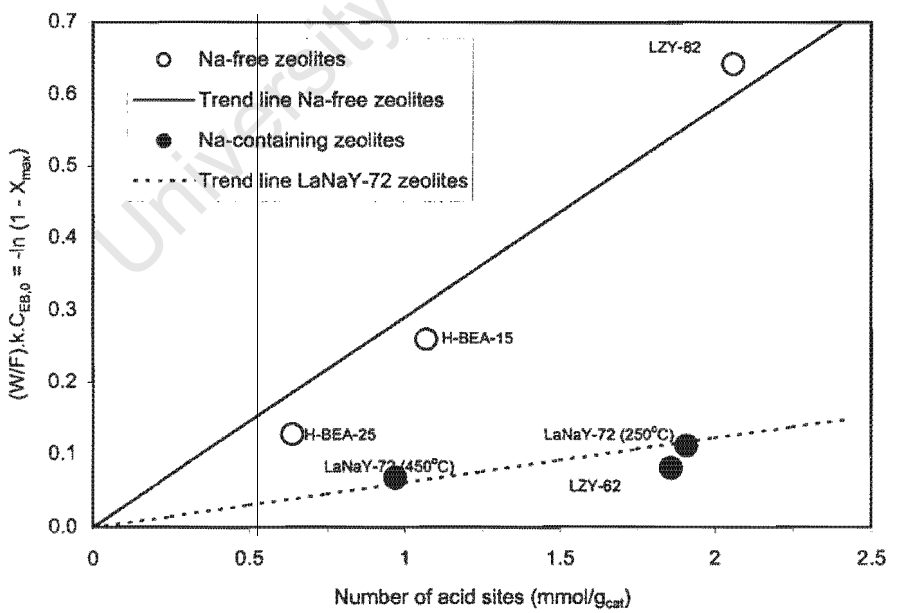

Figure 5-6 **Ethylbenzene conversion as a function of the number of acid sites**

Figure 5-6 shows a plot of the relative first order irreversible rate constant, $\ln(1/(1-X_{max}))$, as a function of the number of acid sites and reveals the same clear trends (see Appendix A3 for derivation). Again the relationship is distinct for the highly active H-zeolites versus that for the sodium-containing samples.

Weiss et al. (1997) found a pronounced difference in activity between LaNaY-72 and LaNaY-92 (Figure 5-7). This was considered not only to be caused by the somewhat higher lanthanum content (from 72 to 92 % of total ion exchange capacity), but also by an increase in the acid strength of the Brønsted sites in LaNaY-92 (H-MAS-NMR measurements). An alternative explanation or conclusion, however, was not given. From the above findings, sodium apparently not only reduces the number, i.e. quantity, of acid sites but also affects the activity of the remaining sites.

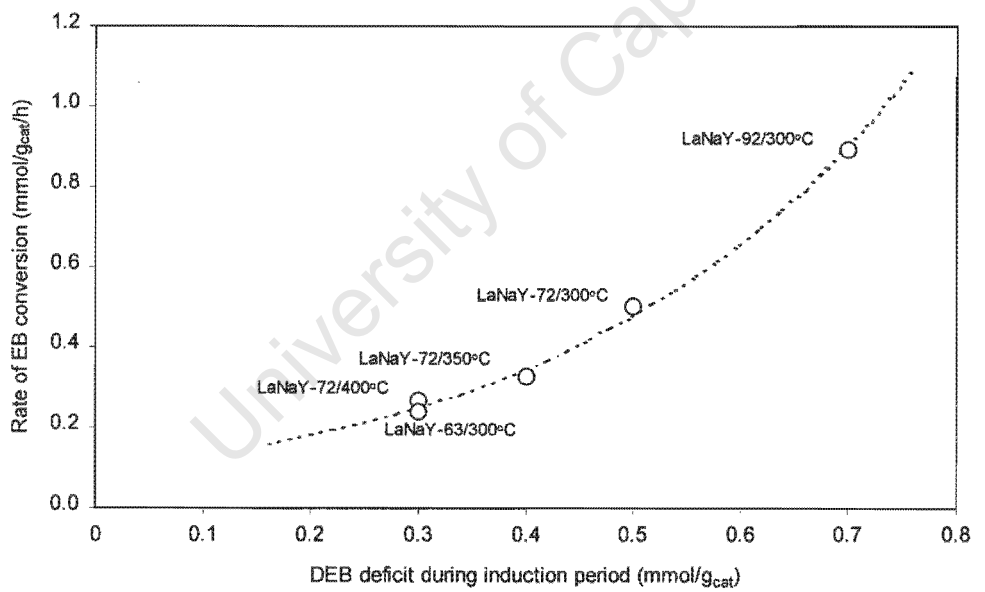

Figure 5-7 Relationship between the rate of ethylbenzene conversion and the deficit of diethylbenzenes during the induction period, both of which were evaluated when steady state was established. (Weiss et al., 1997). Temperatures refer to activation of samples

Figure 5-8 shows the deficit of diethylbenzene during the induction period versus the number of acid sites. Obviously, the accumulation of diethylbenzenes on the catalysts is not a function of the number of acid sites.

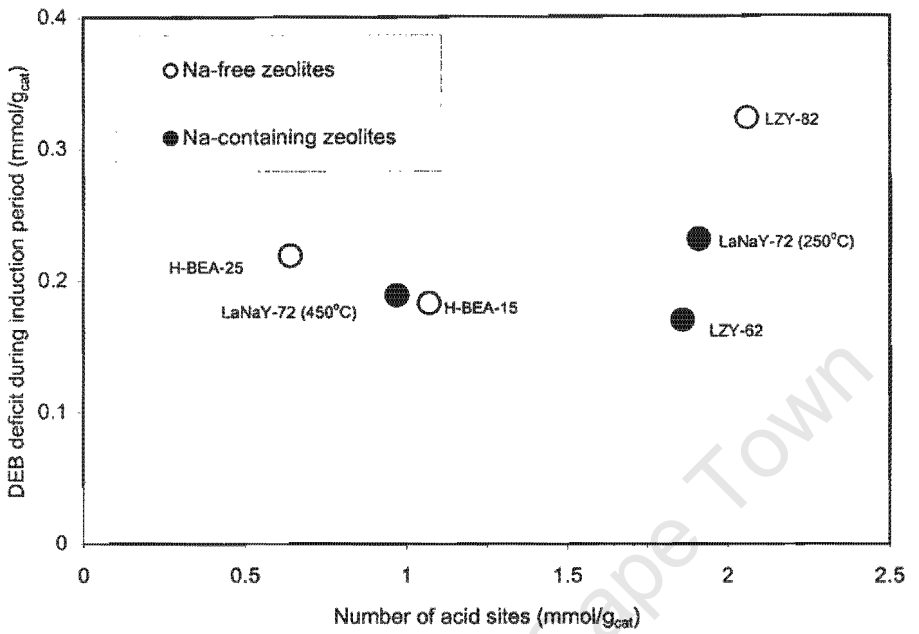

Figure 5-8 Deficit of diethylbenzene during the induction period as a function of the number of acid sites

5.3 ISOMER DISTRIBUTION

Diethylbenzene isomer distributions vary as a function of time-on-stream, as shown in Figures 4-2, 4-15, 4-17 and 4-19. A decline in the para-selectivity during the induction period and a corresponding increase in the ortho- and meta-selectivity are followed by an almost constant isomer distribution throughout the pseudo-steady state period.

Figure 4-21 and Tables 4-6 and 4-7 show that the ortho-diethylbenzene selectivity is far below the thermodynamic equilibrium level and the figures mentioned above show that no ortho-diethylbenzene is being formed at the very beginning of the induction period. In Figure 4-21 catalysts are ordered in

increasing activity during the quasi-steady state and it follows that the higher the activity, the higher the ortho-selectivity. It can be concluded that ortho-diethylbenzene is not a primary product of ethylbenzene disproportionation but is slowly produced via secondary isomerisation.

From Tables 4-6 and 4-7 it can be considered that the meta- and para-isomers approach equilibrium between one another. Figure 5-9 (closed symbols) shows that the para/(para + meta) ratio in the quasi-steady state follows the same trend for all the large pore zeolites investigated. At high conversion, i.e. with the more active samples, the para-content levels out at about 31%, which is considered to approach the thermodynamic equilibrium value of 36 %.

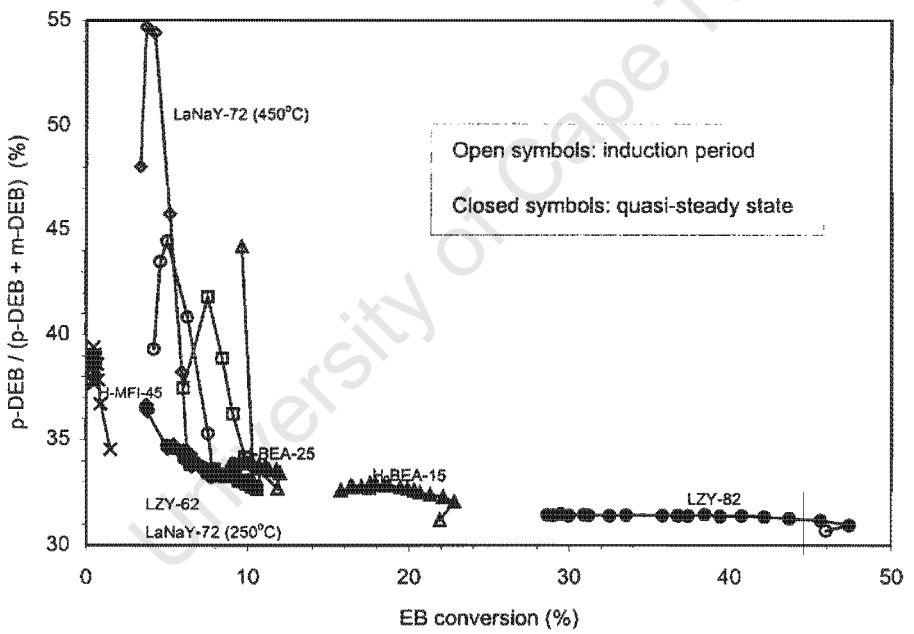

Figure 5-9 Isomer distribution in the diethylbenzene fraction from ethylbenzene disproportionation over various zeolites expressed in terms of para/(para+meta) ratio

At low conversion, i.e. low catalyst activity, there is more para-isomer. It may be concluded that the para-isomer is the kinetically preferred primary product once the catalytic system has been established (i.e. during the quasi-steady state period) which is subsequently isomerised via secondary reactions.

During the induction period, the para-selectivity is not a simple function of conversion (activity). This particular response is readily observed for the less active samples in Figure 5-10, which is an expanded view of Figure 5-9. As depicted in Figure 5-10, for the same conversion level, para-selectivity is much higher during the induction period than during the quasi-steady state period. Moreover, the para-selectivity passes through a maximum value at a point approximately mid-way through the induction period. This is best observed in Figure 5-11 where the para/(para + meta) ratio is shown as a function of the fractional induction period, i.e. as a function of time-on-stream normalised to the length of the induction period. The shapes of the curves coincide as do the positions of the maxima in para-selectivity.

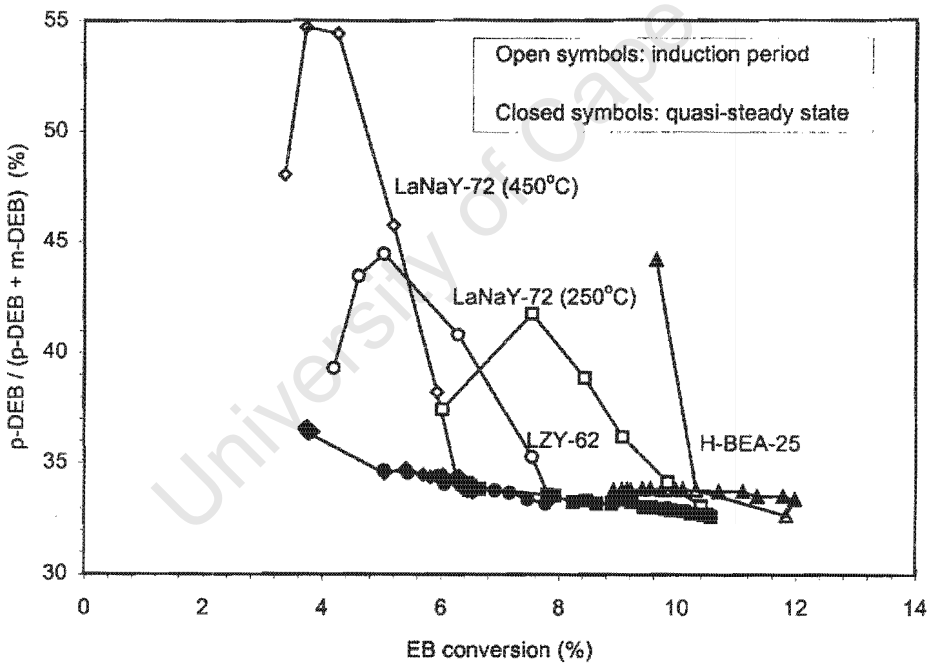

Figure 5-10 An expanded view of Figure 5-9 for the less active samples

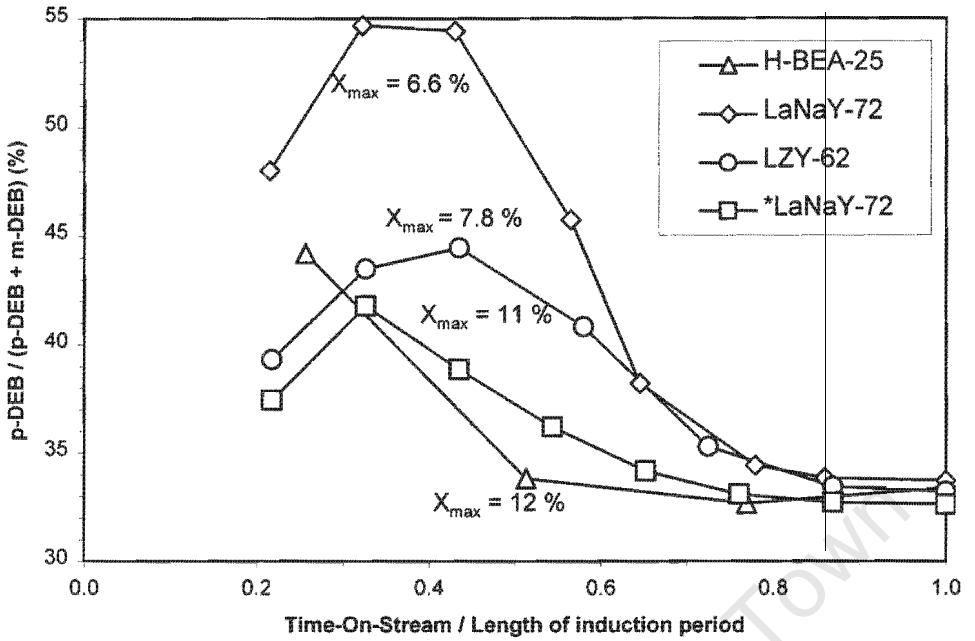

Figure 5-11 Para/(para+meta) ratios as a function of the fractional induction period (*LaNaY-72 - catalyst activation at 250 °C)

The explanation for these selectivity changes may possibly be found in selective and competitive adsorption phenomena occurring during the induction period, however, the present data is insufficient to expand upon this hypothesis.

No consistent correlation or trends were found between the peak temperature of the TPD B-peak (Table 5-1) and the diethylbenzene deficit and/or induction period, across all catalysts of this study.

6 CONCLUSION

The IZA suggested introducing the disproportionation of ethylbenzene as a test reaction for acid zeolites. This suggestion is mainly based on research done by Karge and Weitkamp and co-workers on a multiplicity of H-zeolites and on LaNaY-zeolites in particular, since the early 80s (Karge et al., 1982).

Experiments of this study qualitatively show the same features with respect to time-on-stream behaviour, activity, pore diameter and effect of reaction conditions. Large pore zeolites exhibit the characteristic time-on-stream behaviour in respect of an induction period of increasing activity and initial deficit of diethylbenzene, and a subsequent quasi-steady state of slowly declining activity. Various other general trends and correlations presented in the literature were also observed, e.g. shorter induction periods for increasing WHSV or increasing catalyst activity.

However, this study could not confirm that the diethylbenzene deficit during the induction period correlates with the number of accessible Brønsted acid sites, as has been claimed by Weiss et al. (1997).

Sodium containing (large pore) zeolites as well as lanthanum-sodium containing samples show much less activity per acid site versus sodium-free samples, already at Na/Al ratios around 0.25:1. Consequently, it is concluded that there is a qualitative effect of sodium on the remaining acid sites. With regard to diethylbenzene accumulation during the induction period, there are no differences at all between sodium-free and sodium-containing samples.

The isomer distribution in the diethylbenzene fraction indicates that ortho-diethylbenzene is not a primary product but is formed by secondary isomerisation, however, ortho-selectivity remained far below the thermodynamic equilibrium level for the reaction conditions of this study. Para-diethylbenzene seems to be the primary or kinetically preferred product. The quasi-steady state is characterised by an apparent approach of the

para/(para+meta) distribution to the thermodynamic equilibrium between these two isomers; the higher the activity of the catalyst, the closer the approach to equilibrium.

The behaviour of the para-diethylbenzene selectivity during the induction period is from an initially low para-selectivity via a rather high maximum value to an almost equilibrium distribution between meta and para when approaching maximum conversion and steady state. It is suggested that the selectivity during the induction period might be determined by competitive adsorption of the product isomers, however, data from this work is insufficient to further this hypothesis.

From the findings of this limited study, the disproportionation of ethylbenzene has not been shown to be a robust or simple test reaction for the characterisation of zeolite acidity, pore size and geometry across a range of zeolite materials, as has been previously suggested. The diethylbenzene deficit during the induction period was not found to correlate well with the catalyst acidity and further work will be needed in this laboratory to confirm the value of the test.

REFERENCES

Arsenova, N., H. Bludau, W. O. Haag, and H. G. Karge, Microporous and Mesoporous Materials **23** (1998) 1-10

Arsenova, N., W. O. Haag, and H. G. Karge, in Catalysis by Microporous Materials: Stud. Surf. Sci. Catal. **94** (1995) 441-448

Arsenova, N., W. O. Haag, and H. G. Karge, in Progress in Zeolites and Microporous Materials: Stud. Surf. Sci. Catal. **105** (1997) 1293-1300

Beck, J. S. and W. O. Haag, Handbook of Heterogeneous Catalysis, VCH, Weinheim, vol. **5** (1997) 2139

Benesi, H. A. and B. H. C. Winquist, Advances in Catalysis **27** (1978) 97

Bourdillon, G., C. Gueguen and M. Guisnet, Appl. Catal. **61** (1990) 123-139

Breck, D. W., Zeolite Molecular Sieves, Structure, Chemistry, and Use, Wiley, New York (1974) 29-185

Chen, N. Y., F. T. Degnan Jr. and C. M. Smith, Design and Application of Shape Selective Catalysts, VCH, New York (1994) 55-71

Chen, W., S. Jong, A. Pradhan, T. Lee, I. Wang, T. Tsai and S. J. Liu, Chinese Chem. Soc. **43** (1996) 305-313

Dwyer, J., Zeolite Microporous Solids: Synthesis, Structure, and Reactivity, (E. G. Derouane et al. (eds)), Kluwer, Dordrecht, The Netherlands (1992) 303-319

Ernst S. and J. Weitkamp, Catalysis and Adsorption by Zeolites, Stud. Surf. Sci. Catal. **65** (1991) 645 - 652

Emig, G. and R. Dittmeyer, Handbook of Heterogeneous Catalysis, VCH, Weinheim, vol **3** (1997) 1242-1252

Fasol, R. E., MSc. Thesis, Department of Chemical Engineering, University of Cape Town, (1983) 43-44

Forni, L., S. Amarilli, G. Bellussi, C. Perego and A. Carati, Appl. Catal. A: General, **103** (1993) 173-182

Gilson, J. P., in Zeolite Microporous Solids: Synthesis, Structure, and Reactivity, (E. G. Derouane et al. (eds)), Kluwer, Dordrecht, The Netherlands (1992), 19-48

Hickson, D. A. and S. M. Csicsery, J. Catal., **10** (1968) 27-33

Jansen, J. C., in Introduction to Zeolite Science and Practice, Stud. Surf. Sci. Catal., **58** (1991) 77-136

Kaeding, W. W., J. Catal. **95** (1985) 512-519

Kaeding, W. W., C. Chu, L. B. Young and S. A. Butter, J. Catal., **69** (1981) 392-398

Kapustin, G. I., T. R. Brueva, A. L. Klyachko, S. Beran and B. Wichterlova, Appl. Catal. **42** (1988) 239-246

Karge, H. G., in Zeolite Microporous Solids: Synthesis, Structure, and Reactivity, (E. G. Derouane et al. (eds)), Kluwer, Dordrecht, The Netherlands (1992) 303-319

Karge, H. G., and E. Boldingh, Catal. Today, **3** (1988) 379-386

Karge, H. G., M. Hunger, M. Weihe, U. Weiss and J. Weitkamp, in Progress in Zeolites and Microporous Materials: Stud. Surf. Sci. Catal. **105** (1997) 973-980

Karge, H. G. and J. Ladebeck, Catalysis by Zeolites: Stud. Surf. Sci. Catal. **5** (1980) 151-159

Karge, H. G, J. Ladebeck, Z. Sarbak and K. Hatada, Zeolites **2** (1982) 94-102

Karge, H. G., K. Hatada, Y. Zhang and R. Fiedorow, Zeolites **3** (1983) 13-21

Karge, H. G., S. Ernst, M. Weihe, U. Weiss, and J. Weitkamp, in Zeolites and Related microporous materials: State of the Art, Stud. Surf. Sci. Catal. **84** (1994) 1805-1812

Karge, H. G. and V. Dondur, J. Phys. Chem. **94** (1990) 765-772

Karge, H. G., V. Dondur, and J. Weitkamp, J. Phys. Chem. **95** (1991) 283-288

Kärger, J. and D. M. Ruthven, Diffusion in Zeolites and other Microporous Materials, Wiley, New York, (1992) Chapter 1-2 and 5-16

Klemm, E., H. Scheidat, and G. Emig, Chem. Eng. Sci. **52** (1997) 2757-2768

Klemm, E., J. Wang, and G. Emig, Chem. Eng. Sci. **52** (1997) 3173-3182

Martens, J. A. and P. A. Jacobs, in Handbook of Heterogenous Catalysis, VCH, Weinheim, vol. **5** (1994) 1137-1148

Meier, W. H., and D.H. Olson and Ch. Baerlocher, Atlas of Zeolite Structure Types, 4th ed, Butterworth, New York, (1996)

Moscou, L., in Introduction to Zeolite Science and Practice, Stud. Surf. Sci. Catal. **58** (1991) 1-12

Philippou, A. and M. W. Anderson, J. Catal. **167** (1997), 266-272

Rane, S. J. and D. K. Chakrabarty, Appl. Catal. A: General, **93** (1993) 191-202

Rhodes, N. P. and R. Rudham, J. Chem. Soc. Faraday Trans. I. **89** (1993) 2551-2557

Rohrbaugh W. J. and E. L. Wu, Dev. Am. Chem. Soc. (1989) 279-302

Santilli, D. S. and B. C. Gates, in Handbook of Heterogenous Catalysis, VCH, Weinheim, vol. **5** (1994) 1123-1136

Santilli, D. S., J. Catal. **99** (1986) 327-334

Schulz, H., and S. Nehren, Erdöl und Kohle, **39** (1986) 93

Smith, J. M. and H. C. van Ness, Introduction to Chemical Engineering Thermodynamics, 4th ed. Mc GrawHill. Chapter 15 (1987)

Stull D. R., E. Westrum Jr., G. C. Sinke, The Thermodynamics of Organic Compounds, Wiley, New York, (1969)

Szostak R., Molecular Sieves – Principles of Synthesis and Identification, Van Nostrand Reinhold, New York, (1989) 92-96 284-287 518-527

Uytterhoeven, J. B., L. G. Christner and W. K. Hall, J. Phys. Chem. **69** (1968) 2117-2123

van Koningsveld, H., in Introduction to Zeolite Science and Practice, Stud. Surf. Sci. Catal. **58** (1991) 35-76

van Hooff, J. H. C. and J. W. Roelofsen, Introduction to Zeolite Science and Practice, Stud. Surf. Sci. Catal. **58** (1991) 214-283

Vedrine, J. C., Zeolite Microporous Solids: Synthesis, Structure, and Reactivity, (E. G. Derouane et al. (eds)), Kluwer, Dordrecht, The Netherlands, (1992) 107-131

Weitkamp, J., Private communication to the catalysis commission of the International Zeolite Association, (1994)

Weitkamp, J., S. Ernst, Jacobs, A. and H. G. Karge, Erdöl und Kohle, **39** (1986) 13-18

Weiss, U., H. G. Karge, M. Hunger, M. Weihe and J. Weitkamp, in Progress in Zeolites and Microporous Materials: Stud. Surf. Sci. Catal. **105** (1997) 973-980

A-1 CATALYSTS SUPPLIED AND EXPERIMENTS CONDUCTED

Catalytic experiments conducted

Exp. No.	Catalyst Type	Si/Al Ratio	W_{cat} (mg)	Carrier Gas	T_{rxn} °C	T_{act} °C	(%) NH_4 Exch.	(%) La Exch.
1	LaNaY-72	2.4	290	Nitrogen	180	250	-	72
2*	LaNaY-72	2.4	290	Nitrogen	180	250	-	72
3	LaNaY-72	2.4	290	Nitrogen	180	450	-	72
4	LaNaY-72	2.4	290	Hydrogen	180	250	-	72
5	LaNaY-72	2.4	145	Nitrogen	180	250	-	72
6	LZY-82	5.38	290	Ntrogen	180	450	99	-
7	LZY-62	4.94	290	Nitrogen	180	450	82	-
8	LZY-52	4.74	290	Nitrogen	180	450	0	-
9	H-BEA-15**	14.6	290	Nitrogen	180	450	-	-
10	H-BEA-25**	25	290	Nitrogen	180	450	-	-
11	H-MFI-45**	45	290	Nitrogen	180	450	-	-

* Repeat of experiment 1

** Numbers 15, 25 and 45 indicate Si / Al atomic ratio here

Exp. No. = Experiment number

Si/Al = Silicon to aluminium molar ratio

W_{cat} = Mass of catalyst loaded into the reactor

T_{rxn} = Reaction temperature

T_{act} = Activation temperature

(%) NH_4 Exch. = percentage ammonium exchange level

(%)La Exch. = percentage lanthanum exchange level

A-2 EXPERIMENTAL DATA

Data Work-up

A product chromatogram and analysis is shown below.

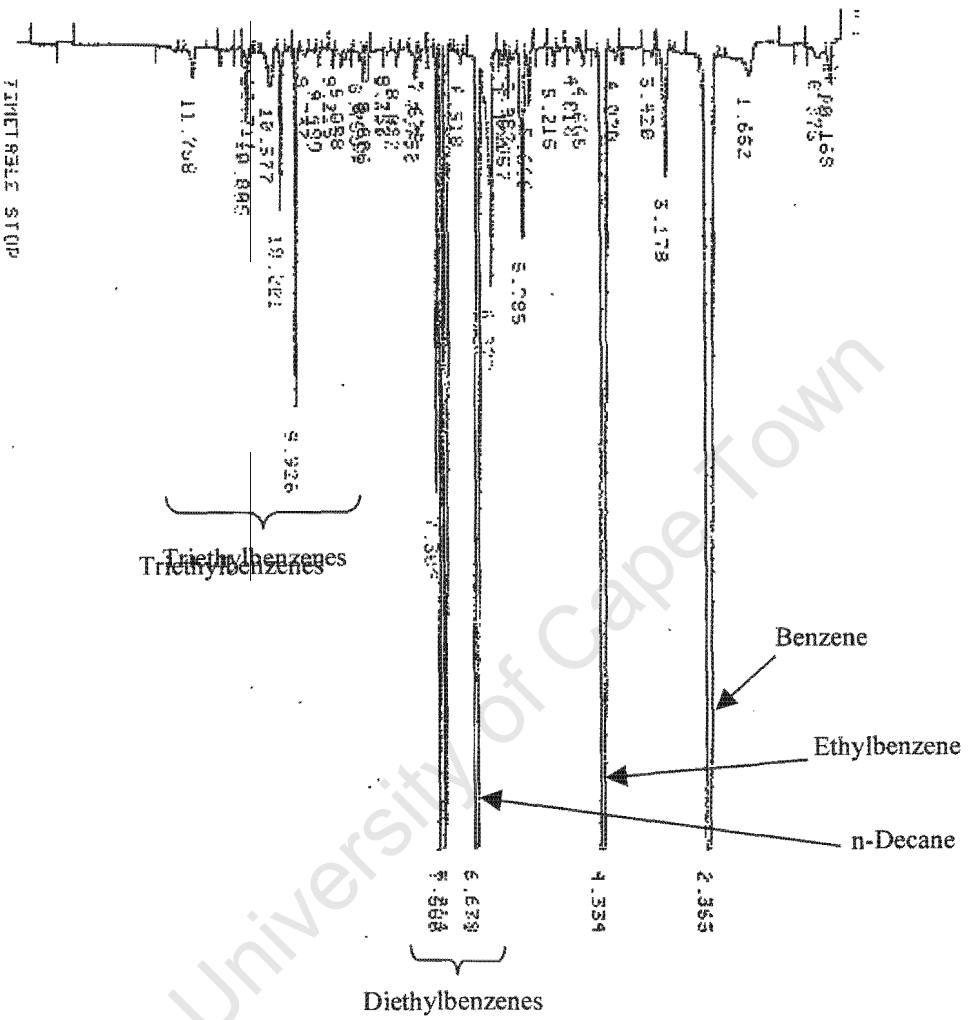

The molar yields of benzene (Y_B) and diethylbenzenes (Y_{DEB}) are calculated from the areas (A_i) of the peaks in the gas chromatogram according to the definition by the IZA (Weitkamp, 1994):

$$Y_B = \frac{A_B / CN_B}{A_B / CN_B + A_{DEB} / CN_{DEB} + A_{EB} / CN_{EB}} \qquad (1)$$

$$Y_{DEB} = \frac{A_{DEB}/CN_{DEB}}{A_B/CN_B + A_{DEB}/CN_{DEB} + A_{EB}/CN_{EB}} \quad (2)$$

where subscripts are

B = Benzene; EB = EthylBenzene; DEB = DiEthylBenzene

A_i = Peak area of compound i in the gas chromatogram;

CN_i = Number of carbon atoms in compound i

Ethylbenzene conversion (X_{EB}) is calculated from the sum of the yields of benzene and diethylbenzenes (Weitkamp et al., 1994):

$$X_{EB} = Y_B + Y_{DEB} \quad (3)$$

The distribution of the DEB isomers with respect to the total DEB product are calculated from the areas of the peaks in the gas chromatogram according to:

$$DEB\_distribution = \frac{A_i}{A_{m-DEB} + A_{p-DEB} + A_{o-DEB}} \quad (4)$$

The molar yield ratio of diethylbenzenes to benzene is calculated as follows:

$$\frac{Y_{DEB}}{Y_B} = \frac{A_{DEB}/CN_{DEB}}{A_B/CN_B} \quad (5)$$

A carbon balance was performed for each sample using equation 6 based on the internal standard n-decane:

$$C_{Total} = \frac{\left(\frac{\sum_i A_i - A_{n-Decane}}{A_{n-Decane}}\right)_{Reactor}}{\left(\frac{\sum_i A_i - A_{n-Decane}}{A_{n-Decane}}\right)_{Bypass}} \quad (6)$$

$\sum_i A_i$ includes all impurities of the feed in case of the bypass sample and all impurities of the feed plus all products in case of the reactor sample. The closer C_{Total} is to 1, the better the total carbon mass balance.

Calculation of WHSV

Ethylbenzene was fed using a saturator and N_2 carrier gas. Vapour pressure is calculated from Antoine equation (Antoine constants taken from Reklaitis 1983):

$$P_{EB}^{sat} = \exp\left(13.9698 - \frac{3257.17}{T_{sat} - 61.0096}\right)$$

where T_{sat} is in K and P_{EB} is in kPa

Assuming ideal gas behaviour, the molar flowrate of ethylbenzene is calculated is estimated as follows:

$$\dot{n} = \frac{P_{EB}^{sat} \dot{V}_{EB}}{RT}$$

EXPERIMENTAL DATA TABLES

Experiment 1

LaNaY-72 catalyst; $W_{cat.}$ = 290mg, T_{act} = 250°C, nitrogen carrier gas

By-pass peak areas: $A_{Ethylbenzene}$ 4032638

$A_{n\text{-}Decane}$ 893013

TOS	Peak area of compounds, A_i						A_i / N_i					Yield (mol%)		Y-ratio	Isomer distribution(%			X(%)	C(%)
hours	B	EB	n-C10	m-DEB	p-DEB	o-DEB	B	EB	m-DEB	p-DEB	o-DEB	B	DEBs	DEBs/B	m-DEB	p-DEB	o-DEB		Balance
0.5	200058	4425174	957981	13047	7810	0	33343	553147	1305	781	0	5.67	0.35	0.06	62.6	37.4	0.0	6.0	107
0.8	220145	4092838	890389	28604	20531	990	36691	511605	2860	2053	99	6.63	0.91	0.14	57.1	41.0	2.0	7.5	109
1.0	251605	4716157	1039361	73497	46727	2897	41934	589520	7350	4673	290	6.51	1.91	0.29	59.7	38.0	2.4	8.4	108
1.3	176257	3461069	771439	85578	48546	3844	29376	432634	8558	4855	384	6.17	2.90	0.47	62.0	35.2	2.8	9.1	108
1.5	210045	4303242	961732	150977	78327	7871	35008	537905	15098	7833	787	5.87	3.98	0.68	63.7	33.0	3.3	9.8	109
1.8	197514	4088930	917366	170312	84249	9995	32919	511116	17031	8425	1000	5.77	4.64	0.80	64.4	31.8	3.8	10.4	110
2.0	234287	5017219	1137603	223159	108529	14327	39048	627152	22316	10853	1433	5.57	4.94	0.89	64.5	31.4	4.1	10.5	109
2.3	208234	4490154	1027680	203986	98721	14005	34706	561269	20399	9872	1401	5.53	5.05	0.91	64.4	31.2	4.4	10.6	108
2.5	193275	4242173	976699	192385	93560	13949	32213	530272	19239	9356	1395	5.44	5.06	0.93	64.2	31.2	4.7	10.5	107
2.8	184452	4017216	917156	178999	87038	13083	30742	502152	17900	8704	1308	5.48	4.98	0.91	64.1	31.2	4.7	10.5	108
3.0	228313	5175824	1202470	229233	111665	16932	38052	646978	22923	11167	1693	5.28	4.96	0.94	64.1	31.2	4.7	10.2	106
3.5	217415	4973379	1142409	215662	105662	16021	36236	621672	21566	10566	1602	5.24	4.88	0.93	63.9	31.3	4.7	10.1	107
4.0	185420	4361002	1005918	185176	90883	13857	30903	545125	18518	9088	1386	5.11	4.79	0.94	63.9	31.3	4.8	9.9	106
4.5	215399	5087696	1165074	211154	104004	15893	35900	635962	21115	10400	1589	5.09	4.70	0.92	63.8	31.4	4.8	9.8	107
5.0	196749	4796560	1094893	194459	95989	14647	32792	599570	19446	9599	1465	4.95	4.60	0.93	63.7	31.5	4.8	9.5	107
5.5	193428	4737907	1081558	188131	92846	14049	32238	592238	18813	9285	1405	4.93	4.51	0.92	63.8	31.5	4.8	9.4	107
6.0	214750	5452605	1241569	213062	106329	15956	35792	681576	21306	10633	1596	4.77	4.47	0.94	63.5	31.7	4.8	9.2	107
6.5	190933	4862576	1103432	183702	92044	13724	31822	607822	18370	9204	1372	4.76	4.33	0.91	63.5	31.8	4.7	9.1	107
7.0	174974	4527965	1004111	169397	85268	12719	29162	565996	16940	8527	1272	4.69	4.30	0.92	63.4	31.9	4.8	9.0	110
7.5	187454	4831181	1100508	176845	87977	12812	31242	603898	17685	8798	1281	4.71	4.19	0.89	63.7	31.7	4.6	8.9	107
8.0	166223	4513789	1017061	162981	81085	11880	27704	564224	16298	8109	1188	4.49	4.14	0.92	63.7	31.7	4.6	8.6	107
8.5	165043	4633178	1058798	165022	82548	12196	27507	579147	16502	8255	1220	4.35	4.11	0.94	63.5	31.8	4.7	8.5	106
9.0	177839	5080643	1148163	174434	86996	12642	29640	635080	17443	8700	1264	4.28	3.96	0.92	63.6	31.7	4.6	8.2	107
10.5	183260	5435184	1227593	176833	89334	12763	30543	679398	17683	8933	1276	4.14	3.78	0.91	63.4	32.0	4.6	7.9	106
11.0	188812	5701901	1292814	183031	92635	13162	31469	712738	18303	9264	1316	4.07	3.74	0.92	63.4	32.1	4.6	7.8	106
18.3	108079	3828320	846038	101534	51996	7026	18013	478540	10153	5200	703	3.51	3.13	0.89	63.2	32.4	4.4	6.6	107
18.7	92775	3353432	742177	89129	45592	6205	15463	419179	8913	4559	621	3.45	3.14	0.91	63.2	32.4	4.4	6.6	107
19.2	84082	3060850	670437	79228	40466	5454	14014	382606	7923	4047	545	3.43	3.06	0.89	63.3	32.3	4.4	6.5	108
19.7	62574	2357597	516729	62206	31926	4385	10429	294700	6221	3193	439	3.31	3.13	0.94	63.1	32.4	4.5	6.4	108
20.3	60680	2189682	479007	56201	28972	3947	10113	273710	5620	2897	395	3.45	3.04	0.88	63.1	32.5	4.4	6.5	108
21.0	67615	2479037	545270	63576	32862	4413	11269	309880	6358	3286	441	3.40	3.04	0.89	63.0	32.6	4.4	6.4	108
21.7	68586	2549518	566240	64471	33343	4423	11431	318690	6447	3334	442	3.36	3.00	0.89	63.1	32.6	4.3	6.4	106
22.3	73353	2693288	619262	69076	35758	4738	12226	336661	6908	3576	474	3.40	3.04	0.90	63.0	32.6	4.3	6.4	103
24.0	53704	1950542	430544	49304	25509	3415	8951	243818	4930	2551	342	3.43	3.00	0.87	63.0	32.6	4.4	6.4	107
24.5	45445	1661307	366034	41770	21595	2840	7574	207663	4177	2160	284	3.41	2.98	0.87	63.1	32.6	4.3	6.4	107

Experiment 2 (repeat of experiment 1)

LaNaY-72 catalyst; $W_{cat.}$ = 290mg, T_{act} = 250°C, nitrogen carrier gas

By-pass peak areas: $A_{Ethylbenzene}$ 3235518
$A_{n\text{-}Decane}$ 735529

TOS	Peak area of compounds, A_i						A_i / N_i					Yield (mol%)		Y-ratio	Isomer distribution(%			X(%)	C(%)
hours	B	EB	n-C10	m-DEB	p-DEB	o-DEB	B	EB	m-DEB	p-DEB	o-DEB	B	DEBs	DEBs/B	m-DEB	p-DEB	o-DEB		Balance
0.5	251062	4301066	1024285	3832	3177	0	41844	537633	383	318	0	7.21	0.12	0.02	54.7	45.3	0.0	7.3	99
1.0	296691	4390566	1101348	34255	22954	1026	49449	548821	3426	2295	103	8.19	0.96	0.12	58.8	39.4	1.8	9.1	95
1.5	280317	4806202	1265562	81661	43277	3691	46720	600775	8166	4328	369	7.07	1.95	0.28	63.5	33.6	2.9	9.0	91
2.0	50683	1259101	297923	50374	23014	2268	8447	157388	5037	2301	227	4.87	4.36	0.90	66.6	30.4	3.0	9.2	103
2.5	279157	5737920	1373312	327541	162547	24566	46526	717240	32754	16255	2457	5.71	6.31	1.11	63.6	31.6	4.8	12.0	105
3.0	209822	4461130	1092838	216520	105457	16445	34970	557641	21652	10546	1645	5.58	5.40	0.97	64.0	31.2	4.9	11.0	102
3.5	202888	4192514	965074	196549	96382	14980	33815	524064	19655	9638	1498	5.74	5.23	0.91	63.8	31.3	4.9	11.0	108
4.0	211456	4812640	1134210	209106	102136	15621	35243	601580	20911	10214	1562	5.26	4.88	0.93	64.0	31.2	4.8	10.1	104
5.5	225932	5264736	1243406	224514	110708	16829	37655	658092	22451	11071	1683	5.15	4.82	0.93	63.8	31.4	4.8	10.0	104
6.0	234635	5530851	1318740	231290	114074	17202	39106	691356	23129	11407	1720	5.10	4.73	0.93	63.8	31.5	4.7	9.8	103
7.0	209448	5226952	1233834	209608	103833	15619	34908	653244	20961	10383	1562	4.84	4.56	0.94	63.7	31.6	4.7	9.4	103
8.0	184346	4796115	1124877	184872	91909	13717	30724	599514	18487	9191	1372	4.66	4.41	0.95	63.6	31.6	4.7	9.1	104
8.5	138814	3666200	846335	136650	67825	9977	23136	458275	13665	6783	998	4.60	4.26	0.93	63.7	31.6	4.7	8.9	105
9.0	198014	5381965	1259842	198649	99197	14691	33002	672746	19865	9920	1469	4.48	4.24	0.95	63.6	31.7	4.7	8.7	104
9.5	175618	4941930	1155979	178711	89237	13059	29270	617741	17871	8924	1306	4.34	4.16	0.96	63.6	31.8	4.6	8.5	103
10.0	162716	4618048	1085243	164488	82381	12152	27119	577256	16449	8238	1215	4.30	4.11	0.96	63.5	31.8	4.7	8.4	103
10.5	168565	4732435	1104831	167926	83198	12094	28094	591554	16793	8320	1209	4.35	4.07	0.94	63.8	31.6	4.6	8.4	104
11.0	132352	3886392	921933	134416	67472	9748	22059	485799	13442	6747	975	4.17	4.00	0.96	63.5	31.9	4.6	8.2	102
11.5	201048	5880179	1368565	200692	101005	14607	33508	735022	20069	10101	1461	4.19	3.95	0.94	63.4	31.9	4.6	8.1	104
12.0	175323	5164848	1193868	175106	87508	12568	29221	645606	17511	8751	1257	4.16	3.92	0.94	63.6	31.8	4.6	8.1	104
13.0	167753	5063408	1201756	167224	84316	12221	27959	632926	16722	8432	1222	4.07	3.84	0.94	63.4	32.0	4.6	7.9	101
14.0	150058	4558042	1053900	145622	73554	10390	25010	569755	14562	7355	1039	4.05	3.72	0.92	63.4	32.0	4.5	7.8	104

Experiment 3

LaNaY-72 catalyst; $W_{cat.}$ = 290mg, T_{act} = 450°C, nitrogen carrier gas

By-pass peak areas: $A_{Ethylbenzene}$ 6438128
$A_{n\text{-}Decane}$ 1320414

TOS	Peak area of compounds, A_i						A_i / N_i					Yield (mol%)		Y-ratio	Isomer distribution(%			X(%)	C(%)
hours	B	EB	n-C10	m-DEB	p-DEB	o-DEB	B	EB	m-DEB	p-DEB	o-DEB	B	DEBs	DEBs/B	m-DEB	p-DEB	o-DEB		Balance
0.7	125870	4885725	1101978	1524	1409	0	20978	610716	152	141	0	3.32	0.05	0.01	52.0	48.0	0.0	3.4	101
1.0	126819	4623037	1054748	5380	6495	0	21137	577880	538	650	0	3.52	0.20	0.06	45.3	54.7	0.0	3.7	100
1.3	111352	3987454	907504	16215	19355	0	18559	498432	1622	1936	0	3.57	0.68	0.19	45.6	54.4	0.0	4.2	101
1.8	142037	5134723	1168740	61431	51809	1096	23673	641840	6143	5181	110	3.50	1.69	0.48	53.7	45.3	1.0	5.2	102
2.0	133273	4784749	1109310	94140	58257	2311	22212	598094	9414	5826	231	3.49	2.43	0.70	60.9	37.7	1.5	5.9	101
2.4	164485	5984960	1382069	144015	75604	5139	27414	748120	14402	7560	514	3.44	2.82	0.82	64.1	33.6	2.3	6.3	102
2.7	144189	5258602	1214265	136160	69685	5967	24032	657325	13616	6969	597	3.42	3.01	0.88	64.3	32.9	2.8	6.4	102
3.1	133877	4943555	1135109	134187	68243	7164	22313	617944	13419	6824	716	3.37	3.17	0.94	64.0	32.6	3.4	6.5	103
3.5	142683	5368291	1222289	143293	73125	8495	23781	671036	14329	7313	850	3.32	3.14	0.95	63.7	32.5	3.8	6.5	104
4.0	119508	4630445	1054630	120205	62118	7744	19918	578806	12021	6212	774	3.22	3.08	0.95	63.2	32.7	4.1	6.3	104
4.5	136204	5296410	1216143	134375	70071	8901	22701	662051	13438	7007	890	3.21	3.02	0.94	63.0	32.8	4.2	6.2	103
5.1	114341	4182056	943155	101607	53354	6583	19057	522757	10161	5335	658	3.42	2.90	0.85	62.9	33.0	4.1	6.3	105
5.5	109404	4375690	974554	106167	55869	6939	18234	546961	10617	5587	694	3.13	2.90	0.93	62.8	33.1	4.1	6.0	106
6.1	111989	4678637	1048445	110244	57807	7065	18665	584830	11024	5781	707	3.01	2.82	0.94	63.0	33.0	4.0	5.8	105
6.5	88243	3799938	858782	87934	46286	5730	14707	474992	8793	4629	573	2.92	2.78	0.95	62.8	33.1	4.1	5.7	104
7.8	95477	4370202	978126	95983	51161	6154	15913	546275	9598	5116	615	2.76	2.65	0.96	62.6	33.4	4.0	5.4	105
8.3	70086	3564677	811959	75684	39936	4637	11681	445585	7568	3994	464	2.49	2.56	1.03	62.9	33.2	3.9	5.1	102
22.7	70270	4620826	1004998	66242	37858	3459	11712	577603	6624	3786	346	1.95	1.79	0.92	61.6	35.2	3.2	3.7	106
23.2	62024	4088110	876772	58979	33726	3246	10337	511014	5898	3373	325	1.95	1.81	0.93	61.5	35.1	3.4	3.8	107
23.5	80665	5187229	1118898	74215	42338	3991	13444	648404	7422	4234	399	1.99	1.79	0.90	61.6	35.1	3.3	3.8	107
23.9	74889	4779610	1034151	67687	38667	3526	12482	597451	6769	3867	353	2.01	1.77	0.88	61.6	35.2	3.2	3.8	106
24.4	59218	3838154	834600	53953	30987	2862	9870	479769	5395	3099	286	1.98	1.76	0.89	61.4	35.3	3.3	3.7	106
24.8	69168	4267283	925802	60265	34505	3223	11528	533410	6027	3451	322	2.08	1.77	0.85	61.5	35.2	3.3	3.8	106
25.2	67846	4317059	932583	59900	34595	3168	11308	539632	5990	3460	317	2.02	1.74	0.86	61.3	35.4	3.2	3.8	106
25.7	62669	4123498	891400	57403	33096	3012	10445	515437	5740	3310	301	1.95	1.75	0.90	61.4	35.4	3.2	3.7	106
26.0	73668	4768979	1042335	66743	38641	3706	12278	596122	6674	3864	371	1.98	1.76	0.89	61.2	35.4	3.4	3.7	105

Experiment 4

LaNaY-72 catalyst; $W_{cat.}$ = 290mg, T_{act} = 250°C, hydrogen carrier gas

By-pass peak areas: $A_{Ethylbenzene}$ 512257
$A_{n\text{-}Decane}$ 92781

TOS	Peak area of compounds, A_i						A_i / N_i					Yield (mol%)		Y-ratio	Isomer distribution(%			X(%)	C(%)
hours	B	EB	n-C10	m-DEB	p-DEB	o-DEB	B	EB	m-DEB	p-DEB	o-DEB	B	DEBs	DEBs/B	m-DEB	p-DEB	o-DEB		Balance
0.5	110451	3049378	699158	10146	7283	0.00	18409	381172	1015	728	0.00	4.59	0.43	0.09	58.2	41.8	0.0	5.0	101
0.8	117047	2612722	594183	17777	12736	0.00	19508	326590	1778	1274	0.00	5.59	0.87	0.16	58.3	41.7	0.0	6.5	103
1.0	174776	3826886	852082	50015	32963	1978	29129	478361	5002	3296	198	5.65	1.65	0.29	58.9	38.8	2.3	7.3	106
1.3	124866	2796654	647554	68440	38588	2382	20811	349582	6844	3859	238	5.46	2.87	0.53	62.6	35.3	2.2	8.3	104
1.5	7304	163756	44078	5625	3510	217	1217	20470	563	351	22	5.38	4.13	0.77	60.1	37.5	2.3	9.5	91
1.8	504695	10186984	2352184	388140	192208	23210	84116	1273373	38814	19221	2321	5.93	4.26	0.72	64.3	31.8	3.8	10.2	106
2.0	144828	3204438	781210	135688	66738	9491	24138	400555	13569	6674	949	5.41	4.75	0.88	64.0	31.5	4.5	10.2	101
2.5	228546	5146746	1194370	224961	110094	16273	38091	643343	22496	11009	1627	5.32	4.90	0.92	64.0	31.3	4.6	10.2	106
2.8	252635	5462544	1223275	230487	112784	17020	42106	682818	23049	11278	1702	5.53	4.73	0.86	64.0	31.3	4.7	10.3	110
3.0	390304	8712307	2011102	378538	188159	29401	65051	1089038	37854	18816	2940	5.36	4.91	0.92	63.5	31.6	4.9	10.3	107
3.3	54340	1293847	279643	61656	28407	6313	9057	161731	6166	2841	631	5.02	5.34	1.06	64.0	29.5	6.6	10.4	114
3.8	232345	5399645	1185523	217207	106291	15976	38724	674956	21721	10629	1598	5.18	4.54	0.88	64.0	31.3	4.7	9.7	112
4.0	250308	5852493	1353778	238506	117827	17768	41718	731562	23851	11783	1777	5.15	4.61	0.90	63.8	31.5	4.7	9.8	106
4.3	263083	5977408	1326063	236617	116915	17598	43847	747176	23662	11692	1760	5.29	4.48	0.85	63.8	31.5	4.7	9.8	110
4.5	41404	1050702	235012	41175	18989	2981	6901	131338	4118	1899	298	4.77	4.37	0.92	65.2	30.1	4.7	9.1	109
5.0	238236	5610266	1257963	217250	107842	16041	39706	701283	21725	10784	1604	5.12	4.40	0.86	63.7	31.6	4.7	9.5	109
5.3	233471	5049584	1143000	190858	93936	13532	38912	631198	19086	9394	1353	5.56	4.26	0.77	64.0	31.5	4.5	9.8	108
5.5	239046	5840698	1280758	216598	107245	16106	39841	730087	21660	10725	1611	4.96	4.23	0.85	63.7	31.5	4.7	9.2	111
5.8	193228	4695914	1033084	168242	83518	12193	32205	586989	16824	8352	1219	4.99	4.09	0.82	63.7	31.6	4.6	9.1	110
6.0	228510	5775824	1289090	214125	106848	15716	38085	721978	21413	10685	1572	4.80	4.24	0.88	63.6	31.7	4.7	9.0	109
6.5	105237	2983050	682934	108550	53805	7845	17540	372881	10855	5381	785	4.30	4.18	0.97	63.8	31.6	4.6	8.5	106
7.0	35376	1005428	229455	35835	17926	2804	5896	125679	3584	1793	280	4.30	4.12	0.96	63.4	31.7	5.0	8.4	106
7.5	97516	2843022	660799	101716	50709	8074	16253	355378	10172	5071	807	4.19	4.14	0.99	63.4	31.6	5.0	8.3	104
8.0	66585	1897654	408918	61944	30211	4419	11098	237207	6194	3021	442	4.30	3.74	0.87	64.1	31.3	4.6	8.0	112
8.5	37078	1057043	235478	34627	15703	2679	6180	132130	3463	1570	268	4.30	3.69	0.86	65.3	29.6	5.1	8.0	108
9.0	92709	2654064	594146	83363	41371	6398	15452	331758	8336	4137	640	4.29	3.64	0.85	63.6	31.5	4.9	7.9	107
9.5	8062	239212	58605	7889	4080	631	1344	29902	789	408	63	4.13	3.88	0.94	62.6	32.4	5.0	8.0	98
10	16205	552263	118296	17029	7616	1861	2701	69033	1703	762	186	3.63	3.56	0.98	64.2	28.7	7.0	7.2	111

Experiment 5

LaNaY-72 catalyst; $W_{cat.}$ = 145mg, T_{act} = 250°C, nitrogen carrier gas

By-pass peak areas: $A_{Ethylbenzene}$ 6438128 $A_{n\text{-}Decane}$ 1320414

TOS	Peak area of compounds, A_i						A_i / N_i					Yield (mol%)		Y-ratio	Isomer distribution(%			X(%)	C(%)
hours	B	EB	n-C10	m-DEB	p-DEB	o-DEB	B	EB	m-DEB	p-DEB	o-DEB	B	DEBs	DEBs/B	m-DEB	p-DEB	o-DEB		Balance
0.3	73173	4364605	939990	14553	7657	0	12196	545576	1455	766	0	2.18	0.40	0.18	65.5	34.5	0.0	2.6	105
0.5	123035	5060413	1110954	31103	20913	1461	20506	632552	3110	2091	146	3.11	0.81	0.26	58.2	39.1	2.7	3.9	104
0.8	117345	4412067	975713	45010	30698	1863	19558	551508	4501	3070	186	3.38	1.34	0.40	58.0	39.6	2.4	4.7	105
1.0	95953	3464797	773932	61719	37539	2683	15992	433100	6172	3754	268	3.48	2.22	0.64	60.5	36.8	2.6	5.7	105
1.3	102026	3680506	806327	82554	45894	3985	17004	460063	8255	4589	399	3.47	2.70	0.78	62.3	34.7	3.0	6.2	108
1.5	138690	5068093	1114092	125451	67628	7245	23115	633512	12545	6763	725	3.42	2.96	0.87	62.6	33.8	3.6	6.4	107
1.8	158712	5823165	1280995	147184	78104	8763	26452	727896	14718	7810	876	3.40	3.01	0.88	62.9	33.4	3.7	6.4	107
2.0	96512	3537224	773538	88450	47379	5677	16085	442153	8845	4738	568	3.41	3.00	0.88	62.5	33.5	4.0	6.4	108
2.5	86416	3426480	748673	85082	45485	5575	14403	428310	8508	4549	558	3.16	2.98	0.95	62.5	33.4	4.1	6.1	108
3.2	92069	3662246	810912	86644	45871	5451	15345	457781	8664	4587	545	3.15	2.83	0.90	62.8	33.2	4.0	6.0	106
3.5	108306	4495626	983931	107670	56321	7085	18051	561953	10767	5632	709	3.02	2.87	0.95	62.9	32.9	4.1	5.9	107
4.0	127684	5501664	1216335	126053	66654	8140	21281	687708	12605	6665	814	2.92	2.75	0.94	62.8	33.2	4.1	5.7	106
4.5	138469	6013360	1321532	131793	70308	8620	23078	751670	13179	7031	862	2.90	2.65	0.91	62.5	33.4	4.1	5.5	107
5.0	138490	6350826	1402293	131879	70838	8468	23082	793853	13188	7084	847	2.75	2.52	0.91	62.4	33.5	4.0	5.3	106
6.0	123309	5906400	1301882	114638	62207	6973	20552	738300	11464	6221	697	2.64	2.37	0.89	62.4	33.8	3.8	5.0	106
7.0	122156	5998336	1315470	114275	62234	6944	20359	749792	11428	6223	694	2.58	2.33	0.90	62.3	33.9	3.8	4.9	106
7.5	123460	6204160	1357889	116314	63286	6930	20577	775520	11631	6329	693	2.53	2.29	0.91	62.4	33.9	3.7	4.8	106
15.8	91942	5145120	1131016	83306	46217	4798	15324	643140	8331	4622	480	2.28	2.00	0.88	62.0	34.4	3.6	4.3	105
16.2	167644	9888179	2133014	159615	88951	9399	27941	1236022	15962	8895	940	2.17	2.00	0.92	61.9	34.5	3.6	4.2	107
16.5	93803	5363914	1167713	85267	47376	4869	15634	670489	8527	4738	487	2.23	1.96	0.88	62.0	34.5	3.5	4.2	106
17.0	87740	5049328	1098198	80232	44622	4623	14623	631166	8023	4462	462	2.22	1.97	0.89	62.0	34.5	3.6	4.2	106
17.5	106258	6366400	1378416	100397	56208	5765	17710	795800	10040	5621	577	2.13	1.96	0.92	61.8	34.6	3.6	4.1	107
18.0	93035	5382064	1157624	84508	47147	4856	15506	672758	8451	4715	486	2.21	1.94	0.88	61.9	34.5	3.6	4.2	107
22.0	99726	5999082	1293621	91030	51078	5204	16621	749885	9103	5108	520	2.13	1.89	0.89	61.8	34.7	3.5	4.0	107
23.0	89200	5515453	1182609	83279	46763	4802	14867	689432	8328	4676	480	2.07	1.88	0.91	61.8	34.7	3.6	3.9	107

Experiment 6
LYZ-82 catalyst; $W_{cat.}$ = 290mg, T_{act} = 450°C, nitrogen carrier gas

By-pass peak areas: $A_{Ethylbenzene}$ 3510964
$A_{n\text{-}Decane}$ 688826

TOS	Peak area of compounds, A_i						A_i / N_i					Yield (mol%)		Y-ratio	Isomer distribution(			X(%)	C(%)
hours	B	EB	n-C10	m-DEB	p-DEB	o-DEB	B	EB	m-DE	p-DEB	o-DEB	B	DEBs	DEBs/B	m-DE	p-DE	o-DEB		Balance
0.5	1210393	2495730	1073824	416463	184349	33485	201732	311966	41646	18435	3349	34.95	10.99	0.31	65.7	29.1	5.3	45.9	90
0.8	1114208	2609514	1154196	708141	317250	58617	185701	326189	70814	31725	5862	29.94	17.48	0.58	65.3	29.3	5.4	47.4	92
1.0	937367	2445352	1020715	653105	295667	54403	156228	305669	65311	29567	5440	27.79	17.84	0.64	65.1	29.5	5.4	45.6	95
1.3	810877	2315470	937612	583068	264971	48208	135148	289434	58307	26497	4821	26.28	17.43	0.66	65.1	29.6	5.4	43.7	95
1.5	666651	2098098	795092	520373	237367	43032	111109	262262	52037	23737	4303	24.50	17.66	0.72	65.0	29.6	5.4	42.2	99
1.8	908330	3063840	1157833	728365	333151	60456	151388	382980	72837	33315	6046	23.41	17.35	0.74	64.9	29.7	5.4	40.8	97
2.0	662750	2388346	844200	544681	248923	44955	110458	298543	54468	24892	4496	22.41	17.01	0.76	65.0	29.7	5.4	39.4	102
2.3	740015	2802230	992649	620670	284706	51234	123336	350279	62067	28471	5123	21.67	16.80	0.78	64.9	29.8	5.4	38.5	100
2.5	629163	2528485	869460	545560	249577	45035	104861	315811	54556	24958	4504	20.78	16.65	0.80	64.9	29.7	5.4	37.4	102
2.8	781957	3226150	1092805	677673	310207	56004	130326	403269	67767	31021	5600	20.43	16.36	0.80	64.9	29.7	5.4	36.8	102
3.0	490187	2112291	711678	427020	195415	35072	81698	264036	42702	19542	3507	19.85	15.98	0.80	64.9	29.7	5.3	35.8	101
4.0	747341	3616154	1153196	673903	308755	55479	124557	452019	67390	30876	5548	18.31	15.26	0.83	64.9	29.7	5.3	33.6	104
4.7	671013	3402784	1079088	606644	277596	49845	111836	425348	60664	27760	4985	17.74	14.81	0.84	64.9	29.7	5.3	32.5	103
5.5	651947	3533309	1086983	596797	273292	48999	108658	441664	59680	27329	4900	16.92	14.31	0.85	64.9	29.7	5.3	31.2	104
6.0	624341	3425109	1053962	568127	260396	47411	104057	428139	56813	26040	4741	16.79	14.13	0.84	64.9	29.7	5.4	30.9	103
6.5	662481	3822328	1146222	612212	280179	50514	110414	477791	61221	28018	5051	16.18	13.82	0.85	64.9	29.7	5.4	30.0	105
7.0	577059	3414021	1022995	533486	245180	44630	96177	426753	53349	24518	4463	15.89	13.60	0.86	64.8	29.8	5.4	29.5	104
7.5	586763	3546288	1050216	542125	248382	44588	97794	443286	54213	24838	4459	15.66	13.37	0.85	64.9	29.7	5.3	29.0	105
8.3	413738	2564210	763442	387788	177820	31964	68956	320526	38779	17782	3196	15.35	13.30	0.87	64.9	29.8	5.3	28.7	104

Experiment 7
LYZ-62 catalyst; $W_{cat.}$ = 290mg, T_{act} = 450°C, nitrogen carrier gas

By-pass peak areas: $A_{Ethylbenzene}$ 4300950
$A_{n\text{-}Decane}$ 931444

TOS	Peak area of compounds, A_i						A_i / N_i					Yield (mol%)		Y-ratio	Isomer distribution(			X(%)	C(%)
hours	B	EB	n-C10	m-DEB	p-DEB	o-DEB	B	EB	m-DE	p-DEB	o-DEB	B	DEBs	DEBs/B	m-DE	p-DE	o-DEB		Balance
0.5	160643	5080589	1120601	6227	4035	0	26774	635074	623	404	0	4.04	0.15	0.04	60.7	39.3	0.0	4.2	104
0.8	209549	6332224	1386152	18654	14352	0	34925	791528	1865	1435	0	4.21	0.40	0.09	56.5	43.5	0.0	4.6	105
1.0	204501	6185293	1369874	37120	29714	1605	34084	773162	3712	2971	161	4.19	0.84	0.20	54.2	43.4	2.3	5.0	104
1.3	197854	5911965	1311038	96042	66282	3440	32976	738996	9604	6628	344	4.18	2.10	0.50	57.9	40.0	2.1	6.3	106
1.7	171702	5037651	1129386	142507	77707	7098	28617	629706	14251	7771	710	4.20	3.34	0.79	62.7	34.2	3.1	7.5	107
2.0	216743	6559659	1517070	215415	108243	12762	36124	819982	21542	10824	1276	4.06	3.78	0.93	64.0	32.2	3.8	7.8	104
2.5	192752	6074269	1380571	203037	100993	14594	32125	759284	20304	10099	1459	3.90	3.87	0.99	63.7	31.7	4.6	7.8	106
3.0	178150	5751843	1290013	180008	90307	13314	29692	718980	18001	9031	1331	3.82	3.65	0.96	63.5	31.8	4.7	7.5	107
3.7	145797	4938560	1107939	147742	75101	10663	24300	617320	14774	7510	1066	3.65	3.51	0.96	63.3	32.2	4.6	7.2	106
4.3	175312	6124400	1367199	175080	89443	12342	29219	765550	17508	8944	1234	3.55	3.37	0.95	63.2	32.3	4.5	6.9	107
5.7	154955	5751171	1281857	149739	77537	10297	25826	718896	14974	7754	1030	3.36	3.09	0.92	63.0	32.6	4.3	6.5	106
7.1	130068	5227274	1154140	129299	66917	8714	21678	653409	12930	6692	871	3.12	2.95	0.95	63.1	32.7	4.3	6.1	107
8.0	152782	6188765	1365507	147801	77574	9889	25464	773596	14780	7757	989	3.10	2.86	0.92	62.8	33.0	4.2	6.0	107
9.4	130706	5870880	1297099	128204	67759	8645	21784	733860	12820	6776	865	2.81	2.64	0.94	62.7	33.1	4.2	5.4	106
11.0	74731	3570560	777622	70595	37503	4307	12455	446320	7060	3750	431	2.65	2.39	0.90	62.8	33.4	3.8	5.0	107

Experiment 8
LYZ-52 catalyst; $W_{cat.}$ = 290mg, T_{act} = 450°C, nitrogen carrier gas

No activity

Experiment 9

H-BEA-15 catalyst; $W_{cat.}$ = 290mg, T_{act} = 450°C, nitrogen carrier gas

TOS	Peak area of compounds, A_i					A_i / N_i					Yield (mol%)		Y-ratio	Isomer distribution(%			X(%)
hours	B	EB	m-DEB	p-DEB	o-DEB	B	EB	m-DEB	p-DEB	o-DEB	B	DEBs	DEBs/B	m-DEB	p-DEB	o-DEB	
0.5	592641	4387584	360288	163257	29143	98774	548448	36029	16326	2914	14.06	7.87	0.56	65.2	29.5	5.3	21.9
0.8	778326	6580858	732294	345604	59349	129721	822607	73229	34560	5935	12.17	10.67	0.88	64.4	30.4	5.2	22.8
1.0	701042	6271088	679881	323845	54858	116840	783886	67988	32385	5486	11.61	10.52	0.91	64.2	30.6	5.2	22.1
1.3	793181	7388275	757628	363015	61254	132197	923534	75763	36302	6125	11.26	10.07	0.89	64.1	30.7	5.2	21.3
1.5	623230	6030912	593138	285388	47968	103872	753864	59314	28539	4797	10.93	9.75	0.89	64.0	30.8	5.2	20.7
1.8	781752	7771443	750270	362604	60783	130292	971430	75027	36260	6078	10.69	9.63	0.90	63.9	30.9	5.2	20.3
2.0	820684	8312611	775535	376259	62730	136781	1039076	77554	37626	6273	10.54	9.36	0.89	63.9	31.0	5.2	19.9
2.5	810196	8476531	770436	375005	62121	135033	1059566	77044	37501	6212	10.27	9.18	0.89	63.8	31.1	5.1	19.4
3.1	664090	7226493	621178	303470	50150	110682	903312	62118	30347	5015	9.96	8.77	0.88	63.7	31.1	5.1	18.7
3.7	544639	6060560	513873	251379	41720	90773	757570	51387	25138	4172	9.77	8.69	0.89	63.7	31.2	5.2	18.5
4.5	503792	5726989	464499	227048	37610	83965	715874	46450	22705	3761	9.62	8.35	0.87	63.7	31.1	5.2	18.0
5.1	742382	8795706	705836	346478	58262	123730	1099463	70584	34648	5826	9.27	8.32	0.90	63.6	31.2	5.2	17.6
5.7	514287	6025184	474004	230471	38153	85715	753148	47400	23047	3815	9.39	8.13	0.87	63.8	31.0	5.1	17.5
6.3	731799	9031443	701046	341730	57119	121967	1129930	70105	34173	5712	8.96	8.08	0.90	63.7	31.1	5.2	17.0
7.2	411352	5258499	384169	187465	30937	68559	657312	38417	18747	3094	8.72	7.67	0.88	63.8	31.1	5.1	16.4
7.8	654034	8350205	621004	302228	50420	109006	1043776	62100	30223	5042	8.72	7.79	0.89	63.8	31.0	5.2	16.5
11.5	235374	3197990	227915	110182	18486	39229	399749	22792	11018	1849	8.27	7.51	0.91	63.9	30.9	5.2	15.8
12.0	527634	7138979	503406	243252	40894	87939	892372	50341	24325	4089	8.30	7.43	0.90	63.9	30.9	5.2	15.7

Experiment 10

H-BEA-25 catalyst; $W_{cat.}$ = 290mg, T_{act} = 450°C, nitrogen carrier gas

TOS	Peak area of compounds, A_i					A_i / N_i					Yield (mol%)		Y-ratio	Isomer distribution(%			X(%)
hours	B	EB	m-DEB	p-DEB	o-DEB	B	EB	m-DEB	p-DEB	o-DEB	B	DEBs	DEBs/B	m-DEB	p-DEB	o-DEB	
0.3	615025	8260928	40809	32324	3035	102504	1032616	4081	3232	304	8.97	0.67	0.07	53.6	42.4	4.0	9.6
0.7	438901	7032090	176287	90087	14309	73150	879011	17629	9009	1431	7.46	2.86	0.38	62.8	32.1	5.1	10.3
1.0	433223	7633411	357366	173417	28370	72204	954176	35737	17342	2837	6.67	5.17	0.77	63.9	31.0	5.1	11.8
1.3	477464	9242854	491657	246506	39457	79577	1155357	49166	24651	3946	6.06	5.92	0.98	63.2	31.7	5.1	12.0
1.8	500092	9783814	504829	254785	41110	83349	1222977	50483	25479	4111	6.01	5.78	0.96	63.0	31.8	5.1	11.8
2.0	412459	8432742	418615	211185	32895	68743	1054093	41862	21119	3290	5.78	5.57	0.96	63.2	31.9	5.0	11.4
2.5	370796	7774995	375610	191415	30187	61799	971874	37561	19142	3019	5.65	5.46	0.97	62.9	32.1	5.1	11.1
3.0	363314	7834845	358095	182440	28344	60552	979356	35810	18244	2834	5.52	5.19	0.94	62.9	32.1	5.0	10.7
4.3	457176	10547208	451642	230975	35921	76196	1318401	45164	23098	3592	5.20	4.90	0.94	62.9	32.1	5.0	10.1
5.0	174045	4001422	165911	84870	13159	29008	500178	16591	8487	1316	5.22	4.75	0.91	62.9	32.2	5.0	10.0
5.8	470233	11157246	453635	231979	36064	78372	1394656	45364	23198	3606	5.07	4.67	0.92	62.9	32.1	5.0	9.7
6.6	407197	9800410	386481	197914	30700	67866	1225051	38648	19791	3070	5.01	4.54	0.91	62.8	32.2	5.0	9.6
7.3	228081	5606186	218726	111923	17320	38014	700773	21873	11192	1732	4.91	4.50	0.92	62.9	32.2	5.0	9.4
8.2	316821	7986669	305400	155926	24029	52804	998334	30540	15593	2403	4.80	4.41	0.92	62.9	32.1	5.0	9.2
8.8	435690	11001552	414995	212040	32845	72615	1375194	41500	21204	3285	4.80	4.36	0.91	62.9	32.1	5.0	9.2
9.4	332144	8494362	317608	162288	25093	55357	1061795	31761	16229	2509	4.74	4.32	0.91	62.9	32.1	5.0	9.1
10.0	366969	9521363	348769	178094	27791	61162	1190170	34877	17809	2779	4.68	4.24	0.91	62.9	32.1	5.0	8.9

Experiment 11

H-MFI-45 catalyst; $W_{cat.}$ = 290mg, T_{act} = 450°C, nitrogen carrier gas

TOS	Peak area of compounds, A_i					A_i / N_i					Yield (mol%)		Y-ratio	Isomer distribution(			X(%)
hours	B	EB	m-DEB	p-DEB	o-DEB	B	EB	m-DE	p-DEB	o-DEB	B	DEBs	DEBs/B	m-DE	p-DEB	o-DEB	
0.2	123844	12067008	14836	7828	0	20641	1508376	1484	783	0	1.35	0.15	0.11	65.5	34.5	0.0	1.5
0.4	53833	11782016	25114	14561	0	8972	1472752	2511	1456	0	0.60	0.27	0.44	63.3	36.7	0.0	0.9
0.8	40645	10913368	23206	14132	0	6774	1364171	2321	1413	0	0.49	0.27	0.55	62.2	37.8	0.0	0.8
1.0	45431	13399960	24886	15650	0	7572	1674995	2489	1565	0	0.45	0.24	0.54	61.4	38.6	0.0	0.7
1.3	31787	11726344	18774	11908	0	5298	1466043	1877	1191	0	0.36	0.21	0.58	61.2	38.8	0.0	0.6
1.8	24257	8768941	11921	7643	0	4043	1096118	1192	764	0	0.37	0.18	0.48	60.9	39.1	0.0	0.5
2.3	33758	12458000	15019	9523	0	5626	1557250	1502	952	0	0.36	0.16	0.44	61.2	38.8	0.0	0.5
2.6	36541	12166176	13848	8825	0	6090	1520772	1385	883	0	0.40	0.15	0.37	61.1	38.9	0.0	0.5
3.4	29809	12132936	12416	7862	0	4968	1516617	1242	786	0	0.33	0.13	0.41	61.2	38.8	0.0	0.5
4.0	28610	12584536	12343	7720	0	4768	1573067	1234	772	0	0.30	0.13	0.42	61.5	38.5	0.0	0.4
4.6	35675	12449024	11728	7396	0	5946	1556128	1173	740	0	0.38	0.12	0.32	61.3	38.7	0.0	0.5
5.1	26340	10157336	9655	5832	0	4390	1269667	966	583	0	0.34	0.12	0.35	62.3	37.7	0.0	0.5
5.8	37634	12891168	11498	7103	0	6272	1611396	1150	710	0	0.39	0.11	0.30	61.8	38.2	0.0	0.5
6.2	31360	11847656	10301	6702	0	5227	1480957	1030	670	0	0.35	0.11	0.33	60.6	39.4	0.0	0.5
6.6	28974	11744696	10272	6251	0	4829	1468087	1027	625	0	0.33	0.11	0.34	62.2	37.8	0.0	0.4
7.0	45045	12851136	11287	7014	0	7508	1607642	1129	701	0	0.46	0.11	0.24	61.7	38.3	0.0	0.6

A-3 EVALUATION OF REACTION RATES

In determining the reaction rates, the following assumptions are made:

- Since the disproportionation of ethylbenzene is almost thermoneutral ($-\Delta H_R^0 = +2kJ/mol$, for the equilibrium product distribution at 180 °C, based on ΔH_f^0 data from Stull et al. (1969)), the conversions can be carried out in a fixed bed micro-reactor with negligible temperature profiles (i.e. isothermal operation).

- Since the ratio of the reactor diameter to the catalyst pellet size is 10 mm / 0.25 mm = 40, wall effects on flow distribution are assumed negligible.

- The ratio of the height of the packed catalyst bed (diluted) preheat zone to the catalyst pellet size is 98 mm / 0.25 mm = 392, thus by-passing can be assumed negligible.

Based on these boundary conditions, plug flow behaviour is assumed to exist throughout the reactor. Thus the material balance for ethylbenzene, EB, is described by the relation:

$$\frac{W}{F} = \int_0^{X_{EB}} \frac{dX}{-r_{EB}}$$

where:
W is the mass of the catalyst (g)
F is the flow rate of ethylbenzene (mol/h)
$-r_{EB}$ is the rate of reaction ($mol/g_{catalyst}.h$)
X is the conversion of reaction

If it is assumed that the ethylbenzene conversion follows first order kinetics (Klemm et al. 1997), then the rate becomes:

$$-r_{EB} = k_{EB} C_{EB0} (1 - X)$$

Consequently, the plug flow equation takes the form:

$$\frac{W}{F} = \frac{1}{k_{EB} C_{EB0}} \int_0^{X_{EB}} \frac{dX}{(1 - X)}$$

Integrating gives

$$\frac{W}{F} = \frac{1}{k_{EB} C_{EB0}} \ln\left(\frac{1}{1 - X}\right)$$

Rearranging gives the relationship for k_{EB}.

$$k_i = \frac{\ln\left(\frac{1}{1 - X}\right)}{(W/F) C_{EB0}}$$

Finally, the rate of consumption of ethylbenzene is given by:

$$-r_{EB} = \frac{\ln\left(\frac{1}{1 - X}\right)}{(W/F)} (1 - X)$$

A-4 CALCULATION OF ACIDITY OF ZEOLITES FROM CHEMICAL COMPOSITION

H-MFI Si/Al = 45 (atomic)

(96-n)/n = 45

46n = 96

n =2.09

On dry basis the hydrogen form of H-MFI-45:

$H_{2.09}[Al_{2.09}Si_{93.91}O_{192}]$ = 5760 g/mol

Acidity (Powder) = 2.09 mol_H/(5760g)

Number of acid sites = **0.363 $mmol_H/g_{cat}$**

H-BEA Si/Al = 25 (atomic)

(64-n)/n = 25

26n = 64

n =2.46

On dry basis the hydrogen form of H-BEA-25:

$H_{2.46}[Al_{2.46}Si_{61.54}O_{128}]$ = 3840 g/mol

Acidity (Powder) = 2.46 mol_H/(3840g)

Number of acid sites = **0.641 $mmol_H/g_{cat}$**

H-BEA Si/Al = 14.6 (atomic)

(64-n)/n = 14.6

15.6n = 64

n = 4.1

On dry basis the hydrogen form of H-BEA-15:

$H_{4.1}[Al_{4.1}Si_{59.9}O_{128}]$ = 3840 g/mol

Acidity (Powder) = 4.1 mol_H/(3840g)

Number of acid sites = **1.068 $mmol_H/g_{cat}$**

Linde-Y (LZY-82) (99% exchanged) Si/Al = 5.38 (atomic)

(192-n)/n = 5.38

$Na_{0.3}H_{29.8}[Al_{30.1}Si_{161.9}O_{384}]$ = 11541 g/mol

Acidity (Powder) = 29.8 mol_H/(11541g

= 2.58 $mmol_H/g_{cat}$

Therefore extrudates (20% Al_2O_3; 80% LZY-82)

Number of acid sites = 0.8*2.58 = **2.06 $mmol_H/g_{cat}$**

Linde-Y (LZY-62) (82% exchanged) Si/Al = 4.94 (atomic)

(192-n)/n = 4.94

$Na_{5.8}H_{26.5}[Al_{32.3}Si_{159.7}O_{384}]$ = 11662 g/mol

Acidity (Powder) = 26.5 mol_H/(11662g)

= 2.27 $mmol_H/g_{cat}$

Therefore extrudates (20% Al_2O_3; 80% LZY-82)

Number of acid sites = 0.8*2.27 = **1.82 $mmol_H/g_{cat}$**

Linde-Y (LZY-52) (0% exchanged) Si/Al = 4.75 (atomic)

(192-n)/n = 4.75

$Na_{33.4}[Al_{33.4}Si_{158.6}O_{384}]$ = 12269 g/mol

Acidity (Powder) = 0.0 mol_H/(12269g)

= 0.0 $mmol_H/g_{cat}$

LaNaY-72 assuming $La(OH)_2^+$ species (activated at 250 °C) Si/Al = 2.4 (atomic)

(192-n)/n = 2.4

$(La(OH)_2)_{13.6}\ H_{27.1}Na_{15.8}[Al_{56.5}Si_{135.5}O_{384}]$ = 14218 g/mol

There are two acid sites per $La(OH)_2^+$ ion in the zeolite

Acidity (Powder) = 2x13.6 mol_H/(14218g)

= 1.91 $mmol_H/g_{cat}$

LaNaY-72 assuming $La(OH)^{2+}$ species (activated at 450 °C) Si/Al = 2.4 (atomic)

(192-n)/n = 2.4

$(La(OH))_{13.6}H_{13.6}Na_{15.8}[Al_{56.5}Si_{135.5}O_{384}]$ = 13973 g/mol

There is one acid site per $La(OH)^{2+}$ ion in the zeolite

Acidity (Powder) = 13.6 mol_H/(13973gl)

= 0.97 $mmol_H/g_{cat}$

A-5 ESTIMATION OF ETHYLBENZENE DEFICIT

The amount of diethylbenzenes remaining on the catalyst can easily be quantified from the integrated benzene and diethylbenzene yield differences during the induction period.

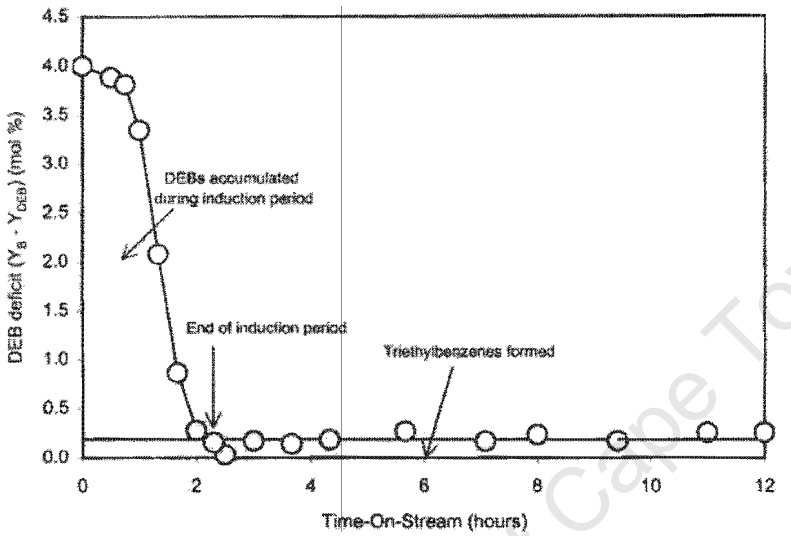

Figure A-1 Quantification of the deficit of diethylbenzenes during the induction period (LZY-62, Experiment 7)

$$D_{DEB} = \int_{t=0}^{t_{ind}} (Y_B - Y_{DEB})dt - \int_{t=0}^{t_{ind}} Y_{TEB}\,dt$$

TEB: triethylbenzenes (see chromatogram in appendix 2)